

©Copyright 2005
Marnie A. Haller

Characterization of Nonlinear Optical Polymers and Dendrimers for Electro-Optic Applications

Marnie A. Haller

A dissertation submitted in partial fulfillment of the requirements for the degree of

Doctor of Philosophy

University of Washington

2005

Program Authorized to Offer Degree: Materials Science and Engineering

UMI Number: 3198795

INFORMATION TO USERS

The quality of this reproduction is dependent upon the quality of the copy submitted. Broken or indistinct print, colored or poor quality illustrations and photographs, print bleed-through, substandard margins, and improper alignment can adversely affect reproduction.

In the unlikely event that the author did not send a complete manuscript and there are missing pages, these will be noted. Also, if unauthorized copyright material had to be removed, a note will indicate the deletion.



UMI Microform 3198795

Copyright 2006 by ProQuest Information and Learning Company.

All rights reserved. This microform edition is protected against unauthorized copying under Title 17, United States Code.

ProQuest Information and Learning Company
300 North Zeeb Road
P.O. Box 1346
Ann Arbor, MI 48106-1346

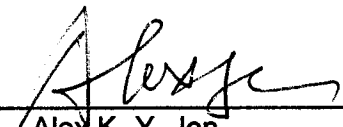
University of Washington
Graduate School

This is to certify that I have examined this copy of a doctoral dissertation by

Marnie A. Haller

and have found that it is complete and satisfactory in all respects,
and that any and all revisions required by the final
examining committee have been made.

Chair of Supervisory Committee:

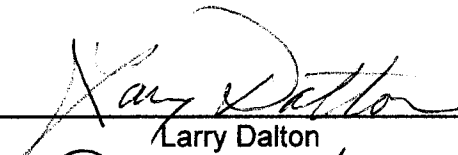


Alex K.-Y. Jen

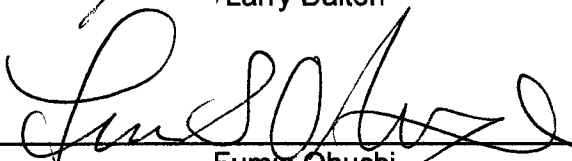
Reading Committee:



Alex K.-Y. Jen



Larry Dalton



Fumio Ohuchi

Date: 9-12-05

In presenting this dissertation in partial fulfillment of the requirements for the doctoral degree at the University of Washington, I agree that the Library shall make its copies freely available for inspection. I further agree that extensive copying of the dissertation is allowable only for scholarly purposes, consistent with "fair use" as prescribed in the U.S. Copyright Law. Requests for copying or reproduction of this dissertation may be referred to Proquest Information and Learning, 300 North Zeeb Road, Ann Arbor, MI 48106-1346, to whom the author has granted "the right to reproduce and sell (a) copies of the manuscript in microform and/or (b) printed copies of the manuscript made from microform."

Signature Marnie Haller

Date 9-12-05

University of Washington

Abstract

**Characterization of Nonlinear Optical Polymers and Dendrimers
for Electro-Optic Applications**

Marnie A. Haller

Chair of the Supervisory Committee:
Professor Alex K-Y Jen
Department of Materials Science and Engineering

Organic second-order nonlinear optical (NLO) polymers have received increasing interest due to their potential for applications in high-speed electro-optic (EO) devices with very broad bandwidth and excellent device performance. Their large EO coefficients and low drive voltages have been demonstrated in prototype EO modulators by using several guest–host poled polymers. Translating the high molecular hyperpolarizabilities (β) of organic chromophores into large electro-optic coefficient (r_{33}) device-quality polymers is one of the most challenging tasks in electro-optic polymer research. Current research at the University of Washington has implemented several innovative approaches to improve the performance of the nonlinear optical polymers through nanoscale architectural control. The ability to synthetically control several critical design parameters, such as size, shape, surface chemistry, flexibility, and topology, has shaped the exploration of a range of novel materials. UW researchers have extensively studied the effects of increasing the effective conjugation length and/or enhancing the donor and acceptor strengths on the basic rigid rod chromophore guest–host systems. They also have conducted comprehensive research on the effects of manipulating chromophore shape by surrounding it with bulky inert substituents to make the chromophore more spherical. Recent work exploiting smartly controlled chemistry and creative processing/poling procedures has significantly improved poling efficiencies. The typical solubility limit of guest molecules in the host matrix has been pushed to much higher doping levels without an increase in dielectric breakdowns through the site isolation effects contributed by fluorinated dendrons. One of our novel synthetic routes was based on free Diels-Alder chemistry, a very mild catalyst. The Diels-Alder reaction allowed the

poling process to occur prior to and separated from the lattice-hardening process and provided materials with high thermal stability and excellent poling efficiency.

TABLE OF CONTENTS

	Page
List of Figures.....	iv
List of Tables.....	vi
Chapter 1 Introduction	1
1.1 Introduction	1
1.2 Waveguide Devices	2
1.2.1 Electro-Optic Modulator	4
1.2.2 Mach-Zehnder Interferometer	4
1.2.3 Performance Parameters.....	5
1.3 Motivation.....	8
1.4 Scope of Research.....	10
Notes to Chapter 1.....	13
Chapter 2 Background	15
2.1 Nonlinear Optical Effect.....	15
2.1.1 Microscopic Polarization	15
2.1.2 Macroscopic Polarization	19
2.2 Poling Process	23
2.2.1 Poling Dynamics	25
2.2.2 Poling Techniques	26
2.2.3 Poling Parameters	27
2.2.4 Shape Engineering	30
2.2.5 Electro-Optic Polymer Systems.....	32
Notes to Chapter 2.....	35

Chapter 3	Experimental Approach	37
3.1	Characterization Techniques.....	37
3.2	Microscopic Measurement	37
3.3	Macroscopic Measurements.....	39
3.4	Simple Reflection Technique Limitations.....	48
3.5	Experimental	50
	Notes to Chapter 3.....	52
Chapter 4	Effects of Chromophore Shape Modification on Poling Efficiency and Stability.....	54
4.1	Introduction	54
4.2	Guest Host Chromophore Systems.....	57
4.2.1	Effects of Chromophore Acceptor and Bridge Design on Poling Efficiency	58
4.2.2	Effects of Bulky Group Additions	63
4.3	Effects of Flourinated Dendrons in Side Chain Systems.....	68
4.3.1	Polystyrene Side Chain Systems	69
4.3.2	Polyimide Series	76
4.4	Stability	78
4.4.1	Background	78
4.4.2	PSDA-CRM Series	81
4.4.3	PSDA-CLD1	87
4.4.4	PSDA-AJL Series	89
4.5	Conclusions and Future Work	91
4.6	Experimental	94
	Notes to Chapter 4.....	96

Chapter 5	Accuracy Limitations of the Simple Reflection Technique	98
5.1	Introduction	98
5.2	Multi-Angle Electro-Optic Measurements	100
5.3	Rigorous Model	103
5.4	Electrode Absorption Contributions	107
5.5	Material Absorption Contributions	115
5.6	Conclusions and Future Work	121
5.7	Experimental	122
	Notes to Chapter 5.....	124
	Bibliography.....	126

LIST OF FIGURES

Figure Number

1.1. Principal of total internal reflection	2
1.2. Waveguide structures	3
1.3. Illustration of a Mach-Zehnder Modulator	5
2.1. Schematic of a Chromophore Design	17
2.2. Representative Chromophore Structure	17
2.3. Poling Process	24
2.4. Contact and Corona Poling Sample Schematics	26
2.5. Experimental Poling Data	28
2.6. r_{33} Versus Temperature Graph	29
2.7. Experimental Electro-Optic Coefficient Data	29
2.8. Electro-Optic Coefficient versus Number Density	31
2.9. Schematic of the Dendrimer Structure	34
3.1. Through Plane Sample Geometry	40
3.2. Experimental Set Up of ATR.....	41
3.3. Constant Bias Set-Up.....	42
3.4. Experimental Set Up of the Simple Reflection Method at UW.....	44
3.5. Output Intensity as a Function of Phase Difference	46
3.6. Experimental Data of the Output Intensity Curve versus Babinet-Soleil Compensator Position	46
3.7. Modulated Intensity versus Modulated Voltage at the UW.....	48
3.8. Modulated Intensity Versus Modulated Voltage	50
4.1. Schematic Drawings of Various Chromophore Systems.....	57

4.2. Chemical Structure of AJL6, 7 and 8 Chromophores	59
4.3. Chemical Structure of AJC139 Chromophore	60
4.4. r_{33} (at 1310 nm) with a Poling Field of 100 V/ μ m Versus Absorption Peak	60
4.5. Stability Summary of the AJL6, AJL7 and AJL8 Chromophores	62
4.6. Chemical Structures of LMAJ22, LMAJ28 and LMAJ28-Bulky Chromophores.....	64
4.7. Chemical Structure of FLDR and TCBD Chromophores	66
4.8. Absorption Spectrum of FLDR and TCBD Chromophores	67
4.9. Chemical Structures of the FTC Side-Chain Series	69
4.10. r_{33} versus Applied Poling Voltage	70
4.11. Chemical Structure of NLO Dendrimer	71
4.12. Chemical Structures of the CLD Side-chain Series.....	73
4.13. Cylindrical Stacking of PS-CLD2	74
4.14. Chemical Structure of PI-CLD1	76
4.15. Long Term Stability of PI-CLD1	77
4.16. Diels-Alder Reversible Reaction	80
4.17. Schematic of Diels-Alder Crosslinking Process	81
4.18. Representation of the Diels-Alder Reactions	82
4.19. Chemical Structure of PSDA-CRM1 and PSDA-CRM2.....	83
4.20. Chemical Structure of PSDA-CRM3 and PSDA-CRM4.....	83
4.21. Normalized Stability Electro-Optic Coefficient versus Time.....	86
4.22. Chemical Structure of PSDA-CLD1	87
4.23. Chemical Structures of PSDA-AJL4 and PSDA-AJL5.....	90
5.1. Intensity and Modulated Intensity for a Compensator Scan (a) Modulated Intensity versus Modulated Voltage (b)	102
5.2. (a) Simple Model (b) Rigorous Model	104

5.3.	Published Data of the Averaged r_{33} Value Measuring at Multiple Angles and Different Wavelengths	107
5.4.	% Transmittance versus Wavelength	108
5.5.	Modulated Intensity versus Modulated Voltage for a Poled Polymer Film on a Commercial ITO Electrode (a) and a NW-ITO Electrode (b) Measured at 1550 nm	110
5.6.	(a) $\delta\phi_{sp}$ versus Measurement Angle at 1315 nm (b) $\delta\phi_{sp}$ versus Measurement Angle at 1550 nm for Abrisa ITO	111
5.7.	(a) $\delta\phi_{sp}$ versus Measurement Angle at 1315 nm (b) $\delta\phi_{sp}$ versus Measurement Angle at 1550 nm for NW-ITO.....	112
5.8.	(a) $\delta\phi_{sp}$ versus Measurement Angle at 1315 nm (b) $\delta\phi_{sp}$ versus Measurement Angle at 1550 nm for NW-ZITO	113
5.9.	$\delta b/b$ versus Measurement Angle for Abrisa ITO Measured at 1315 nm	114
5.10.	Modulated Intensity versus Modulated Voltage.....	116
5.11.	Absorption Spectra of the TCF, AJL8 and AJC135 Chromophores.....	117
5.12.	Chemical Structures of the TCF, AJL8, and AJC135 Chromophores	117
5.13.	(a) $\delta\phi_{sp}$ versus Measurement Angle at 1300 nm for the TCF Chromophore..	118
5.14.	(a) $\delta\phi_{sp}$ versus Measurement Angle (b) $\delta b/b$ versus Measurement Angle at 1300 nm for the AJC135 Chromophore	119
5.15.	Chemical Structure of AJ302 Organic Glass.....	119
5.16.	(a) $\delta\phi_{sp}$ versus Measurement Angle (b) $\delta b/b$ versus Measurement Angle at 1330 nm for the AJ302 Organic Glass	120

LIST OF TABLES

Table Number	Page
1.1. Summary of Material Properties	8
2.1. $\mu\beta$ and r_{33} (pm/V) _{at 1300nm} of Representative NLO Chromophores	18
4.1. Summary of Properties for the AJL6, AJL7, AJL8, and AJC139 Chromophores.....	61
4.2. Summary of Properties for LMAJ22, LMAJ28 and LMAJ28-Bulky Chromophores.....	65
4.3. Summary of Properties for TCBD and FLDR Chromophores.....	68
4.4. Summary of Properties for the PS-FTC Side-Chain Polymers	71
4.5. Summary of Properties for PS-CLD Side-Chain Polymers.....	74
4.6. Summary of Properties for the CRM Series	85
4.7. Summary of Properties for the CLD Materials	88
4.9. Poling Condition Summary for PSDA-AJL4 and 5	91
5.1. Electro-Optic Coefficients (r_{33}) at 1300 nm and 1550 nm.....	114
5.2. Material Properties of Multi-Angle Test Materials.....	121

ACKNOWLEDGMENTS

The author wishes to express appreciation to the faculty of the Department of Materials Science and Engineering for their sustaining encouragement.

The author especially thanks Professor Alex Jen for his assistance, patience, and sponsorship.

The author also acknowledges the members of the Jen Electro-Optics Research Group for their contributions, their exceptional willingness to cooperate and collaborate, and for the extraordinary level of teamwork needed to accomplish this project.

The constant and continuing encouragement and support from mentors, fellow research group members, family, and friends helped make this thesis possible.

Chapter 1: Introduction

1.1 Introduction

Organic nonlinear optical (NLO) materials have attracted an increasing amount of interest over the past decade. This interest in the optical electronic and photonic fields is due to their ability to transmit, process, and store information. Polymeric electro-optical materials have an exceptional bandwidth potential (up to 200 GHz) and low driving voltages (<1 V) in comparison to liquid crystalline, inorganic electro-optic, inorganic electro-absorptive, and inorganic modulated laser materials. Devices made from NLO materials offer versatility, large NLO response, ease of processing, and the possibility of tailoring the physical and chemical properties through molecular engineering. The rapid growth of digital communication devices has created an undeniable need for improved broadband communication technology.[1, 2] The continuing development of organic electro-optic (EO) polymer-based technology is necessary to accommodate future demands, which will depend on the availability of cheap, reliable, and robust optical waveguide devices for routing, switching, and detection. Optical interconnects, components, splitters, combiners, switches, tunable filters, and amplifiers are just a few examples of devices that can be improved through research and development in this field.[3-6]

1.2 Waveguide Devices

Optical waveguide devices are typically used to guide and channel light. They are the fundamental elements interconnecting various components of an optical integrated circuit. Waveguide devices confine and guide light by total internal reflection until it reaches the desired destination. Total internal reflection of light occurs when the light is at a critical angle of incidence, θ_c , and the angles where $\theta > \theta_c$. Under this condition the light rays that are incident on the front face of the waveguide will be trapped and guided through the material as shown in Figure 1.1.[7] Equation 1.1 represents the relationship between the critical angle and the indices of the core (n_1) and cladding layers (n_0).

$$\theta_c = \arcsin\left(\frac{n_0}{n_1}\right); \quad (1.1)$$

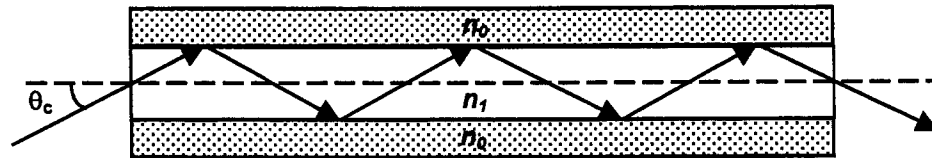


Figure 1.1. Principle of Total Internal Reflection [8]

With the invention of lasers and the development of coherent optics in the 1960s, the need arose for a long-distance transmission medium (optical fiber) and guiding structure with which to build optical components and connect them into optical circuits. Planar optical circuits have proven efficient and show many advantages in electronic circuits at all frequencies up to the microwave range. Planar fabrication and integration were required to develop planar optical waveguides in the form of films and strips.[5]

Waveguide devices can vary in geometry from planar, rectangular, and fibers as illustrated in Figure 1.2.

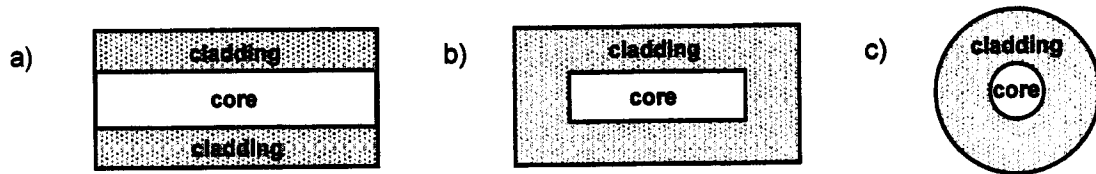


Figure 1.2. Waveguide Structures: a) rectangular slab waveguide, b) rectangular channel waveguide, c) optical fiber [8]

All the above structures consist of a core layer sandwiched or surrounded by a cladding layer. To meet the requirements of total internal reflection, the refractive index of the cladding layer must be less than that of the core layer. In a planar/slab waveguide the cladding layer is deposited onto a substrate, followed by the deposition of the core layer. Another cladding layer is then deposited to cover the core layer. This type of waveguide confines light in one direction. Rectangular waveguides and optical fibers confine light in two dimensions. Studies on these types of waveguides and their applications began in the mid-1960s by Schlosser and interest continues today. Since then, not only has the theory of wave propagation, excitation, and conjugation of optical films and strips advanced to encompass all aspects in the analysis and design of these guiding structures, but also precise and reliable technologies have been developed to fabricate planar optical waveguides and integrated optical circuits.[5, 9]

1.2.1 *Electro-Optic Modulator*

An electro-optic modulator encodes an electrical signal into an optical transmission as an amplitude modulation. Electro-optic modulation depends on the electro-optic effect, which causes the refractive index of certain materials to change with variations in the electric field applied to them. The electro-optic effect occurs when an intense light such as a laser changes the optical properties of a nonlinear optical material. These changes in turn affect the properties of the light beam as it propagates through the material. In the case of NLO polymers for waveguide applications, the refractive index changes with variations in the electric field.

1.2.2 *Mach-Zehnder Interferometer*

A Mach-Zehnder interferometer (MZ) is a typical electro-optic modulator for high-bandwidth optical communication systems. To be considered compatible with the high-speed electronics that drive the modulator, a small half-wave voltage (V_π) of less than 3 V is needed. The half-wave voltage is equal to the voltage needed to produce a π -phase shift of the signal. Improvement in link performance depends on decreasing V_π . The most effective approach to lowering V_π is to increase the electro-optic coefficient (r_{33}). Equation 1.2 illustrates this relationship for the Mach-Zehnder interferometer (MZ) with r_{33} . [10, 11]

$$V_\pi = \frac{\lambda h}{n^3 r_{33} L} \quad (1.2)$$

The other parameters in the above expression are defined as the optical wavelength (λ), which is 1.3 or 1.5 μm for telecommunications, the gap between electrodes (h), the refractive index (n), and the interaction length (L).[11]

Figure 1.3 illustrates a Mach-Zehnder interferometer. In this device the half-wave voltage is equal to the voltage needed to produce a π -phase shift of the signal split at the first Y-junction and cancels out at the second Y-junction, shown in Figure 1.3 (A). If an electric field is not applied, the signals split at the first Y-junction and will recombine into the original signal at the second Y-junction, Figure 1.3 (B).[12-14]

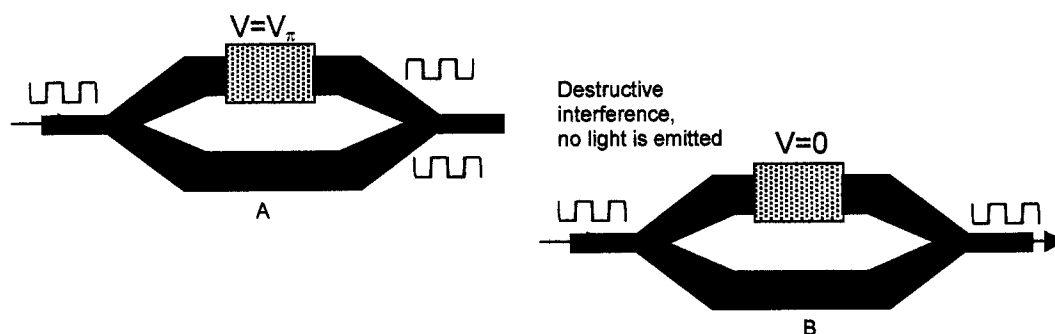


Figure 1.3. Illustration of a Mach-Zehnder Modulator

1.2.3 Performance Parameters

The translation of high molecular hyperpolarizability (β) values of organic chromophores into large macroscopic EO activities (r_{33}) for device-quality-polymers is a challenging task of this research. To obtain device-quality materials, several issues need to be addressed: the design and synthesis of high- $\mu\beta$ chromophores and realization of large macroscopic EO activity in the chromophore-incorporated polymers, and the

maintenance of long-term temporal stability in the EO response of the poled materials in addition to their high intrinsic stability toward the environment such as heat, light, oxygen, moisture, and chemicals.[1, 2] Minimizing optical loss is also an important parameter in the design and processing of materials and for the fabrication and integration of devices. Devices are expected to last approximately 10 years with a minimum thermal stability requirement of no significant change in performance for 1000 hours at 85°C.[1, 2] Photochemical stability is another important parameter. It is necessary to shield electro-optic materials from visible wavelength light. Simple packaging that minimizes oxygen concentration and exposure to visible wavelength light appears to address the problem of photostability sufficiently enough to permit commercial application; however, this matter needs to be continuously studied for each EO material.[1] Another need is to avoid induced chemical reactions and decomposition of the EO polymers.

In addition to stability, EO devices need low optical loss and a clad/core index match. The total EO device insertion loss must be of the order of 5 dB or less. This type of loss has two components: silica optical fiber to EO waveguide coupling loss and EO waveguide loss. Coupling loss is kept to 1 dB or less per connection.[1] EO waveguide loss, which is comprised of both absorption and scattering loss, should be ~ 1 dB/cm or less.[1, 15] Material loss can be limited to the electrical and optical interaction (device electrode) length to a few cm. V_π also depends on interaction length. Bandwidth, drive voltage, and optical loss are not independent issues.

Modulators made from polymeric nonlinear optical materials provide many benefits over conventional inorganic crystals such as lithium niobate (LiNbO_3). The small difference between the refractive index and the square root of the dielectric constant is the main

advantage NLO materials. The refractive index and dielectric constant are determined by the π -electrons, and both properties are relatively independent of frequency. This means that optical and long wavelength (radiowave, microwave, and millimeter wave) fields propagate at the same velocity, permitting exploitation of long interaction lengths. Materials with large dielectric constants, such as lithium niobate, lead to significant velocity mismatch between optical and low-frequency fields, which results in bandwidth and/or drive-voltage limitations. The large dielectrics also lead to power dissipation.[1, 10] As the difference between these two variables decreases, device power consumption decreases and speed of operation increases. Equation 1.3 illustrates the relationship between the bandwidth of a device (Δf) and interaction length (L), the speed of light (c), the refractive index (n), and dielectric constant (ϵ).[3]

$$\Delta fL = \left| \frac{c}{\sqrt{\epsilon} - n} \right| \quad (1.3)$$

Equation 1.3 demonstrates that device performance is significantly improved by decreasing the dielectric constant. If all other variables are equal, the product of the bandwidth and the interaction length (ΔfL) of lithium niobate is 10 GHz-cm due to its high dielectric constant, while an efficient electro-optic polymer's ΔfL would be 200 GHz-cm, providing the electro-optic polymer a considerable advantage over the inorganic materials used today.[3] Broadband transparency, low absorption, low cost, ease of processing, and synthesis modifications are also benefits of EO polymers.[12]

Table 1.1 summarizes several important properties for both organic and inorganic materials. The electro-optic coefficient (r_{33}) listed below in Table 1.1 represents the

amount of electro-optic activity in a material and is an important parameter in describing the performance of an electro-optic modulator.

Table 1.1. Summary of Material Properties [3, 11, 12]

Material Property	EO Polymers	Lithium Niobate
r_{33} (pm/V) _{@ 1.3μm}	>300	31
Dielectric Constant (ϵ)	2.5–4	28
Refractive Index (n)	1.6–1.7	2.2
Optical Loss (dB/cm) _{1.3μm}	0.7-1.1	0.2
Bandwidth-Length Product (ΔfL)	>200	10
Thermal Stability ($^{\circ}$ C)	85	90
V_{π} (V)	1-3	5-10

Device feasibility is determined by the r_{33} values in combination with the above properties.

1.3 Motivation

Rapid growth in broadband communication has created the need for improved broadband communication technologies. Polymer electro-optic modulators provide the possibility for increased transmission speed. However, current materials lack the ability to realize large macroscopic EO activity in the chromophore-incorporated polymers that simultaneously maintain long-term stability toward the environment including heat, light, oxygen, moisture, and chemicals. Presently, the crosslinking processes necessary for long-term stability severely limit the EO activity. Exploration of a range of novel materials is necessary to achieve the large macroscopic EO activity in device-quality-polymers.

Chromophore-incorporated polymers have several limitations in the realization of large electro-optic coefficients. The electric field poling of chromophore-doped polymers is restricted by the chromophore–chromophore electrostatic interactions and the interactions between the chromophore and the host matrix. If the number density is too high a competition occurs between the dipole-poling field and dipole–dipole interactions as shown by theoretical calculations.[12, 14, 16] Most systems have an optimum loading level past which the r_{33} value begins to decrease due to a competition between the dipole-poling field and dipole–dipole interactions. The intermolecular electrostatic interactions must be minimized to achieve a higher electro-optic coefficient. One efficient solution to achieve this goal is to manipulate the chromophore shape to isolate them from each other. Manipulating the chromophore design to a more spherical shape is an approach to take advantage of the site isolation effect and improve EO activity.

Unfortunately, a large EO activity and chromophore design are not the only variables that need to be optimized before a nonlinear optical polymer can be accepted as part of a device. In addition to having a high electro-optic coefficient, the material must also have thermal, chemical, and alignment stability and solvent resistance. The common approach to resolve these problems is to incorporate chromophores covalently into a polymer network and harden the matrix through crosslinking. However, in conventional NLO thermoset polymers the lattice-hardening process and poling occur simultaneously and create several undesirable results. The most important drawback is the “nonlinearity-stability tradeoff” where the full potential of the high optical nonlinearity in organic NLO materials is reduced to only 20–40%.[17] During the crosslinking process the chromophore mobility is limited and the chromophore is unable to orientate under the poling field, thus lowering the EO activity of the polymer. Another limitation of

conventional NLO thermoset polymers is the crosslinking temperature, which is usually much higher than the poling temperature. This can result in chromophore decomposition, sublimation, and/or dielectric breakdown. Overcoming this nonlinearity–stability tradeoff requires a poling process that allows the high rotational freedom of the chromophores. Ideally, this process should be prior to and separated from the lattice hardening process.

1.4 Scope of Research

The scope of this research was to create novel device-quality materials. This process focused on the development of structure property relationships based on the observed material behavior during the characterization process, which involved working with chemists to optimize the chromophore shape, size, conformation, sequence, or functionality of materials in the nanoscale range to improve poling efficiency and stability. Once a material was characterized on the small scale it needed to be translated into a usable device. The following chapters will review the theory and current status of molecular hyperpolarizability and electro-optic activity development, experimental techniques used for electro-optic characterization, and the experimental progress that occurred within the parameters of this research group.

Translating the high molecular hyperpolarizability (β) values of organic chromophores into large electro-optic coefficient (r_{33}) device-quality polymers is one of the most challenging tasks in electro-optic polymer research. The Jen/Dalton research group at the University of Washington has employed innovative nanoscale architectural control

approaches to dramatically improve the performance of the nonlinear optical polymers. The ability to control several critical design parameters, such as size, shape, surface chemistry, flexibility, and topology, has shaped the exploration of a range of novel materials.

This thesis will introduce the effects on poling efficiency and stability for several design approaches that the University of Washington research team has used to improve the performance of the nonlinear optical polymer through nanoscale architectural control. We studied the basic rigid rod-chromophore guest–host systems with no covalent bonds between the chromophore and the polymer host and also side-chain polymer systems consisting of chromophores covalently bonded to the polymer backbone. Extensive characterization research looked at the effects of manipulating chromophore shape by surrounding it with bulky, inert substituents to make the chromophore more spherical. This type of design provides many advantages for the improvement of electro-optic polymers. In general, this globular geometry is referred to as dendrimers. Dendrimers form a class of new macromolecular structures that have a well-defined structure and branching at each repeat unit.[5] An outer shell composed of fluorinated groups improves compatibility with the host material and poling.

The most effective way to prevent the relaxation of the aligned chromophores is to put them in a crosslinkable system. Typically, the chromophores are aligned and then are crosslinked to the polymer backbone or each other. Though crosslinked systems offer the advantages of solvent resistance and high thermal and temporal stability, they also have the drawback of low poling efficiency and increased optical loss.[18, 19] This research also discusses in detail recent novel work to optimize the poling efficiency and

crosslinking relationship. The focal point of this work was the Diels Alder reaction, which allows for high poling efficiency with long-term stability, eliminating the typical tradeoff between the two properties. This crosslinking reaction maintains the poling efficiency and the material gains solvent resistance that makes it feasible for multilayer device fabrication. Initial results indicate that such materials are promising candidates for device-quality materials.

Notes to Chapter 1:

1. Dalton, L.R., *Rational design of organic electro-optic materials*. Journal of Physics: Condensed Matter, 2003. **15**: p. R897-R934.
2. Kajzar, F., K.-S. Lee, and A.K.-Y. Jen, *Polymeric materials and their orientation techniques for second-order nonlinear optics*. Advances in Polymer Science, 2003. **161**: p. 1-85.
3. Kuzyk, M.G. and C.W. Dirk, *Characterization Techniques and Tabulations for Organic Nonlinear Optical Materials*. 1998, New York: Marcel Dekker, Inc.
4. Bosshard, C.H., K. Sutter, Ph. Pretre, J. Hulliger, M. Florsheimer, P. Kaatz, and P. Gunter, *Organic Nonlinear Optical Materials*. 1995, New York: Taylor & Francis.
5. Ma, H., A.K.-Y. Jen, and L. Dalton, *Polymer-based optical waveguide materials, processing, and devices*. Advanced Materials, 2002. **14**(19): p. 1339-1365.
6. Eldada, L., *Advances in telecom and datacom optical components*. Optical Engineering, 2001. **40**(7): p. 1165-1178.
7. Heavens, O.S. and R.W. Ditchburn, *Insight into Optics*. 1991, New York: Wiley and Sons.
8. Wong, S., *Design, synthesis, and characterization of novel perfluorocyclobutyl (PFCB) aromatic ether polymers for optical waveguide applications*, in *Materials Science and Engineering*. 2003, University of Washington: Seattle.
9. Unger, H.G., *Planar Optical Waveguides and Fibres*. 1977, Oxford: Clarendon Press.
10. Chen, A.T., et al., *DC biased electro-optic polymer waveguide modulators with low half-wave voltage and high thermal stability*. Optical Engineering, 1999. **38**(12): p. 2000-2008.
11. Shi, Y.Q., et al., *Low (sub-1-volt) halfwave voltage polymeric electro-optic modulators achieved by controlling chromophore shape*. Science, 2000. **288**(5463): p. 119-122.
12. Dalton, L.R., *Nonlinear optical polymeric materials*. Advances in Polymer Science, 2002. **158**: p. 1-86.
13. Hecht, J., *WDM Solutions*, 2001: p. 100-104.
14. Dalton, L.R., et al., *From molecules to opto-chips: organic electro-optic materials*. Journal of Materials Chemistry, 1999. **9**: p. 1905-1920.

15. Zhou, M., *Low-loss polymeric materials for passive waveguide components in fiber optical telecommunication*. Optical Engineering, 2002. **41**(7): p. 1631-1643.
16. Burland, D.M., R. Miller, and C. Walsh, *Second-order nonlinearity in poled-polymer systems*. Chemical Review, 1994. **94**: p. 31-75.
17. Luo, J.D., et al., *Nanoscale architectural control and macromolecular engineering of nonlinear optical dendrimers and polymers for electro-optics*. Journal Of Physical Chemistry B, 2004. **108**(25): p. 8523-8530.
18. Ma, H., et al., *Highly efficient and thermally stable electro-optical dendrimers for photonics*. Advanced Functional Materials, 2002. **12**(9): p. 565-574.
19. Zhang, C., et al., *Electric poling and relaxation of thermoset polyurethane second-order nonlinear optical materials: role of cross-linking and monomer rigidity*. Macromolecules, 2001. **34**(2): p. 235-243.

Chapter 2: Background

2.1 Nonlinear Optical Effect

The nonlinear optical effect originates from the nonlinear response of a material to an electric field. Nonlinear optical properties arise from the ability of the molecules and atoms to change their polarization in a nonlinear manner under an electric field (E). Interactions with an intense light in such a medium cause a charge displacement resulting in an induced dipole moment or molecular polarization (p).

2.1.1 Microscopic Polarization

Molecular polarization (p) is the result of a charge displacement that produces an induced dipole moment by the interactions of an intense light in a nonlinear optical media. This molecular process works well within an organic crystal or solid polymer since they are generally nonconductive and nonmagnetic, thus restricting the electron motion to within the atomic and molecular orbitals. Equation 2.1 [1] demonstrates the relationship of molecular polarization (p) to the electric field of a light wave.

$$p = \alpha E + \beta EE + \gamma EEE \dots \quad (2.1)$$

Where α is the linear polarizability, β is the first-order hyperpolarizability, γ is the second-order hyperpolarizability, and E is the electric field. A second-order nonlinear optical response requires a noncentrosymmetric material with different electronic properties at

each end of the molecule. Nonlinear optical chromophores are an example of a noncentrosymmetric material.

2.1.1.1 Molecular design

Engineering highly efficient nonlinear optical polymers requires a clear understanding of the atomic bonding properties. The design of organic materials begins with the assumption that intermolecular bonding interactions are much weaker than intramolecular activity. The molecules are thought to function independently of each other and only their net orientations are important to the contribution of the macroscopic properties. This method is known as the oriented gas model and is discussed in section 2.1.2.2 below.

The intramolecular bonding in this research was primarily composed of two types of bonds: 1) a covalent σ -bond ($C_{sp^3}-C_{sp^3}$), which is spatially confined along the internuclear axis of the carbon-carbon bond; and 2) covalent π -bonds, which are regions of delocalized electronic charge distribution above and below the interatomic axis. The two differ considerably in the localization of electron charge density. The delocalization of the π -bonds allows the electron density to be more mobile than the σ -bonds. The extent of this redistribution is measured by the dipole moment, and the ease of redistribution in response to an externally applied electric field is the hyperpolarizability (β). Virtually all nonlinear optical organic molecules exhibit π -bond formations between various nuclei.[2]

The optical nonlinearity or hyperpolarizability (β) of organic molecules has been enhanced by either adding conjugated bonds or by substituting donors and acceptors. The addition of the appropriate functionality at the end of the π system can improve the asymmetric electronic distribution in either or both the ground state and excited state configurations. Functional groups are divided into two categories based on their ability to accept or donate electrons into the π system.[2] Chromophores, for example, are noncentrosymmetric molecules with a donor, π -electron bridge, and acceptor motif, shown in Figure 2.1.

Donor — π -Electron Bridge — Acceptor

Figure 2.1. Schematic of a Chromophore Design

Common donor groups are typified by amines and often have an available electron pair on the p-orbital. Acceptor groups usually are of the nitro, NO_2 , and nitrile, $-\text{C}\equiv\text{N}$ functionalities.[2] Figure 2.2 embodies this concept with a chromophore from our lab that has a tricyanovinyl (TCN) acceptor and an aniline donor. Increasing the effective conjugation length and/or enhancing the donor and acceptor strengths can also increase the optical nonlinearity of a molecule.

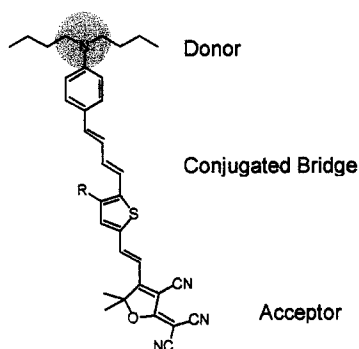


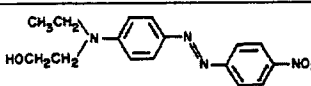
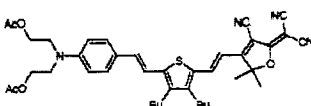
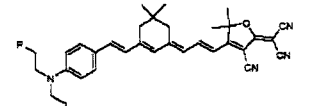
Figure 2.2. Representative Chromophore Structure

When an electric field is applied, an electron travels from the donor to the acceptor, demonstrating an asymmetric electronic response to the polarization. As mentioned earlier, the hyperpolarizability (β) is a measure of the ease of the electron redistribution in response to an applied electric field. A rough approximation of the hyperpolarizability can be made from the two-level model represented in equation 2.2. This model approximates the hyperpolarizability from the transition dipole (μ_{ge}), the difference between the dipole moments ground and excited states ($\mu_{ee}-\mu_{ge}$), and the change in the optical band gap (E_{ge}). [3, 4]

$$\beta = \frac{(\mu_{ee} - \mu_{gg})(\mu_{ge})^2}{(\Delta E_{ge})^2} \quad (2.2)$$

Table 1 illustrates a few representative chromophores developed over the past decade. The table demonstrates how chromophore design has improved the hyperpolarizability and electro-optic coefficient.

Table 2.1. $\mu\beta$ and r_{33} (pm/V)_{at 1300nm} of Representative NLO Chromophores.

NLO Chromophore	Properties
 DR1	$\mu\beta = 580 \cdot 10^{-48}$ esu $r_{33} = 13$ pm/V _{at 1300nm} (30 wt % in PMMA)
 FTC	$\mu\beta = 18000 \cdot 10^{-48}$ esu $r_{33} \sim 35$ pm/V _{at 1300nm} (20 wt % in PMMA)
 CLD	$\mu\beta = 35000 \cdot 10^{-48}$ esu $r_{33} \sim 50$ pm/V _{at 1300nm} (25 wt % in PMMA)

*Disperse Red 1 (DR1) [4-6], FTC [4, 6, 7], Chen-Larry-Dalton (CLD) [4, 6-8]

Hyperpolarizability has increased dramatically (580 versus $35000 \cdot 10^{-48}$ esu) with improvements in the chromophore design. These large nonlinearities were achieved by

combining heterocyclic conjugating units, such as thiophene, with tricyanovinyl acceptors or by employing an extended polyene π -bridge system with strong multicyano-containing heterocyclic electron acceptors.[6] For example, the increase in the hyperpolarizability in CLD from FTC was created by substituting the thiophene unit in FTC with a six-member ring. In the last five years, numerous variations on the FTC and CLD structures have further improved their hyperpolarizability and process-ability.

2.1.2 Macroscopic Polarization

The macroscopic polarization (P) can also be described analogously to the microscopic second-order polarization defined in equation 2.1. In this case, the value of the hyperpolarizability averaged over all orientations of the individual chromophores is P . The dielectric properties of the bulk medium with an externally applied electric field can similarly be described with linear and nonlinear susceptibilities (χ).[1, 9, 10] The macroscopic nonlinear polarization represents the bulk material's response to an electric field. This is the overall effect of how the charges in the material move.

$$P = \chi^{(1)}E + \chi^{(2)}EE... \quad (2.3)$$

The second-order nonlinear susceptibility ($\chi^{(2)}$) relates the square of the electric field strength to the polarization of the medium. For $\chi^{(2)}$ to be a contributing factor and for nonlinear polarization to exist the material must be noncentrosymmetric.

With organic materials, it is thought that intramolecular contributions from the atoms and molecules contribute to polarizability, which depends mainly on electron polarization in

the π -bonding orbitals. The intermolecular bonding (Van der Waals, dipole–dipole interactions, and hydrogen bonds) between these components is considered a secondary effect. In inorganics, with weakly polarizable atoms and complexes, intermolecular material bonding is dominant. Lattice vibrations occurring in a frequency range of typically 1 MHz up to 100 MHz play the primary role in polarizability, thus limiting their use in the higher frequency ranges.[2] Equation 2.4 demonstrates the macroscopic polarization's relationship to the dielectric constant (ϵ), the linear susceptibility (χ), the refractive index (n), electric field (E), and the total electric displacement field within a material (D).[9]

$$D = E + 4\pi P = (1 + 4\pi\chi)E \quad (2.4)$$

$$\frac{D}{E} = 1 + 4\pi\chi = n^2 = \epsilon$$

The dielectric constant and the refractive index are common parameters used to characterize the susceptibility of a material.[11]

2.1.2.1 Relationship between the electro-optic effect and the nonlinear optic effect

The electro-optic effect occurs when the optical properties of a material change in response to an applied electric field that varies slowly compared to the frequency of light. It is triggered from the ability of certain materials to change their refractive index with variations in the applied electric field. These changes in turn affect the properties of the light beam as it propagates through the material. The electro-optic coefficient (r_{33}) is

defined from a variation of the refractive index with the electric field in equation 2.5.[10, 12]

$$\frac{1}{n^2} - \frac{1}{n_o^2} = r_{33} E \quad (2.5)$$

In equation 2.5, n_o and n are defined as the refractive index before and after poling, respectively. The electro-optic coefficient (r_{33}) relationship between the change in refractive index and electric field is more commonly given as equation 2.6.[10]

$$\Delta n = \frac{1}{2} n^3 r_{33} E \quad (2.6)$$

$$\text{where } \Delta n = n_o - n$$

Based on the relationship of nonlinear optics and electro-optics, a direct connection between the EO coefficient and the second-order nonlinear optical susceptibility can be determined, equations 2.7 to 2.11.[2, 10]

$$n_o^2 = 1 + 4\pi\chi^{(1)} \quad (2.7)$$

Based on equation 2.4 and 2.6.

$$n^2 = 1 + 4\pi(\chi^{(1)} + 2\chi^{(2)} E) \quad (2.8)$$

then

$$n^2 - n_o^2 = 8\pi\chi^{(2)} E \quad (2.9)$$

$$\Delta n = \frac{4\pi}{n_o} \chi^{(2)} E \quad (2.10)$$

Equating equation 2.10 with 2.6 gives equation 2.11

$$r_{33} = \frac{\chi^{(2)} 8\pi}{n^4} \quad (2.11)$$

Nonlinear optics and electro-optics are related through equation 2.11. The second-order nonlinear susceptibility quantifies the bulk materials response to an electric field. As the

susceptibility increases, the change in refractive index increases, thus increasing the electro-optic coefficient.

2.1.2.2 Orientated gas model

The noncentrosymmetry needed for $\chi^{(2)}$ to be a contributing factor and for nonlinear polarization to exist is normally achieved through poling. The oriented gas model is often used to describe the theory of poling. The orientated gas model treats the individual chromophores as independent entities from the surrounding polymer matrix. The validity of this theory rests on the much weaker intermolecular interactions in polymer systems compared to intramolecular systems. We can thus think of bulk properties as being built up from the corresponding properties of individual molecules. The change in charge distribution will alter the velocity of light propagating through the material. If the chromophores are randomly oriented, the influence of the individual chromophores will be canceled out as light propagates through the material. If all the chromophores are pointing in the same direction as the applied field, the effect of individual chromophores will be additive.[4, 13]

This model shows that the bulk properties are an accumulation of the microscopic properties, and the bulk electro-optic coefficient is often represented by equation 2.12.

[4]

$$r_{33} = \frac{|2Nf(\omega)\beta \langle \cos^3 \theta \rangle|}{n^4} \quad (2.12)$$

In equation 2.12 the electro-optic coefficient is a result of the number density (N), the local field factors ($f(\omega)$), the hyperpolarizability (β), the refractive index (n), and the order parameter $\langle \cos^3 \theta \rangle$. [10] The number density (N) is the number of molecules per unit volume. The local field factors, number density, hyperpolarizability, and order parameter are related to the nonlinear susceptibility by equation 2.13. The quantity 'F' represents all field effects. [3]

$$\chi^{(2)} = NF\beta \langle \cos^3 \theta \rangle \quad (2.13)$$

Based on these equations, r_{33} should increase linearly by increasing N, β , or the order parameter $\langle \cos^3 \theta \rangle$. However, given the information introduced in table 1.1, other contributions affect the bulk properties since r_{33} only increased by 3 while $\mu\beta$ for the same chromophores increased by 60.

2.2 Poling Process

The concept of poling is essentially inducing polar order through the application of an electric field. Figure 2.3 illustrates the poling process with the chromophores represented by one-dimensional (dipole) vectors. The poling process begins with a thin polymer film containing solute molecules (chromophores) in a host-polymer matrix. At room temperature the chromophores are randomly oriented throughout the glassy polymer matrix. After heating to a temperature close to the glass transition temperature of the polymer matrix, the chromophores become mobile. When an electric field is applied, the chromophores correspondingly align their dipoles. The sample is then

cooled with the electric field applied, freezing the chromophores into their aligned orientation.

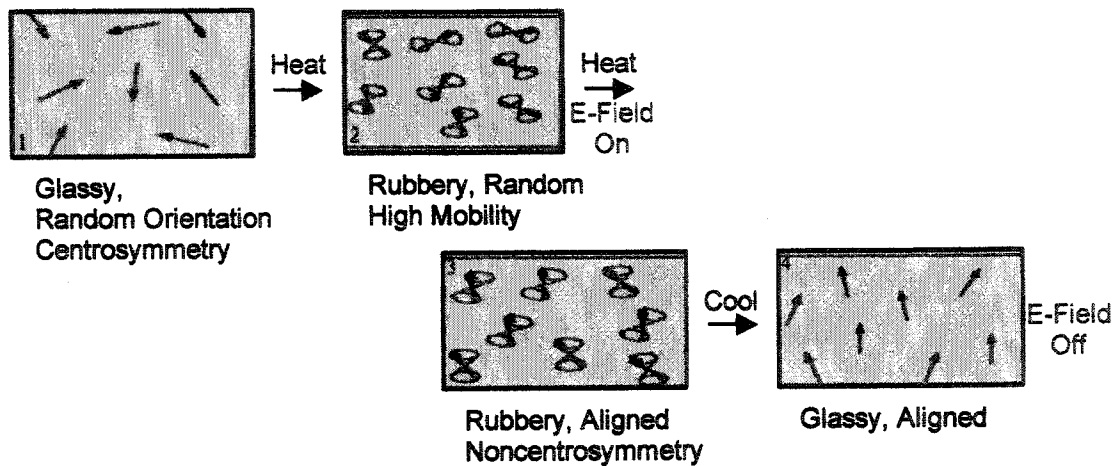


Figure 2.3. Poling Process [1]

At first glance this process seems straightforward: heat the material up and apply an electric field. However, several factors limit the poling process. One major difficulty of poling is dielectric breakdowns caused by film defects, inclusions (voids, impurities, or micro-cracks), thin film morphology, concentration distribution, uneven film thickness, substrate cleanliness, or polymer additives. Dielectric breakdowns can destroy the sample by creating pinhole damage from singular electrical discharges, thus rendering the sample unacceptable for integrated devices or further characterization. Besides material problems, poling dynamics within the material also place limitations on achieving polar order on the microscopic level.

2.2.1 Poling Dynamics

A general approach to describe the poling dynamics of a material is based on equation 2.12. Each parameter to the equation contributes to the overall poling efficiency. The quantity $\langle \cos^3 \theta \rangle$, which represents the amount of polar order, is described in equation 2.14 where the dipole moment is (μ), the temperature in Kelvin is (T), Boltzman's constant is (k), and the electric field felt by the chromophore during poling is (F).[14]

$$\langle \cos^3 \theta \rangle = \frac{\mu F}{5kT}, \quad F = f(0)E_p \quad (2.14)$$

Balancing the tradeoff between the temperature, electric field, and dielectric breakdown is one of the keys to a high poling efficiency and electrode damage prevention. If all other contributions are neglected, the order parameter should increase linearly with the applied electric field (E_p).

The maximum number density (N_{\max}) is also approximated by Boltzman's constant, temperature, and the dipole moment of the chromophore. Equation 2.15 reveals that the stronger the dipole moment, the lower the maximum number density due to electrostatic interactions that can easily saturate N. [14]

$$N_{\max} \approx \left(\frac{kT}{\mu^2} \right) \quad (2.15)$$

Because a high r_{33} is dependent on a high N and order parameter, an approach is needed to reduce the electrostatic interactions that prevent high poling fields and loading densities. When low loading levels are used, the chromophores are isolated from each other, which reduces dielectric breakdowns and allows application of higher electric fields. A requirement is a chromophore design that avoids using extremely low loading levels with high $\mu\beta$ chromophores.

2.2.2 Poling Techniques

Inducing polar order with an applied electric field can be accomplished in a variety of ways. The most common methods of poling are corona and contact poling. In both cases a DC electric field is applied to the polymer at a temperature where the chromophores' dipoles can be readily oriented. In most instances, the largest possible electric field is used for poling to obtain the highest degree of polar order. The thin polymer film is usually sandwiched between two parallel conducting plates, in which case the polar axis is perpendicular to the film's plane. Figure 2.4 shows a schematic of the setup for both a contact (a) and corona (b) poled sample.

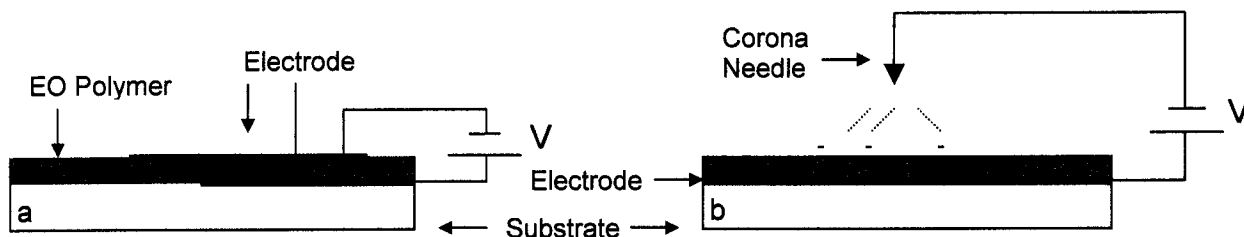


Figure 2.4. Contact (a) and Corona (b) Poling Sample Schematics

In the event of contact poling the electric field is applied through an electrode directly on top of the polymer film. Contact poling usually provides a more evenly poled sample than does corona poling. Corona poling entails two electrodes, one with a shape causing a significantly greater electric field at its surface than that between the electrodes. Typically a sharp needle, wire, or grid is charged with several kilovolts until an electrical discharge ionizes the surrounding atmosphere. Depending on the polarity of the corona needle, either positive or negative ions can be deposited on the surface of the polymer film. With a corona needle the degree of poling decreases outward in a radial fashion.

2.2.3 Poling Parameters

Efficient poling plays an important role in the resulting r_{33} value of a chromophore polymer system. If an electronic breakdown occurs in the material due to excessively high field strength, material impurity or electrode processing pinholes can form. Pinhole formation in the film can substantially reduce the magnitude of the field that can be applied. Increasing the electric field in increments over periodic time intervals or applying the voltage at a low temperature can reduce this problem. Figure 2.5 (a) represents experimental poling data with the voltage applied stepwise and monitoring of the current in the sample to prevent electronic breakdown. Figure 2.6 (b) illustrates experimental poling data for a sample that had 80% of the voltage applied at room temperature, while the temperature was ramped at a constant rate. In this case the final 10% of the applied voltage was added at the desired poling temperature.

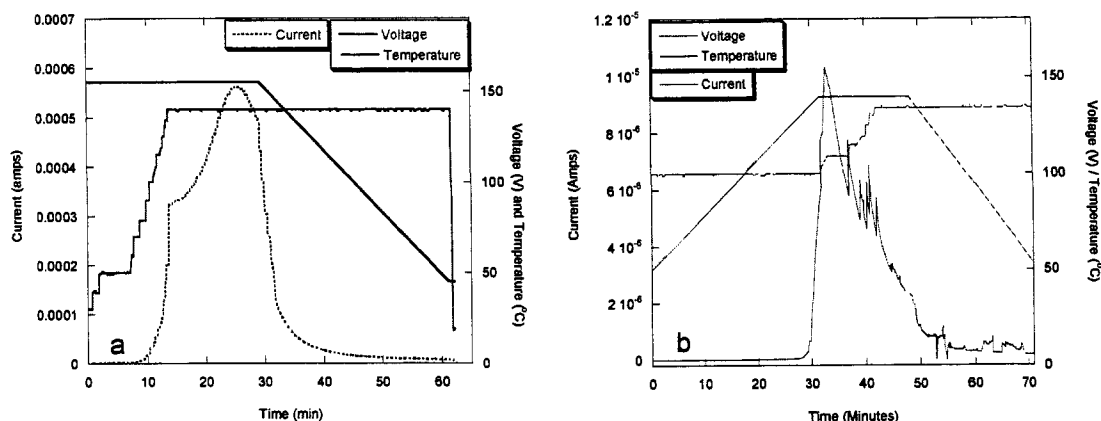


Figure 2.5. Experimental Poling Data

The optimized poling method varies from material to material, and several styles should be tried when characterizing a new material. In both corona and contact poling, the poling temperature, and time are critical to the resulting degree of polar order. The time needed to pole a sample is system dependent. In general, a guest host system can be poled fairly quickly, while side-chain, cross-linkable, and dendrimer systems may require an extremely long time to orient large bulky shapes and/or to crosslink the system. Figure 2.5 (a) is representative of a side-chain system that needed 15 minutes to align before cooling. Slight poling temperature and time changes can be significant. Poling at temperatures above or below the ideal poling temperature can notably lower the r_{33} value or cause damage to the sample as shown experimentally in Figure 2.6.

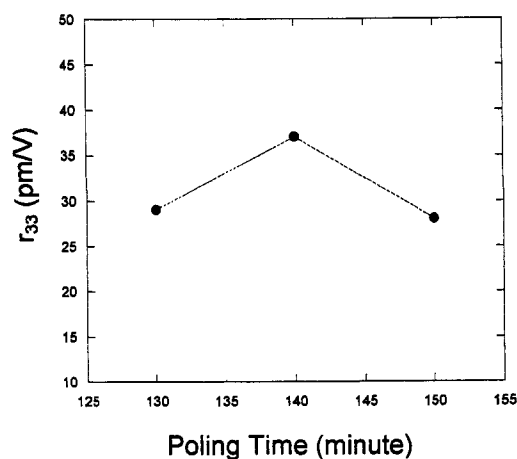


Figure 2.6. r_{33} Versus Temperature Graph

The guest host material in Figure 2.6 experienced an increase of 7 pm/V at the optimized poling temperature opposed to the temperatures above and below it. At a temperature below the optimized temperature the polymer host may not be rubbery, in turn lowering the chromophore mobility. At temperatures above the determined poling temperature the r_{33} value might be lowered due to pinhole damage or chromophore decomposition. The experimental electro-optic coefficient data in Figure 2.7 demonstrates the relationships between the poling time (a), electric field (b), and r_{33} .

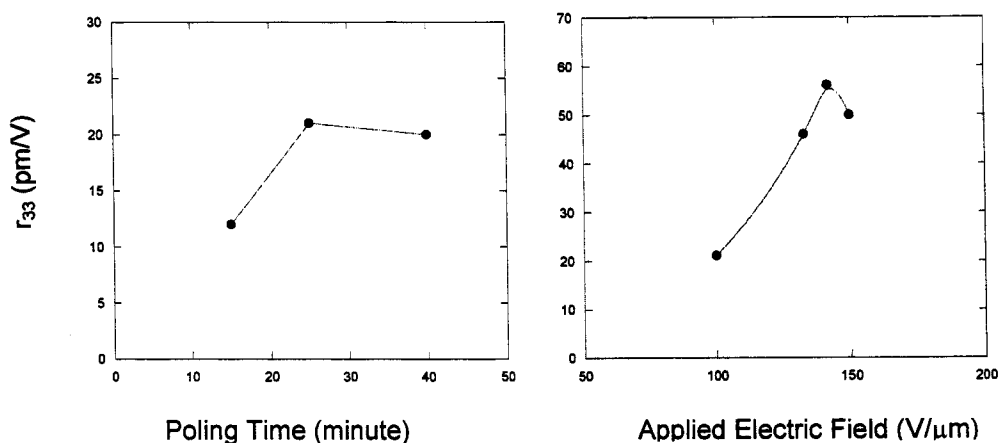


Figure 2.7. Experimental Electro-Optic Coefficient Data

The optimum poling condition of the material in Figure 2.7 was 25 minutes with an applied field of $142 \text{ V}/\mu\text{m}$. By conducting a series of experiments where one parameter was changed and the other two parameters were held constant, we found the optimized poling condition. These data illustrate the importance of optimizing each parameter to achieve the highest degree of polar order. In this case the electro-optic coefficient increased from 12 to 56 pm/V .

Unfortunately, efficient poling is not the only variable that must be optimized for a nonlinear optical polymer to be accepted as part of a device. In addition to having a high electro-optic coefficient, the material must also have thermal, chemical, and alignment stability. Developing device-quality-polymer systems also depends on the chromophore structure.

2.2.4 Shape Engineering

Efficient poling is extremely important for achieving higher EO coefficients. Manipulating the various poling parameters has an enormous impact on the resulting r_{33} value. Our initial hypothesis inferred that the higher the number density of a polymer system the more attractive the result in terms of a higher r_{33} value. Unfortunately, due to the high $\mu\beta$ of the chromophores, the electrostatic interaction played a much larger role than was first thought. Figure 2.8 demonstrates through theoretical calculations that a maximum number density exists for each polymer system.[4, 15] If the number density is too high, a competition occurs between the dipole-poling field and dipole–dipole interactions. To achieve a higher electro-optic coefficient, the intermolecular electrostatic interactions

must be minimized. One efficient solution is to manipulate the chromophore shape.[4, 13, 15]

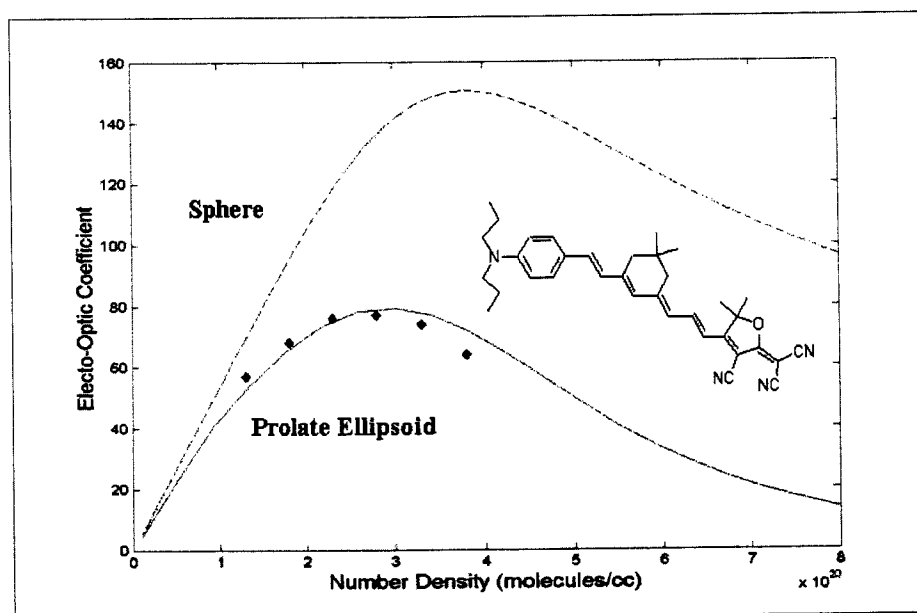


Figure 2.8. Electro-Optic Coefficient versus Number Density [14]

In the above-mentioned study by Dalton et al, shown in Figure 2.8, the theoretical r_{33} value doubled with a spherical shape and was compared to an elliptical one. The site isolation method employed by the Jen/Dalton research groups at the University of Washington manipulates the chromophore shape by surrounding it with bulky inert substituents in a way that makes the chromophore more spherical. This site isolation effect minimizes the intermolecular electrostatic interactions and increases the typical solubility limit of guest molecules in the host matrix.[6, 14-17] This theory in combination with improvements in the ability to synthetically control several critical design parameters, such as size, shape, surface chemistry, flexibility, and topology, has shaped the

exploration of a range of novel materials. Fine tuning the macromolecular architecture of the EO polymers has provided materials ranging from a prolate ellipsoid, to a flattened sphere, an umbrella, a cylinder, and a variety of 3-D shaped dendritic chromophores. [18]

2.2.5 *Electro-Optic Polymer Systems*

Several types of electro-optic polymer systems are commonly used. Three stringent issues must be addressed for device-quality materials: 1) the design and synthesis of high $\mu\beta$ chromophores, 2) the maintenance of long-term temporal stability plus stability toward the environment such as heat, light, oxygen, moisture, and chemicals, and 3) the minimization of optical loss.[6] The most common polymer system is the guest host, where chromophores are doped into host material at weight percentages that range from 5% to 30%. Other typical material systems include side chain, crosslinkable, and dendritic. As expected, each system has advantages and disadvantages.

Chromophore guest–host systems have no covalent bonds between the chromophore and the polymer host. The π -electron orbital interaction inhibits chromophores from bending and twisting extensively, so we can generally consider these to be considered relatively stiff (rigid) objects. Since guest–host systems are not tethered to the host lattice, sublimation at high processing temperatures is a common problem for practical device applications. The effects of increasing the effective conjugation length and/or enhancing the donor and acceptor strengths on the basic rigid rod chromophore in guest–host systems have been extensively studied.[14]

Side-chain polymer systems consist of chromophores covalently bonded to the polymer backbone. Compared to guest–host systems, the side-chain polymer can provide higher chromophore loading densities and improved temporal and thermal stability of the aligned NLO chromophores.[18]

The most effective way to prevent the relaxation of the aligned chromophores is to put them in a crosslinkable system. Typically, the chromophores are aligned first or simultaneously to the crosslinking process. Depending on the material, the polymer backbone may be crosslinked to itself or to the chromophores, or the chromophores could crosslink together. Though crosslinked systems offer the advantages of solvent resistance and high thermal and temporal stability, they also have the drawback of low poling efficiency and increased optical loss.[19] Luo *et al.*[20] have recently achieved novel work in optimizing the poling efficiency and crosslinking relationship, which will be discussed at length in Chapter 4.

One method for manipulating chromophore shape is to surround the chromophore with bulky inert substituents in a way that makes the chromophore more spherical. This type of design provides many advantages for the improvement of electro-optic polymers. The globular geometry of dendrimers is also well suited for modifying chromophores to the ideal spherical shape.[18] Dendrimers form a class of new macromolecular structures that have a well-defined structure and branching at each repeat unit. The dendronic polymer's outer shell is composed of fluorinated groups. The addition of the fluorinated groups not only makes the polymer more spherical, it also imparts high solubility and low viscosity for the materials.[6] The fluorinated group may also contribute to improved

electro-optic activity with the reduction of the chromophore and host-polymer interactions. Fluorinated polymers form a nanodomain with less attracting force to the host polymer than in the guest host system. This nanodomain also benefits poling efficiency by improving rotational mobility.

Chapter 4 extensively discusses the effects of an assortment of dendrimer modifications in guest host, side chain, and crosslinkability of polymeric EO materials. Figure 2.9 represents a schematic multifunctional dendrimer with the center core connected to NLO chromophores.

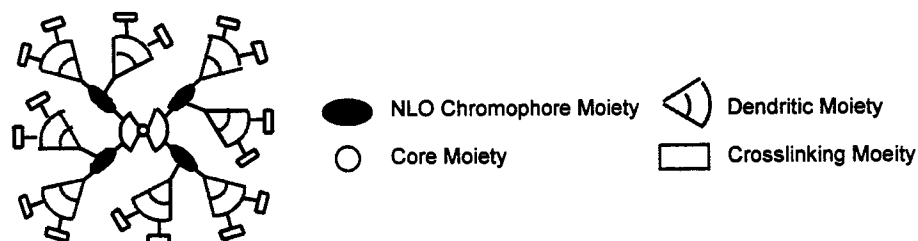


Figure 2.9. Schematic of the Dendrimer Structure

Notes to Chapter 2:

1. Kuzyk, M.G. and C.W. Dirk, *Characterization Techniques and Tabulations for Organic Nonlinear Optical Materials*. 1998, New York: Marcel Dekker, Inc.
2. Bosshard, C.H., K. Sutter, Ph. Pretre, J. Hulliger, M. Florsheimer, P. Kaatz, and P. Gunter, *Organic Nonlinear Optical Materials*. 1995, New York: Taylor & Francis.
3. Dalton, L.R., et al., *Synthesis and processing of improved organic second-order nonlinear optical materials for applications in photonics*. Chemistry of Materials, 1995. 7: p. 1060-1081.
4. Dalton, L.R., *Nonlinear optical polymeric materials*. Advances in Polymer Science, 2002. 158: p. 1-86.
5. Singer, K.D., M.G. Kuzyk, and J.E. Sohn, *2nd-Order nonlinear-optical processes in orientationally ordered materials - relationship between molecular and macroscopic properties*. Journal of the Optical Society of America B-Optical Physics, 1987. 4(6): p. 968-976.
6. Ma, H., A.K.-Y. Jen, and L. Dalton, *Polymer-based optical waveguide materials, processing, and devices*. Advanced Materials, 2002. 14(19): p. 1339-1365.
7. Zhang, C., et al., *Low V electrooptic modulators from CLD-1: chromophore design and synthesis, material processing, and characterization*. Chem. Mater., 2001. 13(9): p. 3043-3050.
8. Grote, J.G., et al., *Effect of conductivity and dielectric constant on the modulation voltage for optoelectronic devices based on nonlinear optical polymers*. Optical Engineering, 2001. 40(11): p. 2464-2473.
9. Marder, S.R., J.E. Sohn, and G.D. Stucky, *Materials for Nonlinear Optics: Chemical Perspectives*. ACS Symposium Series 455. 1991, Washington D.C.
10. Prasad, P. and D.J. Williams, *Introduction to Nonlinear Optical Effects in Molecules and Polymers*. 1991, Hoboken: Wiley-Interscience.
11. Page, R.H., et al., *Electrochromic and optical wave-guide studies of corona-poled electrooptic polymer-films*. Journal of the Optical Society of America B-Optical Physics, 1990. 7(7): p. 1239-1250.
12. Aillerie, M., N. Theofanous, and M.D. Fontana, *Measurement of the electro-optic coefficients: description and comparison of the experimental techniques*. Applied Physics B-Lasers and Optics, 2000. 70(3): p. 317-334.

13. Burland, D.M., R. Miller, and C. Walsh, *Second-order nonlinearity in poled-polymer systems*. Chemical Review, 1994. **94**: p. 31-75.
14. Dalton, L.R., *Rational design of organic electro-optic materials*. Journal of Physics: Condensed Matter, 2003. **15**: p. R897-R934.
15. Dalton, L.R., et al., *From molecules to opto-chips: organic electro-optic materials*. Journal of Materials Chemistry, 1999. **9**: p. 1905-1920.
16. Luo, J.D., et al., *Design, synthesis, and properties of highly efficient side-chain dendronized nonlinear optical polymers for electro-optics*. Advanced Materials, 2002. **14**(23): p. 1763-1768.
17. Robinson, B.H. and L.R. Dalton, *Monte Carlo statistical mechanical simulations of the competition of intermolecular electrostatic and poling-field interactions in defining macroscopic electro-optic activity for organic chromophore/polymer materials*. Journal of Physical Chemistry A, 2000. **104**(20): p. 4785-4795.
18. Luo, J.D., et al., *Nanoscale architectural control and macromolecular engineering of nonlinear optical dendrimers and polymers for electro-optics*. Journal of Physical Chemistry B, 2004. **108**(25): p. 8523-8530.
19. Kajzar, F., K.-S. Lee, and A.K.-Y. Jen, *Polymeric materials and their orientation techniques for second-order nonlinear optics*. Advances in Polymer Science, 2003. **161**: p. 1-85.
20. Luo, J.D., et al., *Highly efficient and thermally stable electro-optic polymer from a smartly controlled crosslinking process*. Advanced Materials, 2003. **15**(19): p. 1635-+.

Chapter 3. Experimental Approach

3.1 Introduction

Nonlinear optical characterization techniques fall into two categories: microscopic and macroscopic. The microscopic techniques experimentally determine the first-order hyperpolarizability (β) for a chromophore. Two common techniques are Hyper-Rayleigh scattering (HRS) and electric field-induced second-harmonic generation (EFISH). The macroscopic second-order nonlinear susceptibility ($\chi^{(2)}$) is usually experimentally determined by a second-harmonic generation (SHG) signal through the marker fringe technique. The electro-optic coefficient (r_{33}) may also be experimentally measured by several techniques that will be discussed in section 3.3.

3.2 Microscopic Measurements

Hyper-Rayleigh scattering (HRS) experimentally determines β by measuring the amount of light incoherently scattered at exactly twice the frequency of an intense incident laser beam by molecules randomly orientated in a dilute solution. The signal arises from a random fluctuation in the density and orientation of the chromophores. HRS can measure molecules with a permanent dipole moment (noncentrosymmetry) and with an octupolar moment (centrosymmetry) because it does not use an externally applied electric field. HRS can acquire β directly and has a less complicated apparatus than does EFISH. The main drawback of HRS is a weak signal.[1-4]

The electric field-induced second-harmonic generation technique determines the second-order nonlinear optical response of molecules. An applied electric field aligns the dipole moments of the nonlinear optical chromophores to remove the inversion symmetry from the solution. This results in an acentrosymmetric orientation, which then allows the bulk second-harmonic generation. The measured quantity is the scalar product of the dipole moment and the vector portion of the susceptibility tensor that is assumed to be parallel. This limits the EFISH technique to the study of compounds with only a permanent electric dipole moment. Another disadvantage is the need to measure the dipole moment in an independent experiment. Also, the presence of an electric field prohibits the measurement of materials containing ionic species. The advantage of EFISH is a signal that is much higher than HRS. HRS and EFISH experiments require a dilute solution and serve as measurements for the molecular nonlinearity.[1-4]

The second-order nonlinear optical susceptibility ($\chi^{(2)}$) is usually determined through a second-harmonic generation (SHG) signal referred to as the marker fringe technique.[3] This technique is a convenient and relatively quick method to determine nonlinearity. This method can also be used to in situ monitor the poling processes, thus providing important information on the optimized poling parameters. A 1.06 μm Nd:YAG laser is commonly used to perform SHG measurements. This measurement prevents obtaining information at the telecommunication wavelengths of 1.3 and 1.55 μm . SHG also typically measures within the absorption region of the chromophore. Since the double frequency of 1.06 μm is within the absorption for most organic chromophores, it generates an amplified SHG signal and therefore an inaccurate result. The SHG

measurement is beyond the scope of this paper and further information can be found in other references.[4, 5]

3.3 Macroscopic Measurements

Macroscopic electro-optic measurements are primarily focused on the electro-optic coefficient (r_{33}). The electro-optic coefficient in a bulk system can be measured by several techniques including attenuated total reflectance spectroscopy (ATR), constant bias, and simple reflection measurement. The research lab at the University of Washington uses the simple reflection technique that was first described by Teng and Man, and also Schildkraut.[6, 7] Simple reflection employs a through-plane sample geometry. ATR and constant bias samples are considered a waveguide geometry. In through-plane mode, light propagates through the narrow poled polymer film at a given angle. In waveguide geometry the light propagates a known distance in the long direction of the film as a guided mode. Figure 3.1 shows a sample schematic of the through-plane geometry.

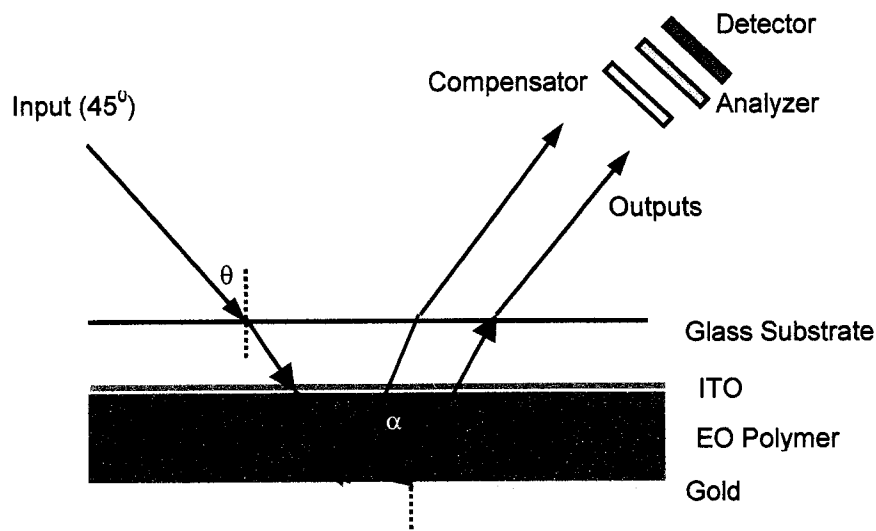


Figure 3.1. Through Plane Sample Geometry

For through-plane geometry, a transparent electrode such as indium tin oxide (ITO) is typically deposited onto a transparent substrate, i.e., glass. The electro-optic polymer is then spin coated into a thin film on the ITO-coated substrate. A second highly reflective gold electrode, approximately 100 nm thick in the case of the University of Washington research, is deposited by sputter coating on the polymer film. This sample geometry is the same as that previously described for poling. The electro-optical behavior is measured as a laser is transmitted through the transparent electrode, through the polymer film, then reflected off the gold electrode and back out of the sample.

Attenuated total reflection (ATR) measurement has the advantage of independent measurements of r_{13} and r_{33} . During this measurement the active polymer material is sandwiched between two thin gold layers or a gold and ITO layer, which is brought into contact with a prism. In some cases, the sample can be directly poled within the ATR set-up. The angle of incidence of the laser entering the prism is varied to find an angle that is sufficient for total internal reflection at the prism base. After a sufficient angle is

found, the light field penetrates the gold, whose thickness is adjusted to optimize the coupling to waveguide mode. When the light is efficiently coupled into waveguide mode, a substantial drop occurs in the reflected intensity.[8]

The electro-optic coefficients are measured by applying a modulating electric field across the two gold electrodes. The applied field causes a small change in the index of refraction of the film and produces a small change in the optimum coupling angle. The electro-optic coefficients are determined from these induced changes. ATR technique can also provide the film thickness and the refractive index of a sample. Although, ATR is an effective technique, the sample preparation and measurement are more complicated than for simple reflection.[1, 5, 8]

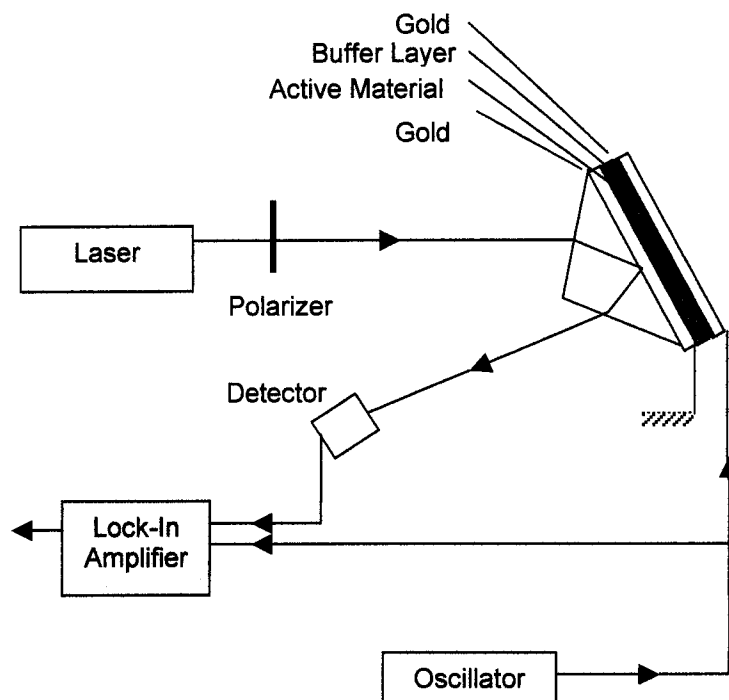


Figure 3.2. Experimental Set Up of ATR.

Constant-bias method experimentally measures V_{π} from which r_{33} can be extracted. This measurement is the most similar to an actual waveguide. Constant-bias method allows the poling and r_{33} measurements to be made simultaneously. This provides valuable information on optimizing the poling condition for the highest possible r_{33} value. Figure 3.3 is a schematic of the constant-bias experimental set-up. To achieve an appropriate poling atmosphere, it is necessary to maintain the temperature of the modulator by a closed-loop system consisting of a temperature controller, a thermoelectric cooler, and a thermistor. The lower electrode is grounded, and a DC bias voltage is applied to the top electrode to create a constant electric field that actively aligns the dipoles of the chromophores. The AC modulating voltage is coupled to the top electrode through a bias tee circuit consisting of a capacitor and a resistor, illustrated in Figure 3.3.[9]

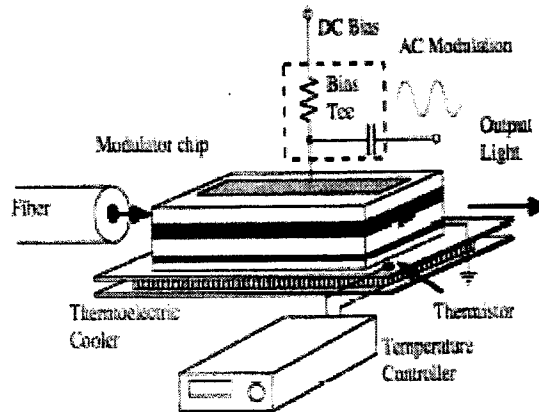


Figure 3.3. Constant Bias Set-Up [9]

The constant-bias device is operated as a birefringent modulator by simultaneously launching both transverse electric (TE, out of plane) and transverse magnetic (TM, in plane) modes into the waveguide with light polarized at 45° . Light is out-coupled with an objective lens and passed through an analyzer oriented at 45° for recombining the two

polarizations. The interference between the two orthogonally polarized modes produces the modulation signal from which V_π can be obtained. A birefringent modulator is a simple configuration to observe modulation. Since the modulations of TE and TM polarization partially cancel each other out, V_π does not represent the lowest achievable V_π of the device.[9]

The simple reflection measurement or Teng-Man technique [6] is the experimental method used in the University of Washington lab. Simple reflection technique has the advantages of easy sample preparation, relatively short measurement times, no measurement-induced sample damage, and straightforward interpretation.

The Teng-Man technique converts a phase modulation into an intensity modulation. This process creates interferences between the s (TE) and p (TM) polarizations.[10] Light polarized at 45° to the plane of incidence is propagated through the ITO electrode and the poled polymer film. The light is subsequently reflected off the gold electrode and continues out of the sample, shown in Figure 3.4. The light then travels through a Soleil Babinet compensator (SBC), which adds a variable phase mismatch between the reflected s and p waves. Finally, the light travels through an analyzer set at negative 45° from the plane of incidence, thus creating a cross-polarizer configuration.

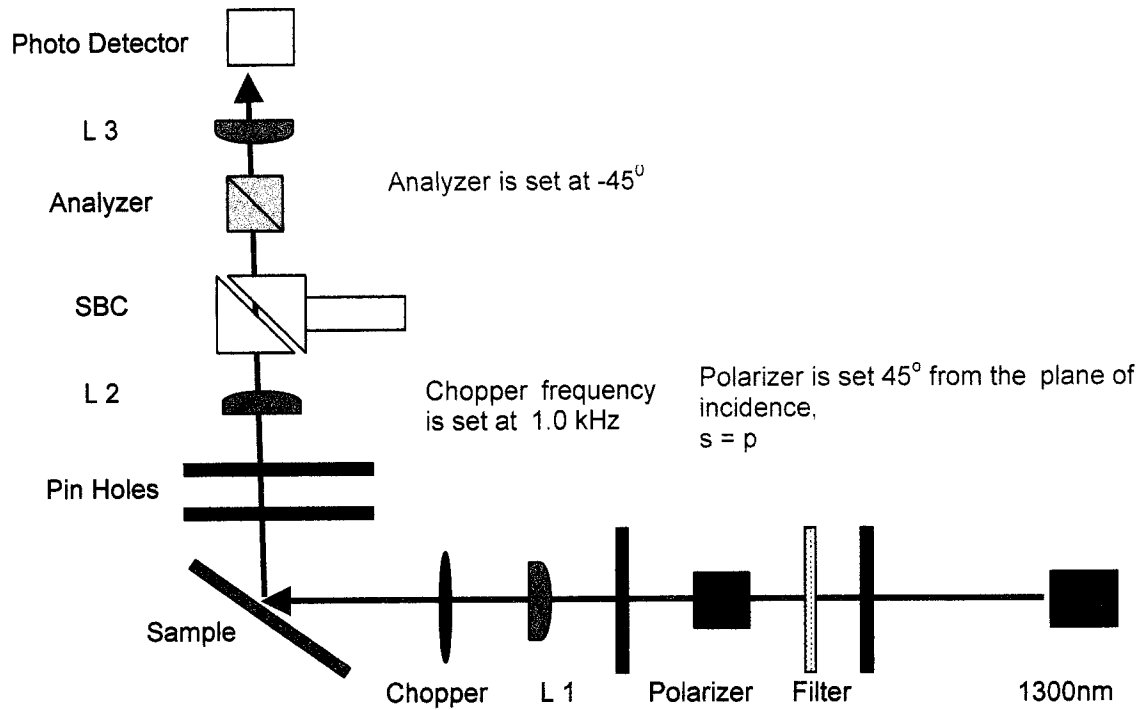


Figure 3.4. Experimental Setup of the Simple Reflection Method at UW

No electric field is applied during the first part of the measurement. The relationship between the phase difference (ϕ_{sp}), compensator position, the output laser intensity (I_o) at the detector and I_c , is equal to half the maximum intensity and is given by equation 3.1.[1, 6, 11]

$$I_o = 2I_c \sin^2 \left(\frac{\phi_{sp} + \phi_c}{2} \right) \quad (3.1)$$

In this configuration the sample experiences equal amounts of polarization of types p (parallel to the angle incidence) and s (perpendicular to the angle of incidence) given that the sample is at 45° . Both the s and p beams have their own refractive index and phase velocity. With reference to Figure 3.1, the angle of incidence (θ) and refraction

(α) inside the film are related to the refractive index by equation 3.2 for the p-ray.[1, 6, 12, 13]

$$\sin \theta = n_p \sin \alpha_p \quad (3.2)$$

With no electric field applied, the static contributions to the total phase shift (ϕ_{sp}) can be found. In general, ϕ_{sp} is described by three components: 1) Γ_o is a static portion due to the differences in the refractive index and path between the two polarizations, 2) Γ_{SB} also is a static contribution as a result of the SBC, and 3) a modulated part from the applied voltage, which is used in the second part of the measurement, as shown in equation 3.3. The first part of the measurement determines the compensator positions at which equation 3.4 is valid.[1]

$$\phi_{sp} = \Gamma_o + \Gamma_{SB} + \Gamma_m(V_m) \sin(\omega t) \quad (3.3)$$

$$\Gamma_o + \Gamma_{SB} = \pi / 2 \quad (3.4)$$

When equation 3.4 is valid it is possible to achieve a linear response and maximum voltage sensitivity. To accomplish this, the compensator is positioned to point A (Figures 3.5 and 3.6) or B (Figure 3.6) where the reflected output intensity is equal to I_c . [1, 6, 11] Figure 3.5 illustrates point A and its relationship to equation 3.1, plus the modulated intensity and voltage. Figure 3.6 demonstrates real data measured and fitted in the University of Washington lab.

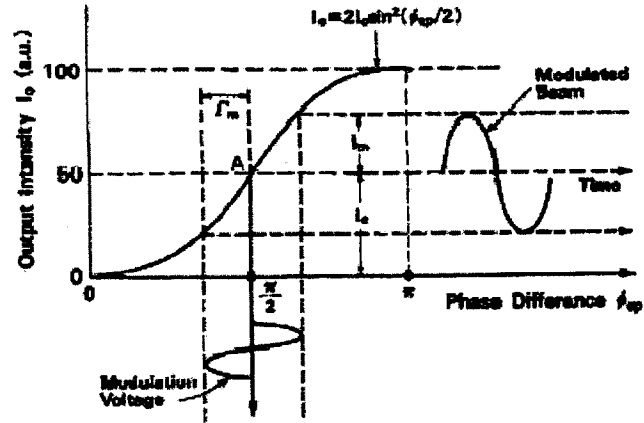


Figure 3.5. Output Intensity as a Function of Phase Difference [6]

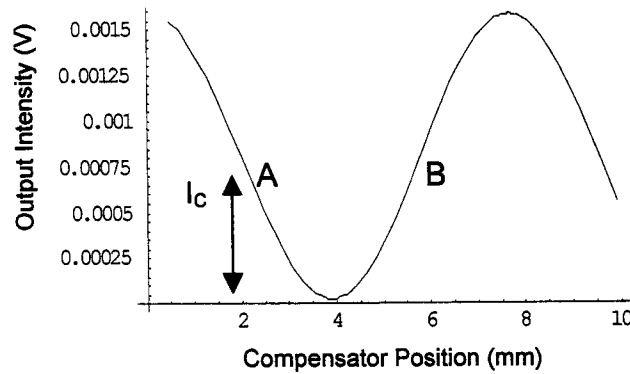


Figure 3.6. Experimental Data of the Output Intensity Curve Versus Babinet-Soleil Compensator Position

Once the compensator is moved to position A or B, the second portion of the measurement can be completed. When a modulated voltage is applied across the electrodes, field-induced changes in the ordinary and extraordinary refractive indices denoted by an 'o' or 'e' result in a differential phase shift ($\delta\phi_{sp}$) between the s and p polarizations and a change in the optical length through the electro-optical material.[1] These relationships are demonstrated by equations 3.5, 3.6, and 3.7.[1, 6, 11]

$$V = V_m \sin \omega_m t \quad (3.5)$$

Equation 3.5 represents the applied modulated voltage. The change in the total phase shift between s and p is represented by equation 3.6, and the modulated phase shift is expressed by equation 3.7.[1, 6, 11]

$$\delta\phi_{sp} = \Gamma_m \sin \omega_m t \quad (3.6)$$

where:

$$\Gamma_m = \left(\frac{2\pi r_{33} V_m}{\lambda} \right) \left[\frac{n_o n_e \sin^2 \theta}{(n_e^2 - \sin^2 \theta)^{1/2}} + \frac{r_{13}}{r_{33}} \left(\frac{n_o^3}{n_e} \right) (n_e^3 - \sin^2 \theta)^{1/2} - \frac{n_o^4}{(n_o^2 - \sin^2 \theta)^{1/2}} \right] \quad (3.7)$$

When the intensity is biased at I_c , the curve in Figure 3.5 is in its most linear region. For small modulations the ratio between the modulated beam intensity (I_m) and I_c is approximated by equation 3.10.[1, 6, 11]

$$\frac{I_m}{I_c} \approx \delta\phi_{sp} \quad (3.10)$$

With this approximation the electro-optic coefficient (r_{33}) of a poled polymer film is simplified to equation 3.11 with the assumptions that $n_o \approx n_e \approx n$ and $r_{33} = 3 r_{13}$. [1, 6, 11]

$$r_{33} = \left(\frac{3\lambda}{4\pi n^2} \right) \left(\frac{I_m}{I_c V_m} \right) \left(\frac{(n^2 - \sin^2 \theta)^{1/2}}{\sin^2 \theta} \right) = \left(\frac{I_m}{V_m} \right) (\text{constant}) \quad (3.11)$$

In equation 3.11 everything except V_m and I_m are constant for a given measurement. At points A and B the intensity is in its most linear region. If the sample is biased in this region, the slope of the modulated intensity over modulated voltage (I_m/V_m) should be equal. Measurements at both working points provide a cross check for the accuracy of the measurement. For a precise measurement the slope at each point should be equal as shown in Figure 3.7.[1, 6, 11, 14-16] Electro-optic coefficient (r_{33}) results are typically reported in pico-meters per volts.

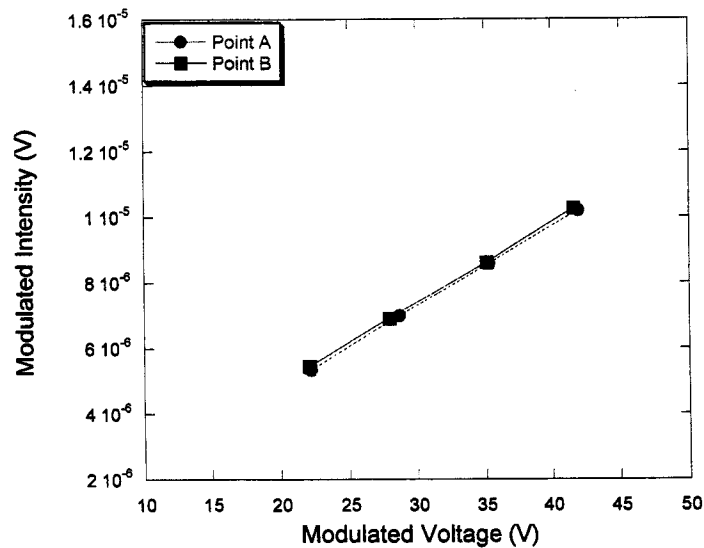


Figure 3.7. Modulated Intensity Versus Modulated Voltage at the UW

3.4 Simple Reflection Technique Limitations

The Teng-Man or simple reflection technique [6, 7] is commonly accepted as a standard method for determining second-order nonlinear optical properties of a poled polymer. This technique is based on several assumptions including no transparent electrode or material absorption, absence of other modulation effects, and no multireflections. The

experiment also assumes the results are a real nonlinear response. In reality, the higher order nonlinear contributions such as electro-mechanical and electro-chromic effects cannot always be neglected.

One of the most fundamental problems with simple reflection is the absorption from the transparent electrode. As described in section 3.1.1 in the Teng-Man technique, the laser beam is assumed to pass twice through the polymer layer of a semitransparent and metal electrode structure: once when entering the structure on the semitransparent electrode side and again after being reflected off the metal electrode. Michelotti et al demonstrated that when the frequently used ITO electrode is in the spectral region where ITO is nearly transparent, the error margin introduced from the ITO electrode is negligible, and when the ITO is absorbing, the two electrodes behave as a Fabry-Perot resonator and electro-optic coefficients are incorrect.[15] As the absorption peak of the new EO material is pushed closer to the near infrared (NIR), the need to accurately measure the EO coefficient at the wavelengths longer than allowed by the transparency of commercial ITOs becomes a critical issue.[14]

Accurate results also depend on a measurement wavelength that is far from material's absorption peak (λ_{max}). The simplified model of the Teng-Man method is only valid when the material absorption is negligible because high absorption leads to high reflectivity which contributes to experimental error.[10] As the materials measured in our lab absorption shifted to longer wavelengths and the chromophore loading increased, so did the separation between the slopes of the modulated intensity over modulated voltage (Im/V_m) (Figure 3.8), which should be equal at the A and B positions (Figure 3.7).

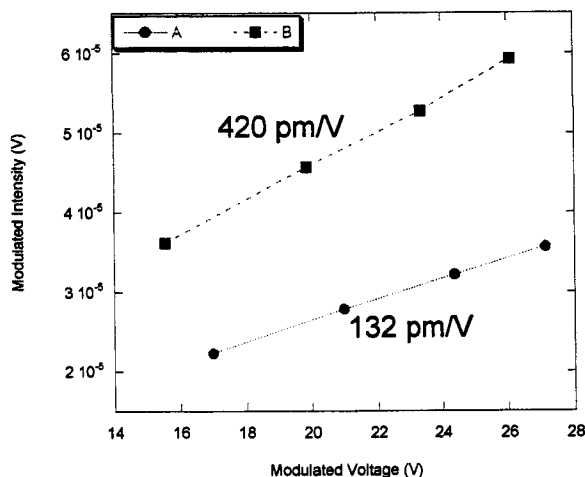


Figure 3.8. Modulated Intensity Versus Modulated Voltage

To further understand how the high $\mu\beta$ chromophores are affecting the accuracy of the simple reflection technique, we must carefully consider the validity of the assumptions upon which the experiment is based. As discussed in Section 3.1.2, this experiment assumes: 1) the contribution of the ITO is negligible, 2) poling-induced birefringence is small ($n_p \sim n_s \sim n_o$), 3) $r_{33} \sim 3r_{13}$, and 4) λ_{\max} is far from the measurement wavelength. Chapter 5 presents a detailed discussion about the error contributions to the measurement that have arisen from material changes in recent years.

3.5 Experimental

The simple reflection technique at the University of Washington was carried out using 630-nm, 830-nm, 1300-nm, and 1550-nm LaserMax diode lasers, a Tektronix TDS520D oscilloscope, a Stanford Research Systems, Inc. (SRS) 560 low-noise pre-amplifier, SRS DS345 synthesized function generator, SRS SR850 DSP lock-in amplifier, SRS

SR540 chopper controller, and a Trek 610C voltage amplifier. All refractive index measurements were made with the Metricon 2010 prism coupler.

Notes to Chapter 3:

1. Kuzyk, M.G. and C.W. Dirk, *Characterization Techniques and Tabulations for Organic Nonlinear Optical Materials*. 1998, New York: Marcel Dekker, Inc.
2. Bosshard, C.H., K. Sutter, Ph. Pretre, J. Hulliger, M. Florsheimer, P. Kaatz, and P. Gunter, *Organic Nonlinear Optical Materials*. 1995, New York: Taylor & Francis.
3. Prasad, P. and D.J. Williams, *Introduction to Nonlinear Optical Effects in Molecules and Polymers*. 1991, Hoboken: Wiley-Interscience.
4. Burland, D.M., R. Miller, and C. Walsh, *Second-order nonlinearity in poled-polymer systems*. Chemical Review, 1994. **94**: p. 31-75.
5. Morichere, D., et al., *Electrooptic effects in 2 Tolane side-chain nonlinear-optical polymers - comparison between measured coefficients and 2nd-harmonic generation*. Journal of the Optical Society of America B-Optical Physics, 1993. **10**(10): p. 1894-1900.
6. Teng, C.C. and H.T. Man, *Simple reflection technique for measuring the electrooptic coefficient of poled polymers*. Applied Physics Letters, 1990. **56**(18): p. 1734-1736.
7. Schildkraut, J.S., *Determination of the electrooptic coefficient of a poled polymer film*. Applied Optics, 1990. **29**(19): p. 2839-2841.
8. Hermienghaus, S., *Electro-optic coefficients in electric-field-poled polymer waveguides*. Journal of the Optical Society of America. B, 1991. **8**: p. 2311-2317.
9. Chen, A.T., et al., *DC biased electro-optic polymer waveguide modulators with low half-wave voltage and high thermal stability*. Optical Engineering, 1999. **38**(12): p. 2000-2008.
10. Chollet, P.A., et al., *Electro-optic coefficient determination in stratified organized molecular thin-films - application to poled polymers*. Thin Solid Films, 1994. **242**(1-2): p. 132-138.
11. Shuto, Y. and M. Amano, *Reflection measurement technique of electro-optic coefficients in lithium niobate crystals and poled polymer films*. Journal of Applied Physics, 1995. **77**(9): p. 4632-4638.
12. Marder, S.R., J.E. Sohn, and G.D. Stucky, *Materials for Nonlinear Optics: Chemical Perspectives*. ACS Symposium Series 455. 1991, Washington D.C.
13. Heavens, O.S. and R.W. Ditchburn, *Insight into Optics*. 1991, New York: Wiley and Sons.

14. Michelotti, F., et al., *Measurement of the electro-optic properties of poled polymers at $\lambda=1.55 \mu m$ by means of sandwich structures with zinc oxide transparent electrode*. Applied Physics Letters, 2003. **83**(22): p. 4477-4479.
15. Michelotti, F., et al., *On the measurement of the electro-optic properties of poled side-chain copolymer films with a modified Teng-Man technique*. Chemical Physics, 1999. **245**(1-3): p. 311-326.
16. Clays, K. and J.S. Schildkraut, *Dispersion of the complex electro-optic coefficient and electrochromic effects in poled polymer films*. Journal of the Optical Society of America B-Optical Physics, 1992. **9**(12): p. 2274-2282.

Chapter 4. Effects of Chromophore Shape Modification on Poling Efficiency and Stability

4.1 Introduction

The design and synthesis of high $\mu\beta$ chromophores is a collaborative effort between the chemists and characterization team. Translating the high molecular hyperpolarizability (β) values of organic chromophores into large electro-optic coefficients (r_{33}) in polymers is the central focus of this type of research. Recent improvements in the performance of the nonlinear optical polymers (NLO) are due to several innovative approaches that capitalize on nanoscale architectural control. The ability to synthetically control several critical design parameters such as size, shape, surface chemistry, flexibility, and topology has shaped the exploration of a range of novel materials. Manipulating the critical design parameters can dramatically advance the NLO polymer's poling efficiency and stability. Optimizing the chromophore design to achieve the highest possible efficient number density by reducing of dipole–dipole interactions and controlling the nanostructure of the chromophore or polymer to attain efficient poling is an effective approach for improving the electro-optic coefficient.

The outcome of increasing the effective conjugation length and/or enhancing the donor and acceptor strengths on the basic rigid rod chromophore guest–host systems has been extensively studied. Comprehensive research has also examined the effects of manipulating chromophore shape by surrounding it with bulky inert substituents in a way that makes the chromophore more spherical and prevents intermolecular interactions.

Recent work exploiting smartly controlled chemistry and creative processing/poling procedures has significantly improved poling efficiencies.

Theoretical analysis suggests that modifying chromophores with bulky substituent groups as spacers to prevent stacking and create a more spherical shape can enhance the maximum realizable EO activity.[1, 2] These bulky groups should not influence the molecular hyperpolarizability but should minimize the effect of unwanted electrostatic interactions. Shape and size changes can improve poling efficiency by increasing the free volume of the material and mobility of the chromophores. The application of this site-isolation effect has led to new achievements in electro-optic activity for guest-host polymer systems, dendritic polymers, side-chain, and psudeo-cylindrical polymer systems. The new poling dynamics of the dendronized polymers have provided higher poling efficiencies that have dramatically enhanced r_{33} values.

Requirements of a device-quality NLO polymer are low optical loss, solvent resistance, thermal and alignment stability, and a high EO coefficient. According to industry standards, devices are expected to last approximately 10 years with a minimum thermal stability requirement of no significant change in performance for 1000 hours at 85°C.[1] The NLO polymers used in these devices are often limited by the lack of poling-induced alignment stability necessary for long-term operation and the required solvent resistance needed for multi-layer device fabrication process.[2-5] The common practice for resolving these problems is to covalently incorporate chromophores into a polymer network and harden the matrix through crosslinking reactions.[3, 5-7] However, this process can significantly reduce the poling-induced alignment, and the high temperatures needed for lattice hardening can induce chemical reactions and

decomposition of the EO polymers. The most important drawback is the “nonlinearity–stability tradeoff” that reduces the full potential of the high optical nonlinearity in organic NLO materials to only 20–40%.[8] The chromophore mobility becomes limited as the polymer begins to crosslink due to the increase in interchain entanglements and the glass transition temperature (T_g). With reduced mobility the chromophore is unable to orientate under the poling field, thus lowering the EO activity of the polymer. Another limitation of conventional NLO thermoset polymers is the crosslinking temperature, which is usually much higher than the poling temperature. This can result in chromophore decomposition, sublimation, low reproducibility, and/or dielectric breakdown. Experimental results from our lab have shown up to a 50% decrease in EO activity when a high-temperature thermoset was used. Overcome this nonlinearity–stability tradeoff requires a poling process that allows the high rotational freedom of the chromophores. To accomplish this, the poling process should occur prior to and separated from the lattice hardening process.

This chapter takes a comprehensive look at the relationships between the molecular design and the macroscopic material properties for guest-host chromophores systems, side-chain chromophore systems, and dendritic materials, shown schematically in Figure 4.1. This chapter also investigates the effects of molecular design on the poling behavior. To be considered as a device-quality material by our collaborators, the poling current must be near or lower than 2 μ Amps while maintaining a high poling efficiency. Manipulating the poling field and temperature can help to control the poling current. We also studied crosslinkable material systems in an effort to develop a device-quality polymer doped with highly efficient chromophores that provides the high alignment stability and solvent resistance necessary for device fabrication.

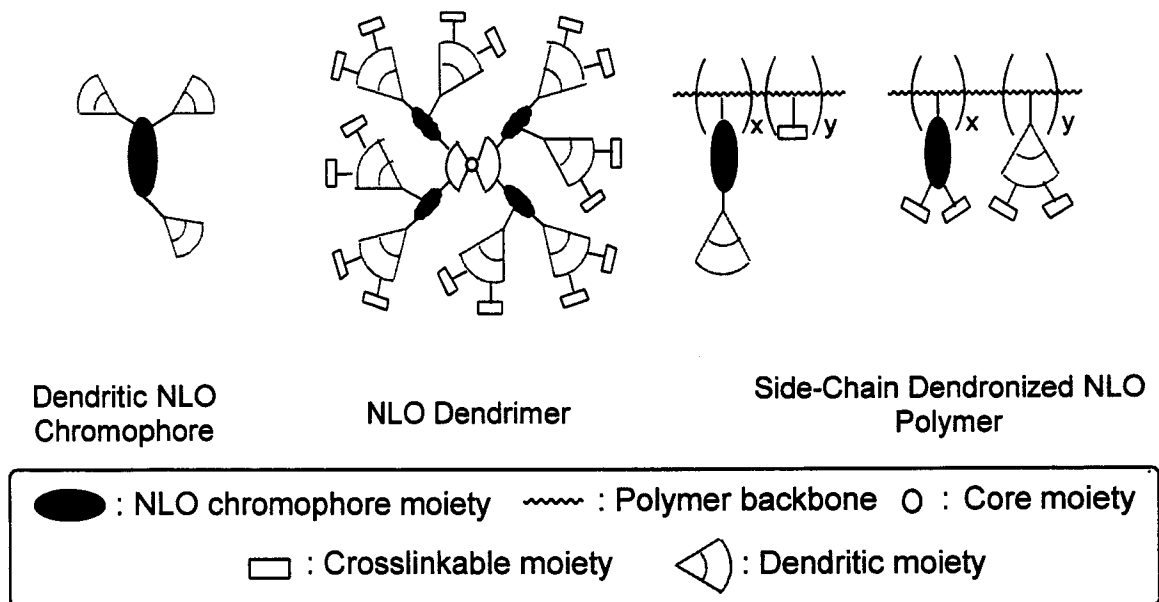


Figure 4.1. Schematic Drawings of Various Chromophore Systems

The Jen research group at the University of Washington designed and synthesized these materials.[9-13] The sample preparation is described in section 4.6. All reported EO coefficients were measured by the simple reflection method described in section 3.3. All the samples were poled by contact poling as described in section 2.2.2.

4.2 Guest-Host Chromophore Systems

Traditional chromophore design includes a donor, π -electron bridge, and acceptor motif. Chapter 2 introduced chromophore changes over the past decade that predominately involved increasing the effective conjugation length and/or enhancing the donor and acceptor strengths. The following sections will address the effects of chromophore design changes for several guest-host systems that include shape modifications on the acceptor, donor, and bridge of the chromophore.

4.2.1 Effects of Chromophore Acceptor and Bridge Design on Poling Efficiency

The development of highly efficient chromophores was one of the driving forces behind this research. Initially, synthetic chromophore research was focused on increasing the donor or acceptor strength. Over time the geometry of these stronger chromophores became longer and flatter, allowing them to easily stack together. However, these chromophores behaved unpredictably during poling and were prone to dielectric breakdowns. In an effort to better understand the relationship between high poling efficiency and chromophore shape, we designed a systemic study that increased the bulk surrounding the acceptor of the chromophore and rigidity of its conjugated bridge.

Previous work by Liu et al [11] demonstrated that the addition of a CF_3 group to the di-cyanomethylene-3-cyano-4,5,5-trimethyl-2,5-dihydrofuran acceptor (TCF) more than doubled the EO activity. This modified acceptor 2-di-cyanomethylene-3-cyano-4,5-dimethyl-5-trifluoromethyl-2,5-dihydrofuran (CF_3TCF) incorporated several improvements: it was more chemically inert than TCF, had a higher T_g , and gave bulk to TCF's very flat geometry, which helped to prevent aggregation.[11] All the chromophores discussed in section 4.2.1 employ the CF_3TCF acceptor. The various chromophore design changes are illustrated in Figures 4.2 and 4.3.

The AJL8 chromophore shown in Figure 4.2 has a CF_3TCF acceptor with a FTC type bridge. AJL8 includes a tert-butyldimethylsilyloxyl-ethyl-aniline (TBDMS) group on the donor, which improves solubility.[14, 15] In comparison to the previously studied CF_3TCF [11] chromophores, the addition of the TBDMS group considerably lowered the poling current, making it more attractive for device fabrication. The change from AJL8 to

AJL6 involved the removal of the five-member thiophene ring from the bridge and replacement with a six-member ring. The six-member ring on the bridge is commonly referred to as a CLD type bridge[14]. The chromophore became more rigid, more thermally stable, and had a 54-nm red shift. This change forced the chromophore into a trans position, which allowed the electrons to move more easily from the donor to the acceptor. The change from the FTC bridge (AJL8) to the CLD bridge (AJL6) increased the EO value by 45%. A phenol group (benzene ring + OH) and a protecting group were added to the AJL7 acceptor. This change made no significant difference in EO activity in comparison to AJL6; however, the extra bulk increased the poling temperature by 10°C, which improved the thermal stability. AJC139 is very similar to AJL6 with the addition of a thiophene to the acceptor. Similar to the change from AJL8 to AJL6, a large red shift occurred the r_{33} value increased.

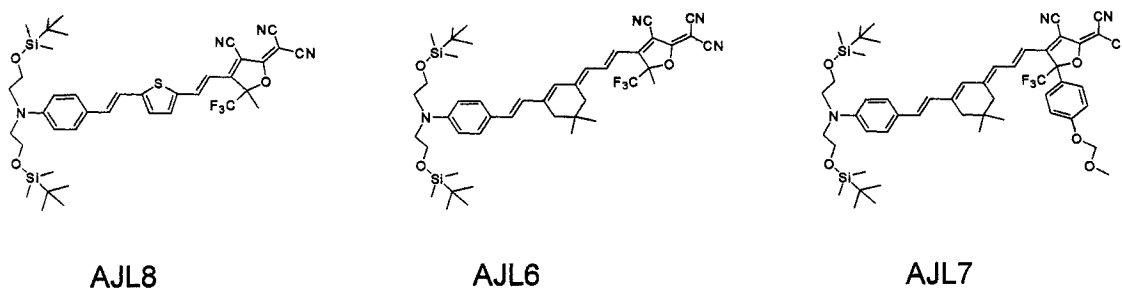


Figure 4.2. Chemical Structure of AJL6, 7, and 8 Chromophores

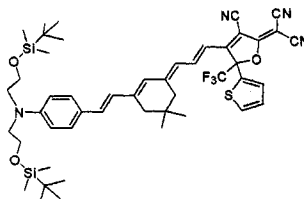


Figure 4.3. Chemical Structure of AJC139 Chromophore

These materials were normalized to 25% by weight in amorphous polycarbonate (APC) and poled with the same applied field for comparison. All of the sample's absorption peaks red shifted as their r_{33} values increased, illustrated by Figure 4.4. This trend is expected following the two-state model introduced in Chapter 2. As the material red shifts, the band gap energy decreases, increasing the hyperpolarizability.

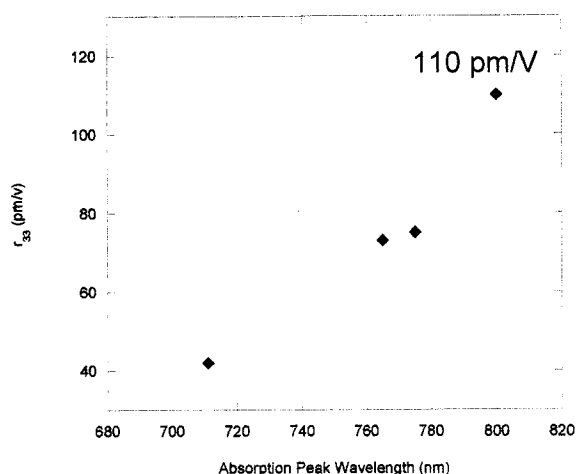


Figure 4.4. r_{33} (at 1310 nm) with a Poling Field of 100 V/ μ m Versus Absorption Peak

The combination of the TBDMS group with the CF_3TCF acceptor afforded the AJL8 chromophore not only a low poling current but also the ability to hold a much higher applied electric field (up to 150 V/ μ m) without dielectric breakdown. A similar

chromophore without the TBDMS group [11] could not be poled above 100 V/ μm without severe electrode damage. Since this chromophore had such a low poling current and predictable poling behavior, the poling temperature and voltage could be quickly applied to reduce the overall material processing time. As the λ_{max} of these materials progressively increased so did their poling current. At 100 V/ μm this change was less significant; however, at 125 V/ μm , for example, the poling current increased from 10 μAmps (AJL8) to 160 μAmps (AJC139). The balance between high poling efficiency and the low poling current required for device fabrication is a constant struggle. It is also important to note the relationship between the poling temperature and applied electric field; as the poling voltages increased the poling temperature had to be lowered, thus lowering the chromophore mobility within the APC host. If the temperature is too low the chromophores will not be able to rotate; if the voltage is too high, a dielectric breakdown or electrode damage will occur. Table 4.1 summarizes the material properties for AJL6, AJL7, AJL8, and AJC139.

Table 4.1. Summary of Properties for the AJL6, AJL7, AJL8, and AJC139 Chromophores

NLO Polymer	Chromophore Content (wt. %)	Poling Temperature ($^{\circ}\text{C}$)	Poling Field (V/ μm)	λ_{max} (nm)	r_{33} (pm/V) _{1300nm}
AJL8-APC	25	140	100	711	42
AJL7-APC	25	150	100	765	73
AJL6-APC	25	160	100	775	75
AJC139-APC	25	158	100	800	110

The long-term stabilities of the AJL-APC polymers were measured at 85 $^{\circ}\text{C}$ under vacuum for more than 500 hours; AJL8 maintained 76% of its original EO activity, AJL7 maintained 83%, and AJL6 maintained 73%. The benzene ring increased the stability of

AJL6 compared to AJL8 or AJL7. The six-member ring on the AJL6 bridge with modification to the acceptor had a slightly lower stability than did the thiophene-containing AJL8. Figure 4.5 illustrates the maintained EO activity for the AJL-APC series. The stability of AJC139 was not measured.

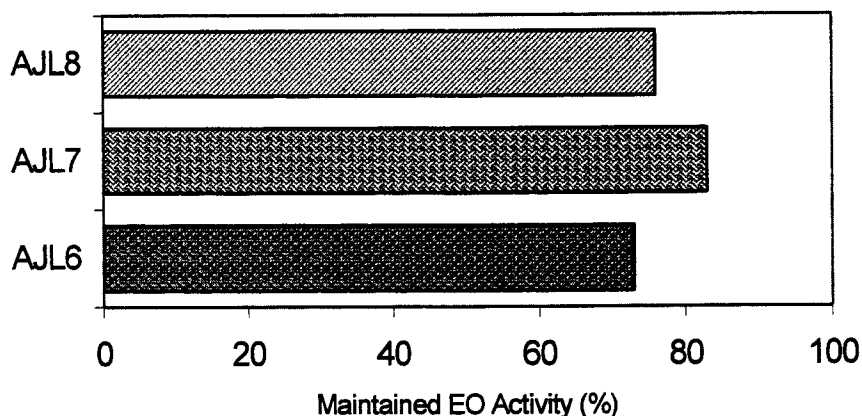


Figure 4.5. Stability Summary of the AJL6, AJL7, and AJL8 Chromophores

Small changes in the chromophore design can have a huge impact on the EO activity and the poling behavior. This research has demonstrated that the electro-optic coefficient can be enhanced by a factor greater than four times by manipulating the donor, bridge, and acceptor and by increasing stability. However, as high $\mu\beta$ chromophores shift more to red, optical loss and poling current increase, which lowers their viability for device applications. To compensate for this problem, researchers are studying the effects of fluorinated dendrons as a way to lower optical loss and improve poling efficiency.[13, 16, 17]

4.2.2 Effects of Bulky Group Additions

Section 4.2.1 demonstrated that adding a small amount of bulk to the acceptor or creating a more ridged chromophore bridge can greatly enhance the EO coefficient. The next phase of this thesis will investigate the addition of fluorinated dendrons on the chromophore and its surrounding matrix.

4.2.2.1 LMAJ series

The LMAJ series investigated adding varying degrees of bulk to the bridge of the chromophore. All the materials tested had a dibutylaniline donor and a CF_3TCF acceptor (Figure 4.6). The LMAJ28 chromophore incorporated a t-butyldimethylsilyl side group to the thiophene of the bridge [9] and LMAJ28-bulky attached a fluorinated dendron to the thiophene of the bridge. Prior experiments demonstrated that the addition of a side group can greatly affect the intermolecular interactions among the chromophores. Substituting different shapes and sizes will create a variable free volume and affect the mobility of the chromophores.[5, 13] The addition of a flexible dendron has increased poling efficiency due to minimization of electrostatic interactions.[18] The LMAJ series was designed with this concept of increasing the bulk with a fluorinated dendron.

The standard chromophore for the LMAJ series was LMAJ22, which had a FTC type bridge and was doped in to polymethyl-methacrylate (PMMA) with a chromophore content of 21% by weight. The LMAJ28-APC polymer had a chromophore content of 20% by weight. LMAJ28-bulky had a chromophore content of 25% by weight , which

included the dendron. This gave the material an active chromophore content of 13% by weight in APC.

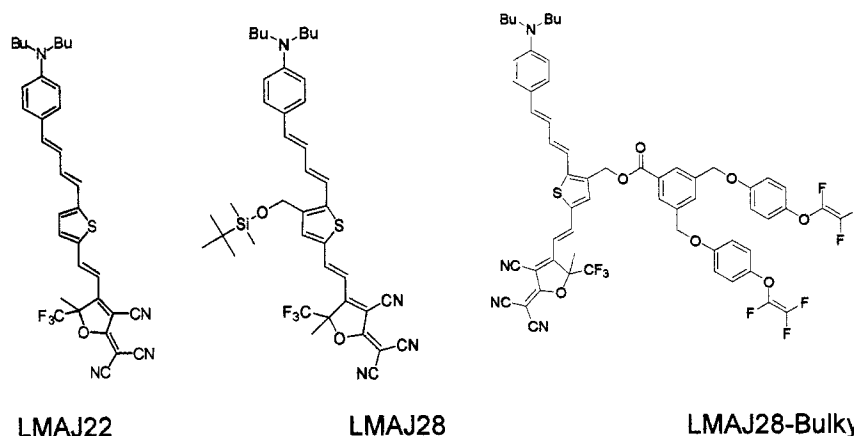


Figure 4.6. Chemical Structures of LMAJ22, LMAJ28, and LMAJ28-Bulky Chromophores

The addition of the *t*-butyldimethylsilyl side group on LMAJ28 provided the chromophore with a higher T_g than the LMAJ22 chromophore. The low T_g ($\sim 90^\circ\text{C}$) of LMAJ22 prevented it from being doped in higher T_g host materials and having an acceptable thermal stability. Though the *t*-butyldimethylsilyl side group on LMAJ28 did not enhance the poling efficiency, it did considerably lower the poling current by isolating the chromophores. The increase in bulk from LMAJ28 to LMAJ28-bulky showed several improvements. Under similar poling conditions the r_{33} value of LMAJ28-bulky was 14% lower with half of the active chromophore present in LMAJ28. Thus, the bulky group greatly increased the poling efficiency. If a much higher poling field of $150\text{ V}/\mu\text{m}$ was used for LMAJ28-bulky, its EO activity could be pushed to 14% higher than LMAJ28 with less chromophore content. LMAJ22 could not withstand the application of such a high poling field without dielectric breakdown. The small side group on LMAJ28 enabled it to

be poled up to 150 V/ μm , but it suffered electrode damage and the poling current was more than four times higher than LMAJ28-bulky under the same field.

Table 4.2. Summary of Properties for LMAJ22, LMAJ28, and LMAJ28-Bulky

Chromophores					
NLO Polymer	Chromophore Content (wt. %)	λ_{max} (nm)	Poling Temperature ($^{\circ}\text{C}$)	Poling Field (V/ μm)	r_{33} (pm/V) _{1300nm}
LMA22-PMMA	21	728	85	100	44
LMAJ28-APC	20	761	130	100	42
LMAJ28-Bulky	13	750	142	150	50
			160	100	36

The previous section showed that an increase in the absorption peak (λ_{max}) typically led to an increase in the resulting r_{33} value; however, in the case of LMAJ28-bulky, the absorption peak decreased while the poling efficiency increased. These results demonstrated that modifying chromophores with fluorinated dendrons can undo some of the problems created by increasing the hyperpolarizability of the chromophore.

These experimental studies have shown that shape modification can considerably enhance the achievable r_{33} value of a highly efficient nonlinear optical chromophore. The addition of a fluorinated side group created more free volume and enhanced the chromophore mobility under an applied electric field. These materials also illustrated that the addition of a side group can increase the T_g of the chromophore and lower the λ_{max} .

4.2.2.2 Dendritic chromophore guest-host systems

This section further explores the effects of the fluoro-rich dendrons on the microenvironments to better understand the effects of increased free volume and site isolation on the poling efficiency. For this study we used a phenyl-tetracyanobutadienyl (Ph-TCBD) thiophene-stilbene-based NLO chromophore [10] as the center core, which was encapsulated with three highly fluorinated aromatic dendrons (highlighted in yellow), shown in Figure 4.7. Encapsulating the chromophore with fluorinated dendrons made its shape more globular-like, close to the ideal spherical shape needed to achieve the theoretically predicted optimum poling efficiency by the site isolation effect.[1] Fluorinated dendrons also add thermal stability, are chemically inert, have low dielectric, and high optical transparency.[16]

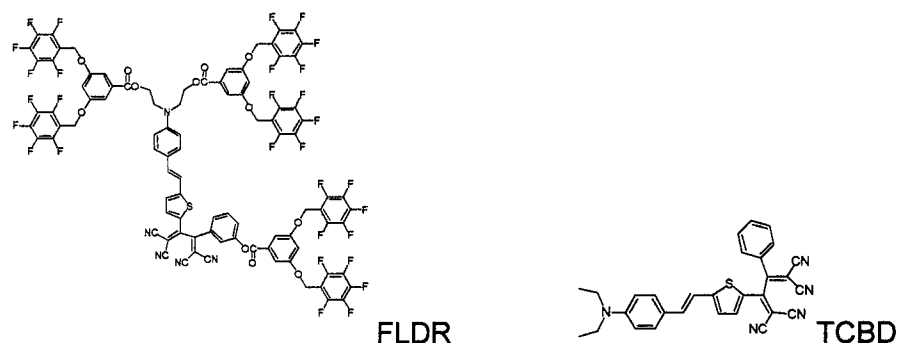


Figure 4.7. Chemical Structure of FLDR and TCBD Chromophores

Both TCBD and FLDR were characterized in an APC host with an active chromophore content of 12% by weight. The encapsulating dendrons created a 40-nm blue shift in the absorption spectrum, as shown in Figure 8. Since both chromophores contain the same NLO active moiety, the blue-shifted λ_{max} was largely due to the fluoro-rich dendrons with

low polarizability, which provided a very low dielectric, constant environment encapsulating the core chromophore.[10, 16, 19] The FLDR chromophore showed the same λ_{\max} in APC or a highly fluorinated polymer. This finding demonstrates that the change in λ_{\max} between FLDR and TCBD was due to the microenvironment created by the fluorinated dendrons of the FLDR chromophore. This change was interesting because the r_{33} values typically decrease as a material blue shifts, as demonstrated in section 4.2.1. The blue-shifted absorption and high C-F content in FLDR also contributed to the material's low optical loss at both 1.33 and 1.55 μm . [10, 16] The optical loss as measured by photothermal deflection ion spectrometry [20] was less than 1 dB/cm. The C-H overtones in the APC matrix were most likely the main contributor to the overall optical loss.[16]

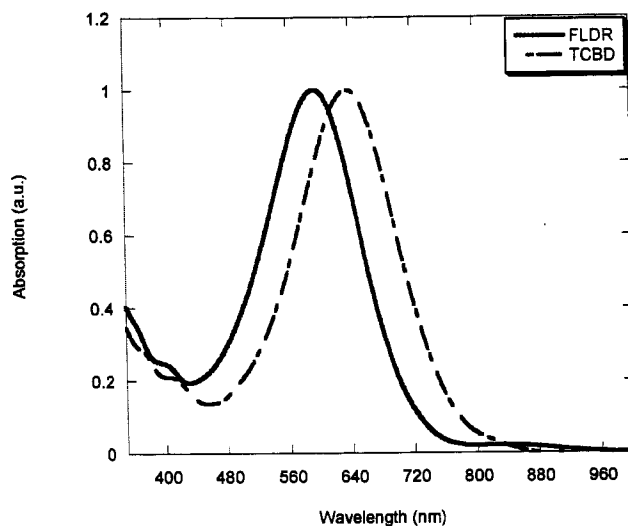


Figure 4.8. Absorption Spectrum of FLDR and TCBD Chromophores

The r_{33} value increased from 5 pm/V to 15 pm/V when compared with the same chromophore (TCBD) in APC. The encapsulation effect of the dendrons allowed the

chromophores to be spatially isolated, and the large voids provided more chromophore mobility for efficient poling.

Table 4.3. Summary of Properties for TCBD and FLDR Chromophores

Polymer	Chromophore Content (wt. %)	λ_{max} (nm)	Poling Temperature ($^{\circ}\text{C}$)	Poling Field ($\text{V}/\mu\text{m}$)	r_{33} (pm/V) _{1300nm}
TCBD	12	635	150	100	5
FLDR	12 % active, 50 % dendron	595	145	100	15

In summary, the dendritic chromophore exhibited a large blue-shifted absorption and three times higher EO activity and lower optical loss when compared to the pristine chromophore. These materials experimentally showed that isolating the chromophore minimized the intermolecular electrostatic interactions. This, in turn, improved the molecular orientation during the poling process.[10, 17] The only drawback of this spherical molecule was the low alignment stability even at room temperature. The increased mobility created by the free volume around the chromophore boosts chromophore alignment and relaxation.[2] To improve the alignment stability while maintaining the positive effects of the dendronized chromophore, we developed several dendronized side-chain materials.

4.3 Effects of Flourinated Dendrons in Side-chain Systems

Side-chain systems have two main advantages over the guest-host chromophore systems: the chromophore can be attached to the main chain at specific places and it possesses the ability to attach bulky groups or dendrons, thus preventing intramolecular interactions between the chromophores in both cases.[2, 5] Side-chain materials offer

improved processibility, less aggregation and phase separation, and also slowed relaxation because the motion of the chromophore is hindered by its attachment to the polymer.[2] This section examines two different polymer backbones and various dendritic shape modifications.

4.3.1 Polystyrene (PS) Side-Chain Series

The polystyrene (PS) series of materials compared a dendritic side-chain chromophore and a pure side-chain chromophore using both the FTC and CLD bridges

4.3.1.1 PS-FTC series

The PS-FTC series compared the LMAJ0 chromophore incorporated onto a PS backbone with a bulky group on the acceptor and without, shown in Figure 4.13. The LMAJ0 guest-host material was also evaluated doped into polyquinaline (PQ-100). Luo et al [9] synthesized these materials.

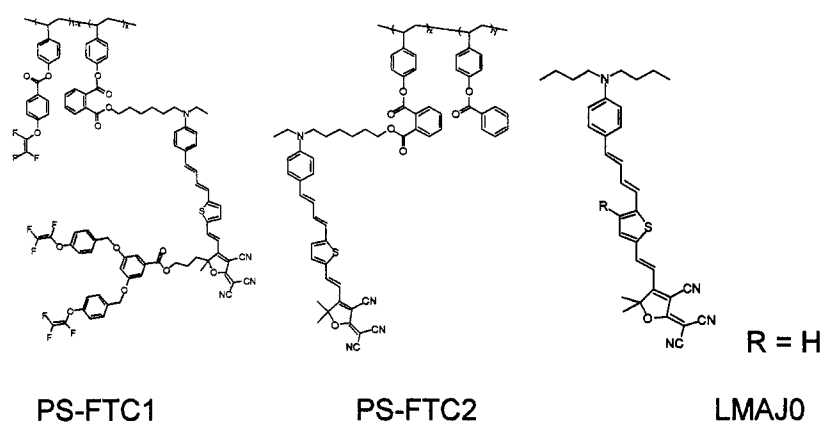


Figure 4.9. Chemical Structures of the FTC Side-chain Series

We conducted a systematic study to find the optimized poling behavior of PS-FTC1. This research indicated that the bulkier side-chain materials needed approximately 15–25 minutes to pole efficiently, versus typical guest-host materials that needed less than 5 minutes. Another interesting feature of the side-chain materials was the application of a much higher electric field without dielectric breakdown. Figure 10 illustrates the effects of poling and electric field on the PS-FTC1 polymer.

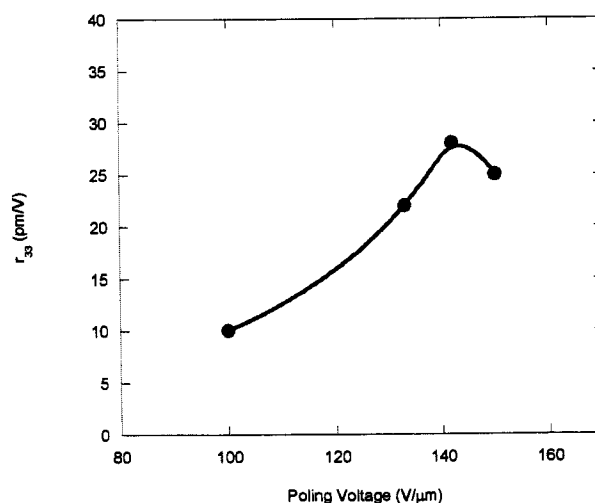


Figure 4.10. r_{33} Versus Applied Poling Voltage

With the same PS backbone and applied electric field during poling, PS-FTC1 had an r_{33} value 1.4 times higher than PS-FTC2. We attributed this result to better site isolation that allowed good special distribution and efficient rotation of the chromophores. The drawback of this higher free volume created by the fluorinated dendrons was significantly lowered T_g and limited possibility of long-term stability. The LMAJ0 chromophore doped in PQ-100 showed a substantially lower r_{33} value in comparison to PS-FTC1, most likely because without the site isolation provided by the fluorinated dendron, LMAJ0 could only withstand up to a 100-V/μm applied field.

Table 4.4. Summary of Properties for the PS-FTC Side-chain Polymers

Structure	Chromophore Content (wt. %)	Poling Temperature (°C)	Poling Field (V/ μ m)	r_{33} (pm/V) _{1300nm}
PS-FTC1	20	95	142	45
PS-FTC2	20	125	140	33
LMAJ0-PQ-100	23	154	100	28
NLO Dendrimer	36	80	110	68

PS-FTC1 design also offers a nice comparison to the NLO dendrimer shown in Figure 4.11 below. Dendrimers have a well-defined structure and branching at each repeat unit.[18] This dendrimer was designed to further minimize chromophore–chromophore electrostatic interactions, to optimize folding under a high electric field, and to improve processibility.[5] The dendrimer material does not need to be doped in a host polymer or connected to a side chain. The chromophore content of this dendrimer was 36% by weight, almost twice that of PS-FTC1. The spatial isolation created by the dendrimer shell allows the chromophore content to be increased to much higher levels, potentially increasing the achievable EO activity.

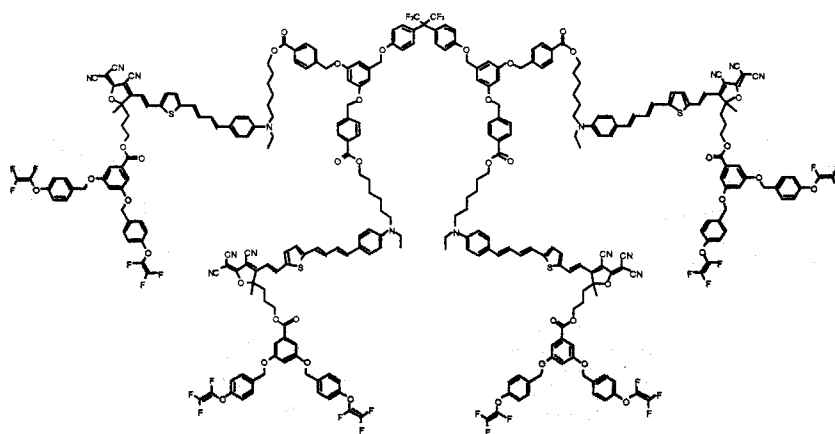


Figure 4.11. Chemical Structure of NLO Dendrimer
(FTC type chromophore is highlighted in blue and the dendron in pink.)

The r_{33} value of the NLO dendrimer was 34% higher than PS-FTC1, which was consistent with its 45% increase in chromophore content. However, without the suppression of the chromophore, electrostatic interactions offered by the dendrimer design, such a high loading level, would not be possible. Another advantage of the dendrimer design was the much lower applied voltage used during poling to achieve the same degree of poling efficiency. The host material did not restrict the NLO dendrimer so it had higher chromophore mobility. The only disadvantage of the NLO dendrimer in comparison to the above materials was an extremely high poling current, approximately five times higher.

Overall, the site isolation provided by fluorinated dendrons dramatically enhanced the poling efficiency. Suppressing the chromophore–chromophore electrostatic interactions allows use of much higher applied fields during poling, which continually increases the r_{33} value without dielectric breakdown. Though the dendronized side-chain polymers preformed better than the guest-host polymer, the fluorinated dendrimer demonstrated the effectiveness of site isolation. With the chromophores protected from each other by the fluorinated dendrons, the chromophore loading could be almost doubled, redefining the chromophore content limit.

4.3.1.2 PS-CLD series

The PS-CLD series, like the PS-FTC series, had a PS backbone; however, these side-chain polymers used the more efficient CLD1 chromophore. Besides a change in chromophore, the PS-CLD series demonstrated the effects of bulky groups on the main chain, chromophore attachment, and bulky-group placement on the chromophore. We

tested three materials in the PS-CLD series: 1) PS-CLD1 was the same as PS-FTC1 with a CLD bridge; 2) PS-CLD2 incorporated several changes that connected the chromophore to the main chain at the acceptor instead of the donor, attached the bulky group to the donor, and added an extra fluorinated group to the main chain; and 3) PS-CLD3 was analogous to PS-FTC2 with the addition of a fluorinated bulky group on to the main chain. The CLD1 chromophore was doped into PS for a guest-host comparison. Figure 4.12 illustrates these materials. The fluorinated bulky group is highlighted in pink, the CLD1 chromophore's donor is in blue, and the acceptor in purple.

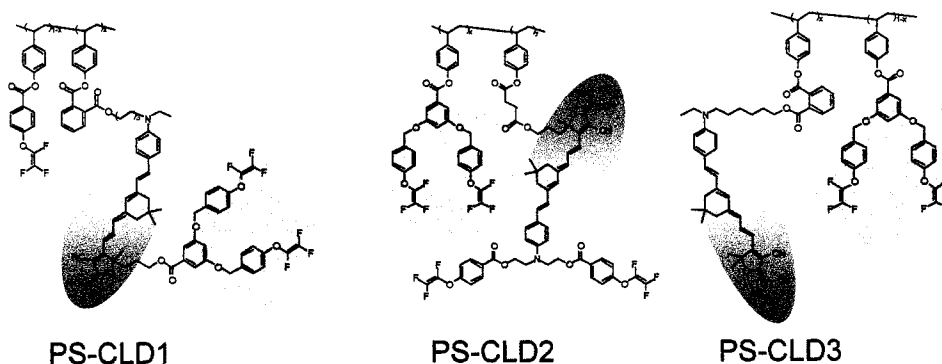


Figure 4.12. Chemical Structures of the CLD Side-chain Series

The structural change from PS-CLD1 to PS-CLD2 introduced the interesting feature of cylindrical packing shown schematically in Figure 4.13. This schematic is based on previous work by Percec and Schöler et al showing that well-organized macromolecular cylinders can be achieved by the self-assembling of densely loaded flat-tapered dendritic moieties along a linear polymer backbone.[17, 21] It was expected that the flat taper-shaped chromophore would be spatially isolated in the channels of such cylindrical structures.[17] The PS-CLD3 polymer included a dendron on the main chain but not on

the chromophore. These three different polymers provide some insight into how the shape of the side-chain chromophores can affect the performance of the polymers.

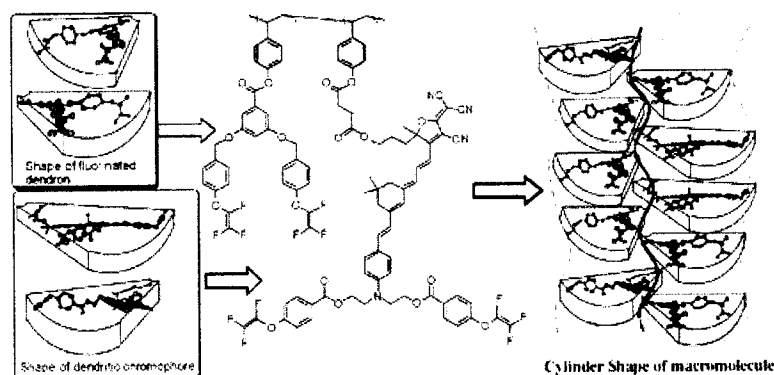


Figure 4.13. Cylindrical Stacking of PS-CLD2 [17]

Table 4.5 summarizes the experimental results for the PS-CLD series. The thin-film UV-vis spectrum of PS-CLD2 showed a 56-nm blue shift when compared to that PS-CLD1. Based on the previously discussed highly fluorinated FLDR, this finding indicates the chromophores have been well isolated by the fluorinated dendrons.

Table 4.5. Summary of Properties for PS-CLD Side-chain Polymers

Structure	Chromophore Content (wt. %)	λ_{max} (nm)	Poling Temperature ($^{\circ}\text{C}$)	Poling Field ($\text{V}/\mu\text{m}$)	r_{33} (pm/V) _{1300nm}
PS-CLD1	20	706	95	140	50
PS-CLD2	20	650	90	115	55
PS-CLD3	20	-	60-80	>100	-
CLD-PS	18	667	90-95	125	29

PS-CLD1 and PS-CLD2 had one T_g near 90–95 $^{\circ}\text{C}$. PS-CLD1 and PS-CLD2 both poled efficiently near their T_g . PS-CLD2 was not able to withstand as high an applied electric field as did PS-CLD1; nonetheless, it demonstrated a higher EO coefficient due to its

more efficient packing. PS-CLD3, however, showed two temperatures transitions, one at 65°C and one at 85°C. The presence of two transitions indicates there may be a significant difference between the PS phase and the dendron phase. Poling PS-CLD3 at 85°C resulted in severe film and electrode damage. At 65°C the polymer was not soft enough to achieve any degree of poling efficiency. Both PS-CLD1 and 2 were much more efficient than the CLD chromophore doped in PS.

The dendronized side-chain polymer PS-CLD1 showed a significantly higher EO activity than the guest-host polymer system with the same chromophore loading level. The excellent poling efficiency of PS-CLD2 can be attributed to the densely packed bulky side groups on the main chain and chromophore pushing against each other and causing the flexible polymer main chain to form a pseudocylindrical conformation.[17] Both results indicate that the strong chromophore–chromophore electrostatic interactions were suppressed with effective site isolation moieties and that the guest-host polymer's lack of site isolation severely limited its attainable EO activity. The PS-CLD3 polymer demonstrated the importance dendron placement. In this case the chromophore was quite free to rotate and the bulky dendrons were more closely attached to the main chain. The dendron is not reducing the interactions between the chromophores, only restricting the polymer chain motion. Both PS-CLD1 and 2 showed excellent thermal stability (90% maintained) at room temperature, but do not have the high temperature thermal stability necessary for device fabrication.

4.3.2 Polyimide (PI) Series

The PS side-chain materials showed a significant improvement in the achievable EO activity, yet they lacked the thermal stability needed for practical applications. To overcome this drawback, we incorporated the CLD1 chromophore in a side-chain system that consisted of a polyimide backbone. Polyimides have excellent thermal stability, and chemical and mechanical properties.[16, 22] This material followed the PS-CLD1 design and is shown in Figure 4.14.

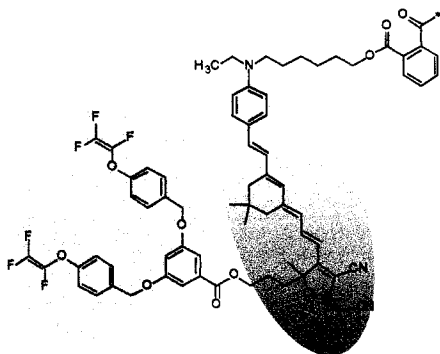


Figure 4.14. Chemical Structure of PI-CLD1 [19]

PI-CLD1 had a chromophore content in polyimide of 25% by weight to compare the poling efficiency with PS-CLD1. PI-CLD1 was poled at 155°C with an 85-V/ μm applied field, unlike PS-CLD1, which had a 140-V/ μm applied field. The current during poling of PI-CLD1 was approximately 10 times higher than the previously tested PS-CLD1, which makes it difficult to use a high poling field. The r_{33} value for PI-CLD1 was 35 pm/V, about 30% less than the PS-CLD1 value of 50 pm/V. However, this is quite reasonable considering that the poling voltage was 40% less than that applied to PS-CLD1. If a higher poling field could have been applied to PI-CLD1, its r_{33} value could have been as

high or higher than that of PS-CLD1. The use of PI with NLO chromophores has been limited in our lab due to its extremely high poling current, and only a few chromophores can tolerate its high T_g .

The long-term stability of PI-CLD1 was measured over 600 hours at 85°C under vacuum and maintained 90% of its original value as shown in Figure 4.15. The thermal stability of PI-CLD1 meets the industry expectations but does not have the low poling current necessary for multi-layer device fabrication.

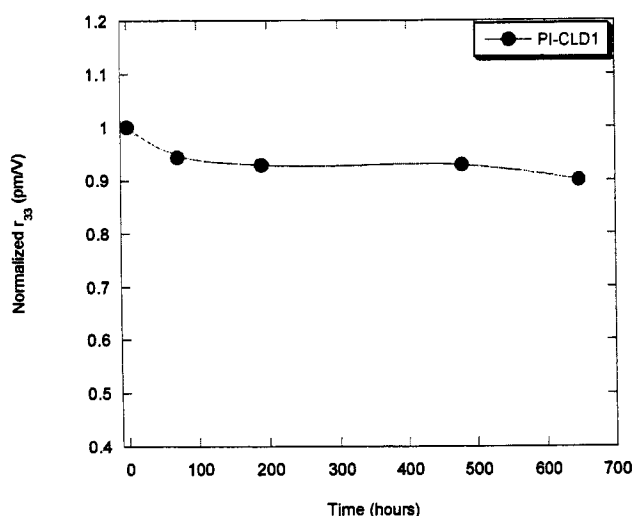


Figure 4.15. Long-term Stability of PI-CLD1

The polyimide backbone had a high glass transition temperature and has shown it can provide long-term stability at 85°C. Unfortunately, its high poling current limits its usefulness in future device fabrication. Researching different variations on the poling process or modifying the PI chain itself might be effective ways to lower the conductivity.

4.4 Stability

To be considered device-quality, an NLO polymer must have low optical loss, solvent resistance, plus thermal and alignment stability in addition to a high EO coefficient. According to industry standards, devices are expected to last approximately 10 years with a minimum thermal stability requirement of no significant change in performance for 1000 hours at 85°C.[1] The NLO polymers used in these devices are often limited by the lack of poling-induced alignment stability necessary for long-term operation and by the required solvent resistance needed for multi-layer device fabrication process.[2-5, 12] To resolve these problems, the common practice in this field is to covalently incorporate chromophores into a polymer network and harden the matrix through crosslinking reactions.[3, 5, 7] However, this process can significantly reduce the poling-induced alignment, and the high temperatures needed for lattice hardening can induce chemical reactions and decomposition of the EO polymers.

4.4.1 Background

In conventional NLO thermoset polymers, the lattice hardening and poling processes occur simultaneously and create several undesirable results. The most important drawback is the “nonlinearity-stability tradeoff” that reduces the full potential of the high optical nonlinearity in organic NLO materials to only 20–40%.[8] The chromophore mobility becomes limited as the polymer begins to crosslink due to the increase in interchain entanglements and the glass transition temperature (T_g). With reduced mobility the chromophore is unable to orientate under the poling field, lowering the EO

activity of the polymer. Another limitation of conventional NLO thermoset polymers is a crosslinking temperature that is usually much higher than the poling temperature. This can result in chromophore decomposition, sublimation, low reproducibility, and/or dielectric breakdown. Experimental results from our lab have shown up to a 50% decrease in EO activity with use of a high-temperature thermoset. Overcoming this nonlinearity-stability tradeoff requires a poling process that allows the high rotational freedom of the chromophores. To accomplish this, the poling process should occur prior to and separated from the lattice-hardening process.

4.4.1.1 Diels-Alder crosslinking systems

To maintain the achieved chromophore alignment, it is necessary to trigger the crosslinking reactions by a very mild condition, preferably without further temperature elevation. Taking all of these requirements into account, Luo and colleagues developed a novel lattice-hardening approach using the Diels-Alder [4+2] cycloaddition reaction.[8] The Diels-Alder (DA) reaction generally involves the coupling of a “diene” with a “dienophile.”[8, 23] This reaction allows the poling process to occur prior to and separated from the lattice-hardening process, providing the materials with high thermal stability and excellent poling efficiency.

4.4.1.2 Diels-Alder process and dynamics

Diels-Alder crosslinkable polymers involve two types of diene moieties. One is the pristine diene molecule (furan) capped to the dienophile (maleimide) to prevent the crosslinking reaction from occurring prior to the lattice-hardening step, Figure 4.16. The

low-boiling-point diene can be cleaved by the retro-Diels-Alder reaction and easily evaporated from the material by heating the polymer within the temperature range of 110°C to 150°C.[8] Once the furan is cleaved, or while it is evaporating, the polymer can be efficiently poled. Using this type of protection method prevents over-crosslinking prior to poling. It also isolates the poling and hardening processes.

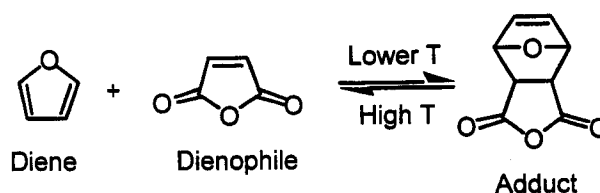


Figure 4.16. Diels-Alder Reversible Reaction

The Diels-Alder poling/crosslinking process is shown schematically in Figure 4.17. Initially the polymer is heated to the deprotection temperature (T_d , 110–150 °C) so the furan can begin to evaporate. As the furan is evaporating, an electric field (E) can be applied to align the chromophores. After a sufficient amount of evaporation/poling time the polymer is cooled to its crosslinking temperature ($T_{\text{crosslink}}$).

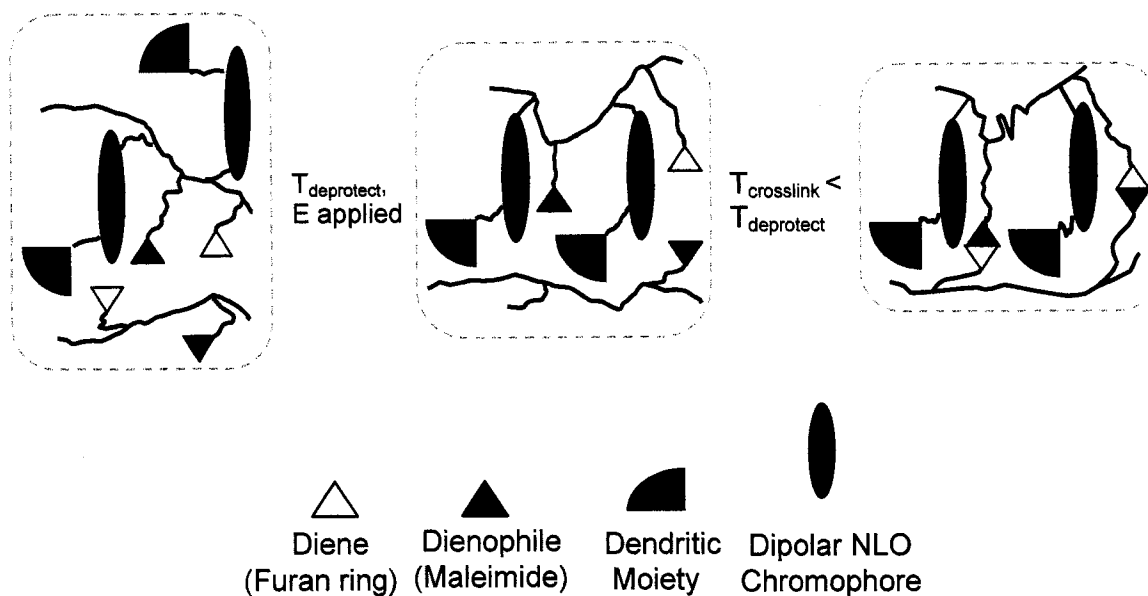


Figure 4.17. Schematic of Diels-Alder Crosslinking Process

The polystyrene-based Diels-Alder (PSDA) low-temperature, crosslinkable polymers show a lot of promise for electro-optic activity and long-term stability. Three different chromophores have been incorporated into PSDA crosslinking systems: a chromium-based chromophore (CRM), the CLD1 chromophore, and the AJL8 chromophore. The CLD1 and AJL8 chromophores provide a nice comparison to the previously discussed PS-CLD series and the PM series.

4.4.2 PSDA-CRM Series

The PSDA-CRM series was the first set of materials to be characterized by this novel crosslinking approach. Initially, we attempted several poling conditions to find the right balance between crosslinking density and poling efficiency. Once an understanding of the two was established, efficient poling could be successfully achieved with a high

crosslinking density. Figure 4.18 is a representation of the diene moieties (highlighted in pink) that can provide reversible or nonreversible crosslinking. The four polystyrene-based Diels-Alder (PSDA) crosslinking derivatives PSDA-CRM1, 2, 3, and 4 are shown in Figures 4.19 and 4.20, respectively. The chromone-type chromophore (CRM) is highlighted in pink. The PSDA-CRM materials included four diene moieties and thermally stable adducts for the purpose of lattice hardening, which are also highlighted with various colors.

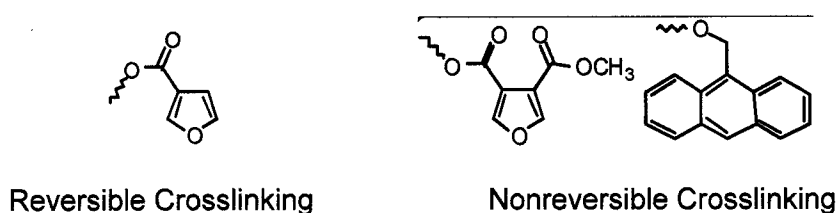


Figure 4.18. Representation of the Diels-Alder Reactions [24]

PSDA-CRM1 was a thermally reversible polymer. PSDA-CRM2 was a thermally nonreversible crosslinked polymer below 250°C created by using a more deactivated furan diester. Attaching an ester group onto the furan of PSDA-CRM3 increased the temperature for the retro-DA reaction by 45°C. The crosslinking between the imido and anthryl groups in polymer PSDA-CRM4 were nonreversible below 110°C and reversible crosslinking above 140°C.[24]

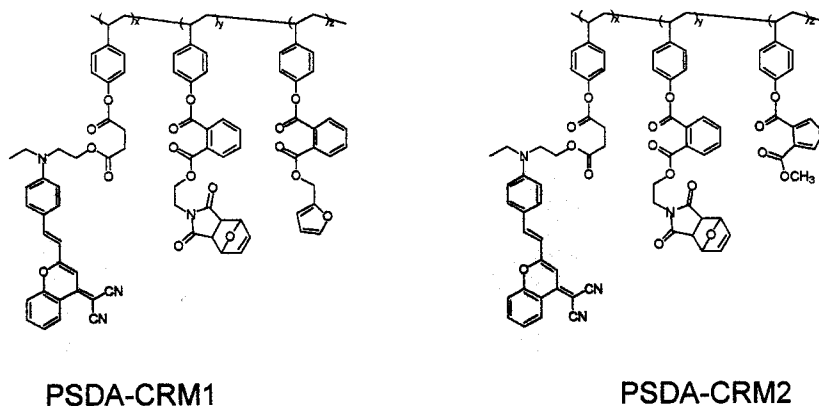


Figure 4.19. Chemical Structure of PSDA-CRM1 and PSDA-CRM2

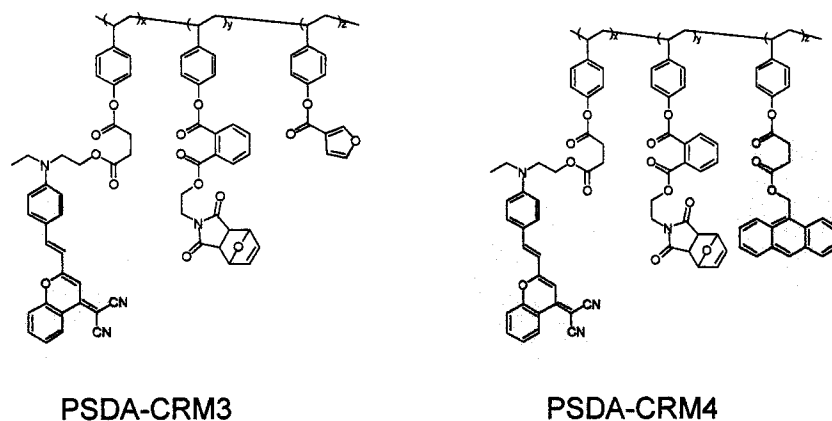


Figure 4.20. Chemical Structure of PSDA-CRM3 and PSDA-CRM4

The initial material characterized (PSDA-CRM1) used a very lengthy deprotection/crosslinking procedure. The material was initially heated to 120°C for 40 minutes for deprotection before depositing the gold electrode. After electrode deposition the sample was reheated to 120°C for 10 minutes to remove any crosslinking that occurred upon cooling from the deprotection step. Then the temperature was lowered to 110°C and the poling voltage was applied (150 V/ μm). The sample was then systematically cooled in varying time and temperature intervals. This poling/crosslinking scheme could take up to 5 hours to accomplish. In an effort to reduce the

poling/crosslinking time needed, an isothermal heating test was done at 110°C for 30 minutes. This demonstrated a weight loss of ~4.5% by weight, which was in good agreement with the furan content used for protection.[24] After isothermal heating the sample became completely insoluble even though it was rapidly quenched to room temperature. Based on this finding, we poled all the subsequent samples and simultaneously crosslinked them to reduce the poling/crosslinking time to 30 minutes without the loss of crosslinking density.

The PSDA-CRM2 polymer had the highest r_{33} value of the series, likely due to a slower crosslinking reaction, which allowed more time for the sample to pole. PSDA-CRM3 had a slightly lower r_{33} value and was thought to have a faster crosslinking reaction, thus causing less chromophore alignment under the same condition. PSDA-CRM4 had the lowest r_{33} value. The relatively lower EO activity of polymer PSDA-CRM4 was mainly due to the large temperature difference between the poling temperature and its intrinsic T_g (110°C vs. 75°C). When materials are poled well above their T_g , the chromophores tend to aggregate, lowering the poling efficiency. Table 4.6 lists all of the optimized poling results for the PSDA-CRM series.

§

To demonstrate the poling efficiency of the crosslinkable polymers, we doped the chromone-type CRM chromophore into a poly(methyl methacrylate) (PMMA) host at the same loading level of 25% by weight. The guest-host sample was poled at 75°C with an electric field of 100 V/ μm for an optimized r_{33} value of 15 pm/V. To make a parallel comparison, we poled the PSDA-CRM3 polymer under the same electric field, in which produced exactly the same EO coefficient, 15 pm/V. This proves that almost the same

high poling efficiency can be reproduced in the PSDA polymers as those exhibited in a guest-host polymer. It is also interesting that applying a high electric field (150 V/ μm versus 100 V/ μm) for PSDA-CRM3 only increased the r_{33} by 1 pm/V. The rate of the PSDA-CRM3 crosslinking reaction dominated the poling efficiency.

Table 4.6. Summary of Properties for the CRM Series

Chromophore	Chromophore Content (wt. %)	Poling Temperature ($^{\circ}\text{C}$)	Poling Field (V/ μm)	r_{33} (pm/V) _{830nm}
PSDA-CRM1	25	110	150	10
PSDA-CRM2	25	110	150	19
PSDA-CRM3	25	110	150	16
		110	100	15
PSDA-CRM4	25	110	150	13
CRM-PMMA	25	75	100	15

These NLO polymers demonstrated the ability to overcome the nonlinearity-stability tradeoff. Their success can be attributed to the significantly delayed the crosslinking of the deprotection step when the poling field was applied, as crosslinking can only be triggered after sufficient deprotection.[8, 23, 24] This “additional” deprotection step separated the poling process from the lattice hardening without disrupting the crosslinking or lowering the alignment. During the further lattice-hardening process, dense crosslinking occurred even with a constant temperature of 110 $^{\circ}\text{C}$. This mild crosslinking condition provides the necessary dense crosslinking needed for solvent resistance. The low-temperature crosslinking also affords very low poling currents during deprotection and crosslinking.

The alignment stability of the PSDA-CRM series was monitored under vacuum at 85 $^{\circ}\text{C}$ for 500 hours (Figure 4.21). After the initial relaxation, PSDA-CRM1, 2, and 3 all

retained ~70% of their original r_{33} values. PSDA-CRM4 was not measured for stability because of its low T_g . Due to the efficient lattice hardening of DA reaction, these materials also exhibited very promising temporal alignment stability.

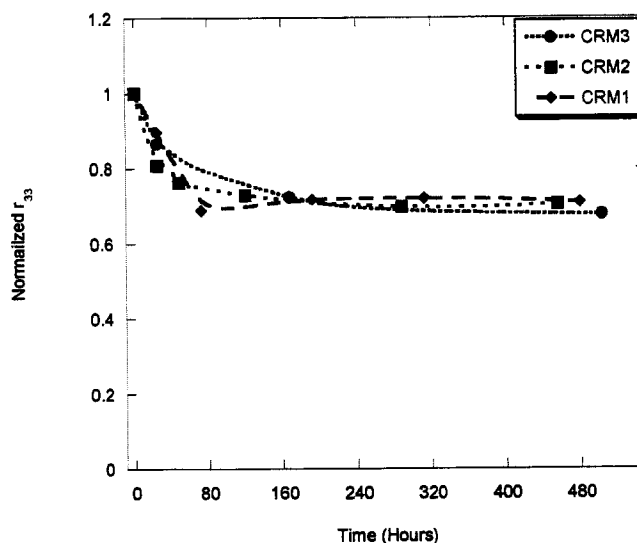


Figure 4.21. Normalized Stability Electro-Optic Coefficient Versus Time

In conclusion, through this innovative Diels-Alder lattice-hardening process, we have been able to overcome the “nonlinearity-stability tradeoff” and reproduce the poling efficiency of a guest-host system while sustaining thermal stability of densely crosslinked polymers. The resultant materials exhibited a combination of excellent poling efficiency and good temporal stability at 85°C. Furthermore, modifying the crosslinking moieties allows us to tune the processing temperature window or reversibility of the Diels-Alder reactions, and achieve hardened lattice with variable stability and processibility.

4.4.3 PSDA-CLD1

The PSDA-CRM materials demonstrated that efficient poling and crosslinking was possible; however, the r_{33} of the CRM chromophore was not enough to meet industry device standards. To overcome this shortcoming, we incorporated the more efficient CLD1 chromophore into a PSDA crosslinkable system following design of the side-chain PS-CLD1 chromophore (Section 4.3.1.2) with the addition of a capped dienophile and diene onto the polymer backbone.[8] This material not only demonstrated the PSDA system with a more efficient chromophore, it also established that the PSDA system was compatible with bulky chromophores.

The PSDA-CLD1 polymer had a chromophore content of 15% by weight and its structure is illustrated in Figure 4.22. In Figure 4.26 the protected dienophile is dormate after heating above 110°C and the dienophile will be deprotected and ready to crosslink. The fluorinated dendron is highlighted in pink, the CLD1 donor blue, CLD1 acceptor purple, the diene green, and the dienophile in yellow.

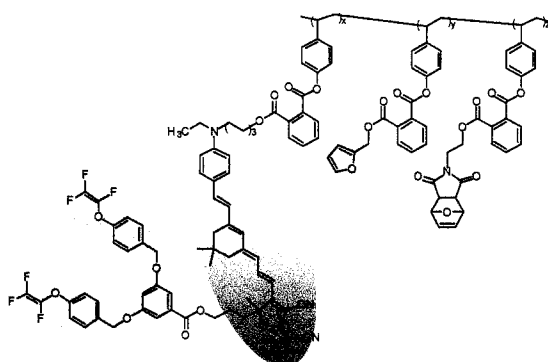


Figure 4.22. Chemical Structure of PSDA-CLD1

The highest temperature used throughout the poling/deprotection process was $\sim 125^{\circ}\text{C}$. Under such conditions the trifluorovinylether functional groups will not polymerize or interfere with the DA crosslinking reaction as dienophiles.[8] After hard baking overnight, the films were baked at 125°C for 30 minutes to evaporate the furan-protecting group. The samples were cooled and a thin layer of gold was deposited for poling. Since the polymer was slightly crosslinked upon cooling, the films were again baked at 120°C for 1 hour to revert them to their thermoplastic precursors. This uncrosslinked film was then cooled to 100°C and poled with a DC field of $142\text{ V}/\mu\text{m}$. The poling temperature was very close to the onset temperature of the retro-DA reaction (110°C) and slightly higher than the typical temperature range used for DA crosslinking ($60\text{--}80^{\circ}\text{C}$). At this temperature, the material possesses the characteristics of a typical thermoplastic polymer. After the poling process, a sequential cooling/curing process (85°C for 1 hour, 75°C for 1 hour, and 65°C for 1 hour) annealed and crosslinked the polymer through the DA reaction. The resulting r_{33} value of PSDA-CLD1 was 42 pm/V . Table 4.7 summarizes PSDA-CLD1 and the other CLD1 samples reported in this thesis.

Table 4.7. Summary of Properties for the CLD Materials

Structure	Chromophore Content (wt. %)	Poling Temperature ($^{\circ}\text{C}$)	Poling Field ($\text{V}/\mu\text{m}$)	r_{33} (pm/V) _{1300nm}
PSDA-CLD1	15	120	140	42
PI-CLD1	25	155	85	35
PS-CLD1	20	95	140	50
CLD1-PS	14	100	100	21

With crosslinking, the poling efficiency of PSDA-CLD1 was comparable to PS-CLD1 because it had a lower chromophore content. The thermally stable PI-CLD1 had a

similar poling efficiency to PSDA-CLD1 given PI-CLD1 had a higher chromophore content and a 27% lower r_{33} value, but applied a 40% lower electric field during poling. The real advantage of PSDA-CLD1 was the poling current, which was 25 times lower than for PI-CLD1. PSDA-CLD1's poling current was consistent with PS-CLD1 and the guest-host CLD1-PS polymers. The r_{33} value of PSDA-CLD1 was significantly higher than that for the guest-host CLD1-PS.

The alignment stability of PSDA-CLD1 was measured at 70°C under vacuum for 300 hours and maintained 80% of its original value. This is lower than PI-CLD1's alignment stability of 90% at 85°C, yet the PI matrix did not offer solvent resistance or a low enough poling current to be feasible for device fabrication.

This PSDA-CLD system demonstrated comparable results to the previously tested CLD side-chain polymers with crosslinking, and that dendronized chromophores can be successfully incorporated in crosslinkable systems.

4.4.4 PSDA-AJL Series

The PSDA-AJL series incorporated the AJL8 chromophore into a PSDA polymer. AJL8 offers the advantage of high poling efficiency in combination with a very low poling current. PSDA-AJL4 and PSDA-AJL5 evaluated the effect of decreasing bulk on the donor of the chromophore. PSDA-AJL4 had an extra benzene ring (yellow) providing bulk at the donor, Figure 4.23. The chromophore content of PSDA-AJL4 and 5 was normalized to 20% by weight.

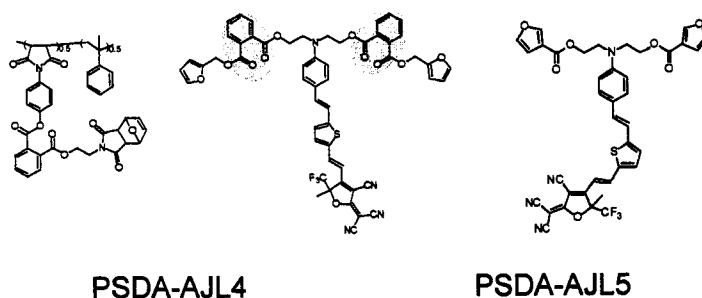


Figure 4.23. Chemical Structures of PSDA-AJL4 and PSDA-AJL5

The optimal poling condition for PSDA-AJL4 involved heating the sample to 125°C for 20 minutes to dissociate the material before applying the voltage. This step attempted to give the sample the rotational freedom of a guest-host system. Next, a 100-V/ μm electric field was applied and held for 10 minutes. The sample was then cooled to 90°C for 1 hour to crosslink and finally cooled to room temperature. The current for this type of poling condition met the required 2 μAmps and the resulting optimized r_{33} value was 43 pm/V, which is slightly higher than the guest-host AJL8-APC polymer.

The first sample PSDA-AJL5 followed PSDA-AJL4's poling guideline and had a disassociation step prior to poling. However, the second sample skipped this step and was heated directly to the poling temperature of 130°C. Since the poling temperature was higher than the disassociation temperature, poling and disassociation could occur simultaneously. Table 4.9 is a summary of the two poling conditions and their results.

Table 4.9. Poling Condition Summary for PSDA-AJL4 and 5

Polymer	Chromophore Content (wt. %)	Poling Temperature (°C)	Poling Field (V/ μ m)	r_{33} (pm/V) _{1330nm}
PSDA-AJL4	20	125	100	43
PSDA-AJL5	20	135	100	19
AJL8-APC	20	140	100	39

Unfortunately, r_{33} value of the less bulky PSDA-AJL5 was half the 43 pm/V value of PSDA-AJL4. It did, nonetheless, demonstrate that dissociation and poling could be achieved simultaneously without the loss of EO activity or a huge increase in current, shortening the poling/crosslinking process considerably. PSDA-AJL4 meets the requirements of a device-quality material: it had a fairly high EO coefficient, good thermal and alignment stability at 85°C (maintained 85%), low poling current, and solvent resistance.

4.5 Conclusions and Future Work

This chapter took a comprehensive look at the relationships between the molecular design and the macroscopic material properties for guest-host chromophore systems, side-chain chromophore systems, and dendritic materials. This chapter also investigated the effects of molecular design on the poling behavior and alignment stability. Crosslinkable material systems were studied in an effort to meet the material requirements of device fabrication.

The guest-host chromophores experimentally confirmed that changes in the chromophore design can have a huge impact on the EO activity. This research

demonstrated that over four times the EO activity can be achieved by manipulating the donor, bridge, and acceptor, and by increasing stability. Suppressing the chromophore–chromophore electrostatic interactions allows use of much higher applied fields during poling and increases the r_{33} value without dielectric breakdown. However, as high $\mu\beta$ chromophores shift more to red, optical loss and poling current increase, lowering their viability for device applications. To compensate for this problem, our current research examined the effects of fluorinated dendrons as a way to lower optical loss and improve poling efficiency.

The dendritic guest-host chromophores exhibited a large blue-shifted absorption, three times higher EO activity, and lower optical loss when compared to the pristine chromophore. The increased mobility created by the free volume around the chromophore enhanced the chromophore alignment and, unfortunately, the chromophore alignment relaxation. These experimental studies have shown that the achievable r_{33} value of a highly efficient nonlinear optical chromophore can be considerably enhanced by shape dendritic modification.

To prevent the loss of the alignment stability while maintaining the positive effects of the dendronized chromophore, we studied several dendronized side-chain materials. Dendronized side-chain polymers performed better than their guest-host polymer counterparts. The site isolation provided by the carefully designed fluorinated dendrimer (4.3.1.1) demonstrated that the chromophore content could be almost doubled through suppressed chromophore–chromophore interactions. Varying how the chromophore and dendrons were attached illustrated how dendron placement can affect the resulting r_{33} value. As a whole these materials demonstrated that attaching a dendron can

significantly improve the EO coefficient and thermal stability if the chromophore has the flexibility to rotate.

The innovative Diels-Alder crosslinking process established a way to overcome the “nonlinearity-stability tradeoff” and reproduce the poling efficiency of guest-host systems while sustaining the thermal stability of densely crosslinked polymers. These polymers exhibited an impressive combination of large optical nonlinearity, tunable processibility, solvent resistance, and high thermal stability. Their ability to cross-link at lower temperatures than are needed to orientate the chromophores has enabled them to be poled with the same rotational freedom as a guest-host system. Furthermore, modifying the crosslinking reagents created a tunable processing temperature window or reversibility of Diels-Alder reactions to achieve a hardened lattice with variable stability and processibility without the risk of damage to the electrode or chromophore sublimation. This DA crosslinking process has been used for device fabrication with the AJL8 chromophore.

The site isolation provided by fluorinated dendrons dramatically enhanced the poling efficiency by allowing the applications of higher poling fields. Optimizing the chromophore design to achieve the highest possible efficient number density by reducing of dipole–dipole interactions and controlling the nanostructure of the chromophore or polymer to attain efficient poling is an effective approach for further improving the electro-optic coefficient. The NLO dendrimer demonstrated that protecting the chromophores with fluorinated dendrons pushes the typical solubility limit of guest molecules in the host matrix to much higher doping levels without an increase in dielectric breakdowns. This approach circumvents the typical poling behavior in which

electrode damage and dielectric breakdown accompany the chromophore loading level increases. This phenomenon prevents the application of a high electric field and adequate chromophore alignment. Future work should be focused on manipulating the chromophore shape and creative poling to find the balance for redefining the allowable number density of high $\mu\beta$ chromophores. Preliminary work with highly doped materials has shown exceptionally high r_{33} values (>200 pm/V), reproducibility, and thermal stability.

4.6 Experimental

All solutions were filtered through the 0.2 μm PTFE filter prior to spin coating. The thin-film preparation for all materials included spin coating onto half-etched ITO substrates. Spin-coating speeds typically ranged from 800–1200 rpm depending on the solid content and desired film thickness. On average the film thickness ranged from 1–2 microns and solid content varied from 8–15% by weight in cyclopentanone. The samples were soft baked at 65°C for approximately 10 minutes and hard baked under vacuum for more than 12 hours after spin coating. All samples were baked under vacuum in a Napco 5851 oven. In general, the guest-host APC samples were hard baked under vacuum at 85°C while guest-host PMMA and PS samples were hard baked at 65°C. The side chain PS and PI samples were hard baked under vacuum at 65 and 85°C, respectively. The dendrimer and PSDA samples were hard baked at 85°C. All thicknesses were measured with a Daktak 3030 profilometer. Each sample was sputter coated with a Denton Desk II sputter coater for 2 minutes, resulting in a gold electrode approximately 100nm thick. We measured the UV/VIS spectrum for all discussed materials by using a Perkin-Elmer

Lambda 9 UV/VIS/NIR spectrophotometer. We conducted poling under an N_2 atmosphere and used a fresh sample for each measurement. All poling was done with a Mettler FP800 oven, Stanford Research Systems, Inc. (SRS) high-voltage power supply PS 350, and a Keithley 617 programmable electrometer.

Notes to Chapter 4:

1. Dalton, L.R., *Rational design of organic electro-optic materials*. Journal of Physics: Condensed Matter, 2003. **15**: p. R897-R934.
2. Burland, D.M., R. Miller, and C. Walsh, *Second-order nonlinearity in poled-polymer systems*. Chemical Review, 1994. **94**: p. 31-75.
3. Dalton, L.R., *Nonlinear optical polymeric materials*. Advances in Polymer Science, 2002. **158**: p. 1-86.
4. Shi, Y.Q., et al., *Low (sub-1-volt) halfwave voltage polymeric electro-optic modulators achieved by controlling chromophore shape*. Science, 2000. **288**(5463): p. 119-122.
5. Kajzar, F., K.-S. Lee, and A.K.-Y. Jen, *Polymeric materials and their orientation techniques for second-order nonlinear optics*. Advances in Polymer Science, 2003. **161**: p. 1-85.
6. Bosshard, C.H., K. Sutter, Ph. Pretre, J. Hulliger, M. Florsheimer, P. Kaatz, and P. Gunter, *Organic Nonlinear Optical Materials*. 1995, New York: Taylor & Francis.
7. Jen, A.K.Y., et al., *Synthesis and characterization of highly efficient, chemically and thermally stable chromophores with chromone-containing electron acceptors for NLO applications*. Advanced Materials, 1999. **11**(6): p. 452.
8. Luo, J.D., et al., *Highly efficient and thermally stable electro-optic polymer from a smartly controlled crosslinking process*. Advanced Materials, 2003. **15**(19): p. 1635-+.
9. Luo, J.D., et al., *Design, synthesis, and properties of highly efficient side-chain dendronized nonlinear optical polymers for electro-optics*. Advanced Materials, 2002. **14**(23): p. 1763-1768.
10. Luo, J.D., et al., *Large electro-optic activity and low optical loss derived from a highly fluorinated dendritic nonlinear optical chromophore*. Chemical Communications, 2002(8): p. 888-889.
11. Liu, S., et al., *Focused microwave-assisted synthesis of 2,5-dihydrofuran derivatives as electron acceptors for highly efficient nonlinear optical chromophores*. Advanced Materials, 2003. **15**(7-8): p. 603-607.
12. Kim, T.-D., et al., *Molecular engineering of highly efficient and thermally stable nonlinear optical polymers for electro-optics*. Polymeric Materials: Science and Engineering, 2004. **91**: p. 273.

13. Ma, H., et al., *Highly efficient and thermally stable electro-optical dendrimers for photonics*. Advanced Functional Materials, 2002. **12**(9): p. 565-574.
14. Zhang, C., et al., *Low V electrooptic modulators from CLD-1: chromophore design and synthesis, material processing, and characterization*. Chemistry of Materials, 2001. **13**(9): p. 3043-3050.
15. Harper, A.W., et al., *Translating microscopic optical nonlinearity into macroscopic optical nonlinearity: the role of chromophore-chromophore electrostatic interactions*. Journal of the Optical Society of America B-Optical Physics, 1998. **15**(1): p. 329-337.
16. Zhou, M., *Low-loss polymeric materials for passive waveguide components in fiber optical telecommunication*. Optical Engineering, 2002. **41**(7): p. 1631-1643.
17. Luo, J.D., et al., *Nanoscale architectural control and macromolecular engineering of nonlinear optical dendrimers and polymers for electro-optics*. Journal of Physical Chemistry B, 2004. **108**(25): p. 8523-8530.
18. Ma, H., A.K.-Y. Jen, and L. Dalton, *Polymer-based optical waveguide materials, processing, and devices*. Advanced Materials, 2002. **14**(19): p. 1339-1365.
19. Luo, J.D., et al., *A side-chain dendronized nonlinear optical polyimide with large and thermally stable electrooptic activity*. Macromolecules, 2004. **37**(2): p. 248-250.
20. Pitois, C., A. Hult, and D. Wiesmann, *Absorption and scattering in low-loss polymer optical waveguides*. Journal of the Optical Society of America B-Optical Physics, 2001. **18**(7): p. 908-912.
21. Percec, V., et al., *Visualizable cylindrical macromolecules with controlled stiffness from backbones containing libraries of self-assembling dendritic side groups*. Journal of the American Chemical Society, 1998. **120**(34): p. 8619-8631.
22. Cai, Y.M. and A.K.Y. Jen, *Thermally stable poled polyquinoline thin film with very large electro-optic response*. Applied Physics Letters, 1995. **67**(3): p. 299-301.
23. Kwart, H. and K. King, *The reverse Diels-Alder or retrodiene reaction*. Chemical Review, 1968. **68**(4): p. 415-447.
24. Haller, M., et al., *A novel lattice-hardening process to achieve highly efficient and thermally stable nonlinear optical polymers*. Macromolecules, 2004. **37**(3): p. 688-690.

Chapter 5. Limitations of the Simple Reflection Technique

5.1 Introduction

The Teng-Man or simple reflection technique [1] is commonly accepted as a standard method for determining the electro-optic properties of a poled polymer. This technique is based on several assumptions including no transparent electrode or material absorption, no other modulation effects, no multireflections, negligible birefringence, and $r_{33} \approx 3r_{13}$. The experiment also assumes the results are a purely real nonlinear response. In reality, the higher order nonlinear contributions cannot always be neglected. This chapter will examine the effects of these assumptions on the measurement accuracy and possible modifications to account for these contributions.

The reduction in experimental accuracy from electrode and material contributions is an interrelated problem. As the EO material's absorption peak is pushed closer to the near infrared (NIR), it has become critical to accurately measure the EO coefficient at longer wavelengths than the transparency of commercial ITO allows. Levy et al demonstrated that accurate results with the simple Teng-Man model depend on the ITO transparency and that the material's absorption peak (λ_{max}) is far from the measurement wavelength.[2] The measurement assumes that the ITO is completely transparent, there is no absorption from the polymer film, and the light is only reflected at the gold electrode. An ITO or EO polymer film that is absorbing also will be reflecting. Earlier work has shown that measurements at different angles of incidence can lead to a more reliable estimation of the EO coefficient even when the absorption band of the polymer is near the measurement wavelength.[2-5] The dependence of

the measurement accuracy on ITO's transparency and the material absorption will be discussed in detail in sections 5.4 and 5.5. When the assumptions of the Teng-Man method are no longer valid, it is necessary to use a numerical calculation that applies anisotropic Fresnel relationships.[2-5] This type of calculation requires a precise knowledge of the refractive index and thickness of each layer.

Absorption is commonly represented by the extinction coefficient (κ), which is part of complex refractive index (\hat{n}) described by equation 5.1.[6]

$$\hat{n} = n + i\kappa \quad (5.1)$$

Since the EO coefficient is based on the change in refractive index with respect to an applied electric field it can also be complex. Similar to the definition of the real part of the EO coefficient (r_{33}) introduced in Chapter 2 and equation 5.2, the imaginary part of the electro-optic coefficient (s_{33}) corresponds to changes in the extinction coefficient with an applied electric field, equation 5.3.[2, 3, 7, 8]

$$\delta n_o = -\frac{1}{2} n_o^3 r_{13} \frac{\delta V}{d} \text{ and } \delta n_e = -\frac{1}{2} n_e^3 r_{33} \frac{\delta V}{d} \quad (5.2)$$

$$\delta \kappa_o = -\frac{1}{2} n_o^3 s_{13} \frac{\delta V}{d} \text{ and } \delta \kappa_e = -\frac{1}{2} n_e^3 s_{33} \frac{\delta V}{d} \quad (5.3)$$

Clays and Schildkraut demonstrated that electrochromic effects can be quantified by the imaginary part of the EO coefficient and their presence can lead to a possible over or underestimation of the real portion of the EO coefficient.[7] Electrochromic effects can arise from the large difference between the ground- and the excited-state dipole

moments.[7] Fitting an averaged r_{33} and s_{33} through a modified multi-angle Teng-Man technique can determine the contributions of the real and imaginary parts of the measured electro-optic coefficient and the presence of higher order effects.[5, 7]

5.2 Multi-Angle Electro-Optic Measurement

Previous work has shown that fitting an averaged r_{33} and s_{33} value by measuring several angles can be useful in determining presence of other contributions.[5] Variations in the measured results that depend on angle of incidence are due to multiple reflections while modulation changes depend on material absorption.[3] Multi-angle experiments typically fit an entire intensity profile of a given compensator scan.[2, 5, 7] Fitting the data in this manner also provides a way to calculate the imaginary electro-optic coefficient (s_{33}). Equation 5.4 was previously introduced in Chapter 3 to express the intensity for a compensator scan during the first part of the simple reflection measurement when no electric field is applied. The phase difference is represented by ϕ_{sp} , the compensator position by ϕ_c , and the output laser intensity at the detector as I_o and I_c is equal to half the maximum intensity.[1, 5, 9, 10] Equation 5.4 can be rewritten as equation 5.5.[2, 3, 5, 7]

$$I_o = 2I_c \sin^2 \left(\frac{\phi_{sp} + \phi_c}{2} \right) \quad (5.4)$$

$$I_o = I_{dc} = a + b \cos(\phi_{sp} + \phi_c), \quad b = I_c \quad (5.5)$$

In Chapter 3 the change in the phase shift was approximated by equation 5.6. The real part of the electro-optic coefficient was calculated by fitting the linear relationship

between the changes in the modulated intensity and the modulated voltage, equation 5.7 assuming $n_o \approx n_e \approx n$ and $r_{33} = 3 r_{13}$. [1, 9, 10]

$$\frac{I_m}{I_c} \approx \delta\phi_{sp} \quad (5.6)$$

$$r_{33} = \left(\frac{3\lambda}{4\pi n^2} \right) \left(\frac{I_m}{I_c V_m} \right) \left(\frac{(n^2 - \sin^2 \theta)^{1/2}}{\sin^2 \theta} \right) = \left(\frac{I_m}{V_m} \right) (\text{constant}) \quad (5.7)$$

For multi-angle measurements the modulated voltage (V_m) is held constant. The modulated intensity is measured over all the compensator positions and shown in Figure 5.1(a). According to the assumptions of the Teng-Man measurement at positions A and B, the modulated intensity should be equal, at a maximum, and phase shifted. Figure 5.1(a) shows this is approximately true and the corresponding slopes are similar for the modulated intensity versus applied field, Figure 5.1(b). However, more absorptive materials are typically shifted and the intensities are significantly different, which corresponds to the difference in the separation of the two slopes, Figure 5.5. In this situation the material no longer fits in the parameters of the TMT.

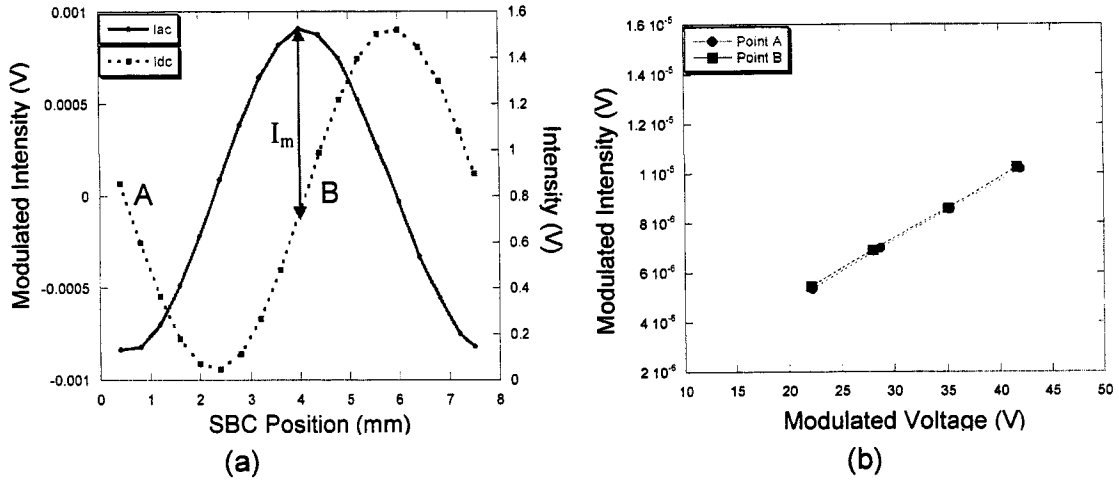


Figure 5.1. (a) Intensity and Modulated Intensity for a Compensator Scan and (b) Modulated Intensity versus Modulated Voltage

The I_{ac} curve is then fit to equation 5.8 to find the value of I_m (Figure 5.1(a)), which is similarly related to $\delta\phi_{sp}$ by equation 5.9.[2] The real portion of the EO coefficient is then calculated by equation 5.10 and the imaginary portion of the EO coefficient is similarly calculated with equation 5.11.[3, 5, 7] Again, the assumptions that $n_o \approx n_e \approx n$, $r_{33} = 3 r_{13}$ and $s_{33} = 3 s_{13}$ are used.[1, 9, 10]

$$I_{ac} = \delta a + \delta b \cos(\phi_{sp} + \phi_c) + b \sin(\phi_{sp} + \phi_c) \delta \phi_{sp} \quad (5.8)$$

$$\frac{I_{m1} - I_{m2}}{2} \frac{1}{b} = \frac{I_{m1} - I_{m2}}{2} \frac{1}{I_c} = \frac{I_m}{I_c} \approx \delta \phi_{sp} \quad (5.9)$$

$$\delta \phi_{sp} = \left(\frac{n^2 \sin^2 \theta}{(n^2 - \sin^2 \theta)^{1/2}} \right) \left(\frac{4\pi V_m r_{33}}{3\lambda} \right) \quad (5.10)$$

$$\frac{\delta b}{b} = \left(\frac{n^2 (n^2 + \sin^2 \theta)}{(n^2 - \sin^2 \theta)^{1/2}} \right) \left(\frac{4\pi V_m s_{33}}{3\lambda} \right) \quad (5.11)$$

When multiple angles are measured an average r_{33} and s_{33} value can be determined and used in the above equations. Michelotti et al introduced the normalized variable

(Λ) represented by equation 5.12, which is a function of the average electro-optic coefficient (\bar{r}_{33}), the refractive index (n), and the angle of incidence (θ) to compare the experimental results.[5] If the material is within the assumptions of the TMT, the experimental results at each angle and the results fitted will be the same.

$$\Lambda(\theta) = \bar{r}_{33} \frac{n^2 \sin^2 \theta}{\sqrt{n^2 - \sin^2 \theta}} \quad (5.12)$$

When the material does not fit the simplified Teng-Man model a rigorous model must be used to accurately determine the contribution of each layer to the real and imaginary electro-optic coefficients.

5.3 Rigorous Model

When a sample does not fit into the assumptions of the TMT, a rigorous model needs to be employed to account for multireflections and material and/or ITO absorption. Park et al recently published a rigorous model that represented the data in a way that clearly showed the error between the simplified Teng-Man model and the rigorous fit.[3] The Teng-Man approach only considers the polymer film's contribution to the phase shift and assumes the glass and ITO are transmitting perfectly and the gold (Au) is reflecting perfectly, Figure 5.2(a). The rigorous fit includes the Fresnel reflection coefficients for all six layers, Figure 5.2(b).

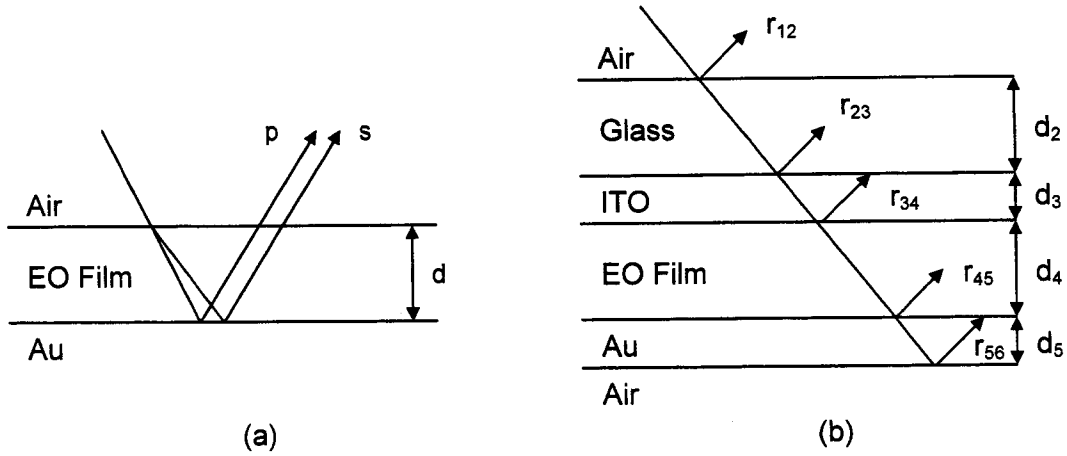


Figure 5.2. (a) Simple Model (b) Rigorous Model

In both models the EO coefficients are determined by Frensel reflection coefficients. Equation 5.5 can be rewritten as 5.13 and the coefficients a and b can be expressed as equation 5.15 in terms of the Frensel reflection coefficients for the s and p polarizations (r_s and r_p). [2, 3, 6, 7, 10, 11] The relationship between Frensel coefficients (r_s and r_p), the ellipsometric parameter ($\tan\Phi$), and the phase shift is described by equation 5.16. [3, 6, 7, 11]

$$I_{dc} = a + b \cos(\phi_{sp} + \phi_c) = \frac{I_o}{4} |r_s e^{i\phi_c} - r_p|^2 = \frac{I_o}{4} |e^{2i\beta_s d} e^{i\phi_c} - e^{2i\beta_p d}|^2 \quad (5.13)$$

$$I_{ac} = \delta a + \delta b \cos(\phi_{sp} + \phi_c) + b \sin(\phi_{sp} + \phi_c) \delta \phi_{sp} \quad (5.14)$$

$$a = \frac{I_o}{4} (|r_s| - |r_p|)^2, \quad b = \frac{I_o}{2} |r_s| |r_p| \quad (5.15)$$

$$\frac{r_p}{r_s} = \tan \Phi e^{-i\phi_{sp}} \quad (5.16)$$

For the simple model r_s and r_p are expressed as equation 5.17. In equation 5.18 β is the complex propagation constant ($\beta = \beta_r + i\beta_i$), d is the EO polymer film thickness, and $\hat{\alpha}$ is the complex propagation angle.

$$r_s = -e^{2i\beta_s d}, \quad r_p = -e^{2i\beta_p d} \quad (5.17)$$

$$\beta_s = \frac{2\pi}{\lambda} \hat{n} \cos(\hat{\alpha}_s), \quad \beta_p = \frac{2\pi}{\lambda} \hat{n} \cos(\hat{\alpha}_p) \quad (5.18)$$

Equation 5.19 and 5.20 demonstrate that the phase shift only depends on the real phase retardation in the film.[3]

$$\phi_{sp} = 2d(\beta_{sr} - \beta_{pr}) \quad (5.19)$$

$$\delta\phi_{sp} = 2d(\delta\beta_{sr} - \delta\beta_{pr}) \quad (5.20)$$

$$\delta b = -2db(\delta\beta_{si} - \delta\beta_{pi}) \quad (5.21)$$

In the case of the rigorous model, all the layers are considered to create a more complicated Fresnel coefficient, equation 5.22.[2] The reflection coefficient for each layer is defined by equation 5.23.

$$r = \frac{r_{23} + r'_{34} e^{2i\beta_3 d_3}}{r_{23} r'_{34} e^{2i\beta_3 d_3}} \quad r'_{34} = \frac{r_{34} + r'_{45} e^{2i\beta_4 d_4}}{r_{34} r'_{45} e^{2i\beta_4 d_4}} \quad r'_{45} = \frac{r_{45} + r'_{56} e^{2i\beta_5 d_5}}{r_{45} r'_{56} e^{2i\beta_5 d_5}} \quad (5.22)$$

$$r_{ij} = \frac{Z_j - Z_i}{Z_j + Z_i} \quad Z_s = \frac{1}{\sqrt{\hat{n}_s^2 - \sin^2 \theta}} \quad Z_p = \frac{1}{\hat{n}_s} \sqrt{1 - \left(\frac{\sin \theta}{\hat{n}_p} \right)^2} \quad (5.23)$$

The simple model is related to the rigorous through the coefficients U_s and U_p and by rewriting equation 5.13 as 5.26.[3]

$$U_s = r_s e^{-2i\beta_{4s}d_{4s}} = \frac{r_{23s} + r'_{34s} e^{2i\beta_{3s}d_{3s}}}{r_{23s} r'_{34s} e^{2i\beta_{3s}d_{3s}}} e^{-2i\beta_{4s}d_{4s}} \quad (5.24)$$

$$U_p = r_p e^{-2i\beta_{4p}d_{4p}} = \frac{r_{23p} + r'_{34p} e^{2i\beta_{3p}d_{3p}}}{r_{23p} r'_{34p} e^{2i\beta_{3p}d_{3p}}} e^{-2i\beta_{4p}d_{4p}} \quad (5.25)$$

$$I_{dc} = \frac{I_o}{4} \left| U_s e^{i\phi_c} e^{2i\beta_{4s}d_{4s}} - U_p e^{2i\beta_{4p}d_{4p}} \right|^2 \quad (5.26)$$

This method provides a comparison of the experimental and fitted data in a slightly different manner than the previously explained method by Michelloti.[5] In equations 5.27 and 5.28, $\text{Im}(\delta U_c / U_c)$ and $\text{Re}(\delta U_c / U_c)$ are the error correction terms to the simple model. They are additive to the simple model because the rigorous model approaches the simple model when r_{23} , r_{34} , and r_{56} vanish and r_{45} goes to 1.[3] Equations 5.10 and 5.11 define $(\delta\phi_{sp})_{\text{simple}}$ and $(\delta b/b)_{\text{simple}}$ and the rigorous fit is determined by adding the error correction terms to the simple model.

$$(\delta\phi_{sp})_{\text{rigorous}} = (\delta\phi_{sp})_{\text{simple}} + \text{Im}\left(\frac{\delta U_c}{U_c}\right) \quad (5.27)$$

$$\left(\frac{\delta b}{b}\right)_{\text{rigorous}} = \left(\frac{\delta b}{b}\right)_{\text{simple}} + \text{Re}\left(\frac{\delta U_c}{U_c}\right) \quad (5.28)$$

$$\left(\frac{\delta U_c}{U_c}\right) = \left(\frac{\delta U_s}{U_s}\right) + \left(\frac{\delta U_p}{U_p}\right)^* \quad (5.29)$$

$$U_c = U_s U_p^* \quad (5.30)$$

The example published by Park et al demonstrated the r_{33} value was underestimated due to the material absorption.[3] The following experiments were conducted to determine the effects of the variations in the ITO and material absorption on the measured r_{33} value.

5.4 Electrode Contributions

The effects of the ITO absorption on the accuracy of the measurement was first studied by Michelotti et al.[5] His multi-angle experiment demonstrated that when the frequently used ITO electrode is in the spectral region where ITO is nearly transparent, the error margin introduced from the ITO electrode is negligible, Figure 5.3(A).[5] When the ITO is absorbing it becomes more reflective and the two electrodes behave as a Fabry-Perot resonator and the electro-optic coefficients obtained through this method are incorrect, illustrated in Figure 5.3(B).[5]

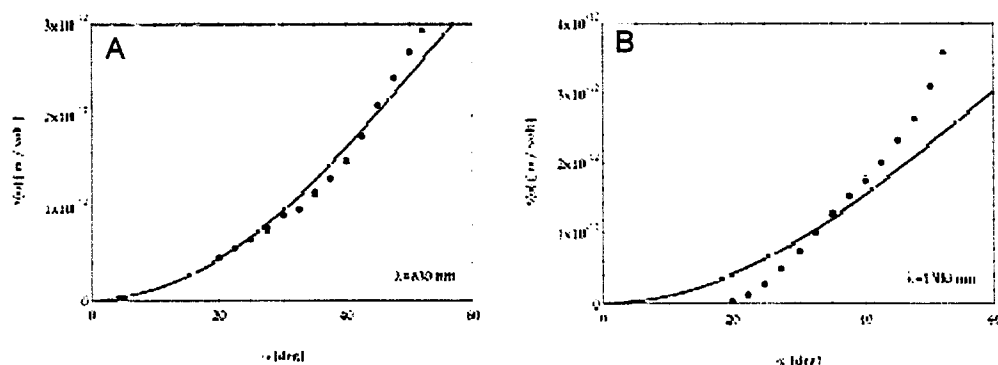


Figure 5.3 Published Data of the Normalized Variable (Δ) at Multiple Angles and Different Wavelengths [5]

Since the polymer used in this experiment was DR1 (Table 2.1) with an absorption peak (λ_{max}) that is far from the measurement wavelength, the error increase at 1315 nm

was thought to be dependent on the ITO absorption. The transparency of current commercial ITO begins to diminish beyond 1200 nm, raising concern around its use at 1550 nm.[12]

The following experiment compared three semitransparent electrodes. The first was the commercially available ITO from Abrisa/USPG Glass & Coatings/Worldwide. A second ITO-coated sample and a zinc-doped (ZITO) sample made by Northwestern University (NW) were also tested.[13] The transparency of each electrode coating was measured, Figure 5.4.

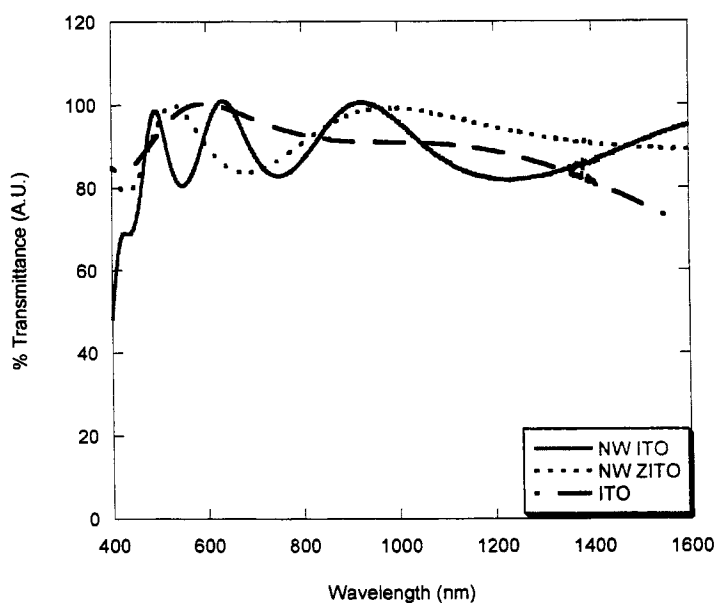


Figure 5.4. Percent Transmittance versus Wavelength

Figure 5.4 illustrates that the transparency of the commercial ITO began to diminish past 1200 nm. The NW-ZITO offered a higher transparency at 1315 nm but its transparency also decreased at the longer wavelengths. The NW-ITO sample's transparency is somewhat misleading because of its increased film thickness. Thicker

films will exhibit a greater number of oscillations over a given wavelength range, while thinner films will exhibit fewer oscillations over the same range.[14] The true transparency of the NW-ITO could be found by fitting the entire curve however the trend of the oscillation peaks gives an approximate transparency. The change in NW-ITO's deposition parameters in comparison to the commercial ITO demonstrated an overall improved transmittance. ITO's optical properties depend on the correct oxygen content to minimize absorption and the film's thickness. These properties affect the spectral transmittance and reflectance of the film. Commercial ITO has a thickness of approximately 150 nm, the ZITO had a thickness of 300 nm, and the NW-ITO had a thickness 450 nm. The sheet resistance of the Abrisa ITO was 50 Ω/sq , the NW-ZITO was 87 Ω/sq , and the NW-ITO was 1836 Ω/sq .

Identical samples were prepared with the AJL8 chromophore (Section 4.2.1) to compare measurement accuracy and poling efficiency on each of the different transparent electrodes. Since the two NW electrodes had not previously been tested at the University of Washington, we used a more conservative poling sequence to ensure that no electrode damage occurred during poling. We measured the real electro-optic coefficient (r_{33}) for each sample by using the multi-angle scan at 1315 nm and 1550 nm.[3, 5, 7]

Michelotti and colleagues demonstrated that measurements made in the transparent region of the semitransparent electrode at the two bias points (A and B) can generate an averaged r_{33} value with an 8% error.[5, 12] This experiment also confirmed that measuring at only one bias point instead of determining an averaged r_{33} value can give results that are completely wrong. Figure 5.5 shows the experimental results for the

poled polymer film on the commercial ITO electrode and on the NW-ITO electrode when measuring the slope at both Babinet-Soleil compensator positions (A and B) for the 1550 nm laser. On the graph of the poled polymer film on commercial ITO (a) the slopes of the two lines are significantly different, resulting in considerably different r_{33} values, 35 and 22 pm/V. In contrast, graph (b) of the poled polymer on the NW-ITO electrode has two approximately equal slopes with similar r_{33} values, 28 and 30 pm/V.

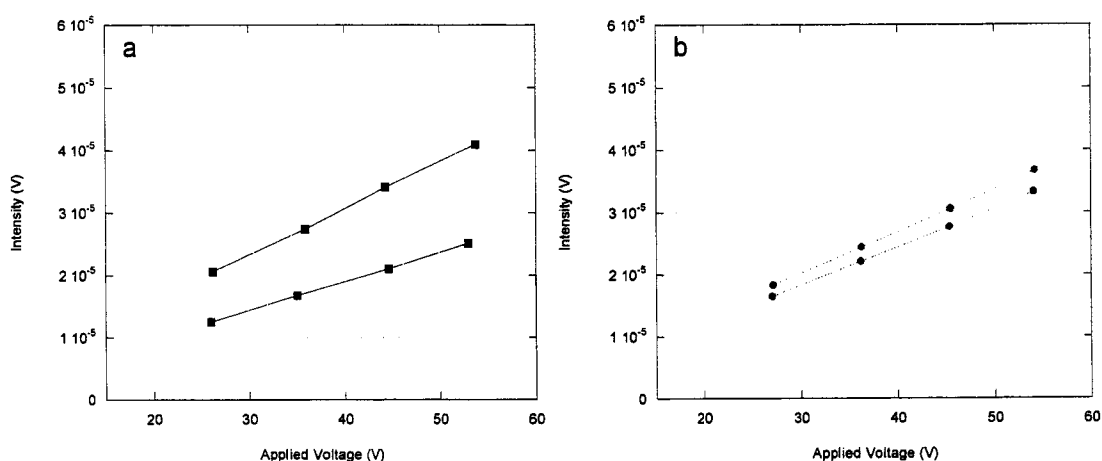


Figure 5.5. Modulated Intensity versus Modulated Voltage for a Poled Polymer Film on a Commercial ITO Electrode (a) and a NW-ITO Electrode (b) Measured at 1550 nm

Measuring at one angle demonstrates an increase in the experimental error at 45° but it does not give the full picture. When the data is fitted with the rigorous model, which does not consider the ITO to be completely transparent, the effects of the changes in the different ITO become more apparent.

The results for the commercial ITO sample shown in Figure 5.6 demonstrate a departure from the simple model at the higher angles. Since the transparency of commercial ITO has improved, the change is not as extreme as those published in 1990. The experimental data reveal a more noteworthy roll-off at 1550 nm, which

could possibly be attributed to misalignment during the measurement process.

Ideally the sample would be carefully remeasured.

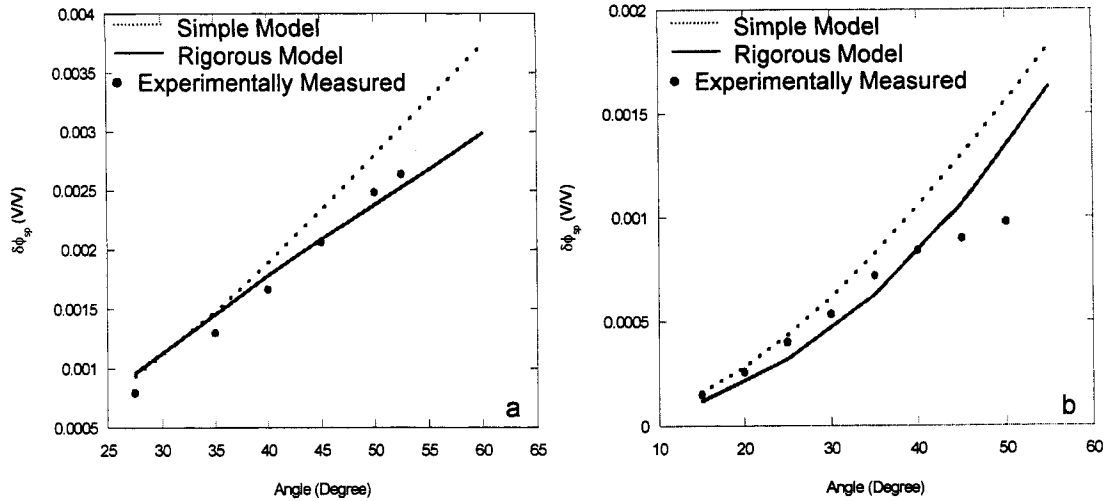


Figure 5.6. (a) $\Delta\phi_{sp}$ versus Measurement Angle Measured at 1315 nm (b) $\Delta\phi_{sp}$ versus Measurement Angle Measured at 1550 nm for Abrisa ITO

Figure 5.7 illustrates the results of the NW-ITO. They showed a very close match to the simple model below $\sim 50^\circ$. The polymer film thickness of the NW-ITO sample was the same as the Abrisa ITO; however, the ITO thickness was considerably higher, changing the fit of the rigorous model at 1315 nm. The difference between the NW-ITO simple model and the rigorous fit at 45° and 1550 nm was 2×10^{-4} , which corresponds quite well to the experimental data. The Abrisa ITO, however, shows a significant difference between the simple model and the experimental data. This large variation from the simple model would have produced a separation between the two slopes at A and B, shown above in Figure 5.5.

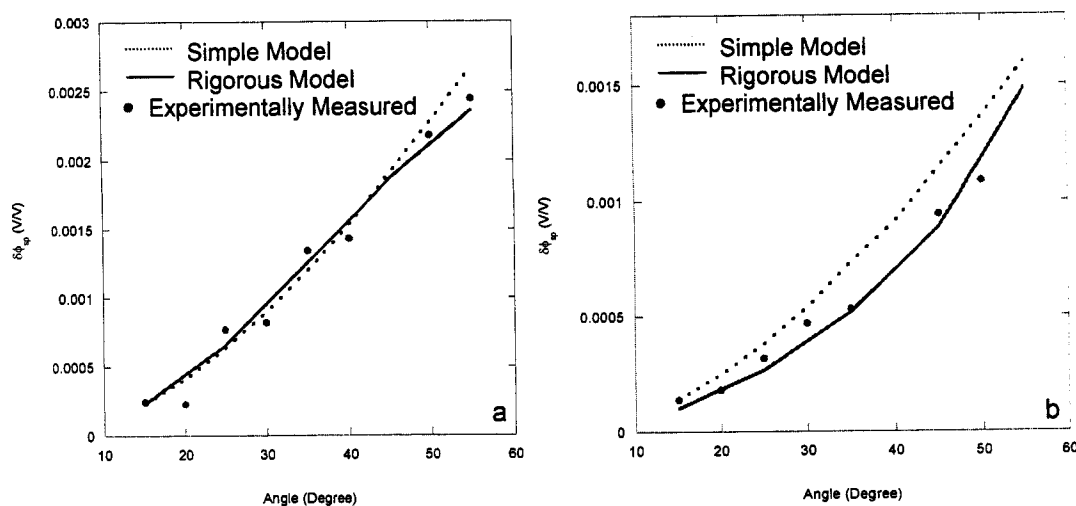


Figure 5.7. (a) $\delta\phi_{sp}$ versus Measurement Angle Measured at 1315 nm (b) $\delta\phi_{sp}$ versus Measurement Angle Measured at 1550 nm for NW-ITO

Figure 5.8 shows the experimental data, the simple and rigorous fits for the NW-ZITO. The rigorous model accounts for the contribution of the refractive indices and thickness polymer film and ITO that create the deviation from the simple model at the higher angles when measuring at 1315 nm and 1550 nm. The rigorous model more accurately follows the trend of the data at both wavelengths. It is interesting to note the change in the behavior of the rigorous model at the higher angles for 1315 nm when the thickness of the polymer film and ITO recipe/index changed.

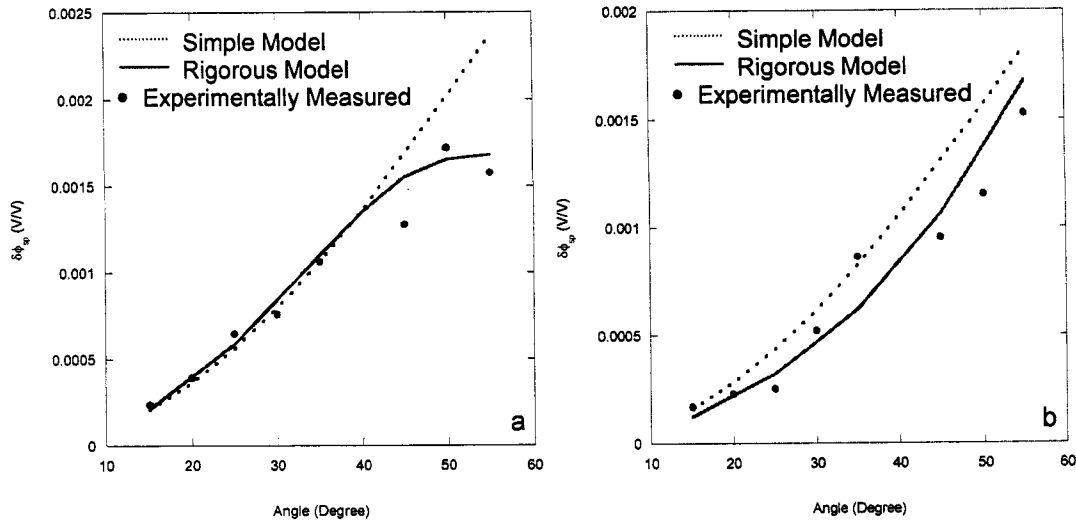


Figure 5.8. (a) $\delta\phi_{sp}$ versus Measurement Angle Measured at 1315 nm (b) $\delta\phi_{sp}$ versus Measurement Angle Measured at 1550 nm for NW-ZITO

Figure 5.9 represents $\delta b/b$ versus measurement angle for the NW-ITO (a) and the Abrisa ITO (b) at 1315 nm. The correction term for $\delta b/b$ is dependent on the real parameters of the rigorous model and is the dominant factor in the rigorous model's fit with the experimental results. In the more absorptive EO polymer cases the rigorous model is very sensitive to the polymer film thickness, which in this instance is the same. This example demonstrates that the change in ITO thickness and index has a profound effect on the experimental results. This result also shows that the simple model is not effective in calculating the imaginary electro-optic coefficient (s_{33}). The fitted imaginary EO coefficient (s_{33}) for the Abrisa ITO was 0.5 pm/V.

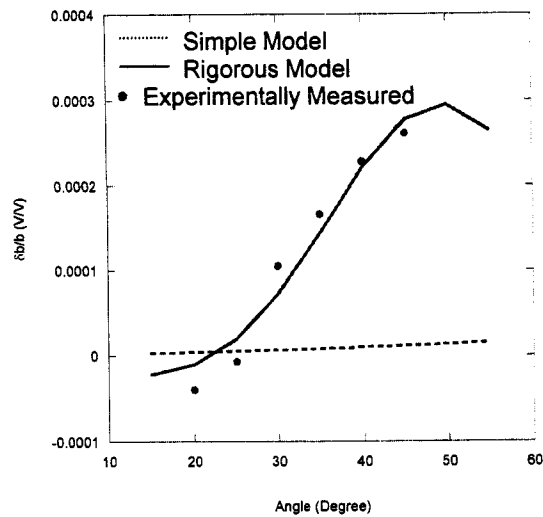


Figure 5.9 $\delta b/b$ versus Measurement Angle for Abrisa ITO Measured at 1315 nm

Table 5.1 lists the fitted r_{33} values for each electrode using the simple and rigorous models. The various electrodes showed similar values for the real EO coefficients from both models.

Table 5.1. Electro-Optic Coefficients (r_{33}) at 1315 nm and 1550 nm.

Wavelength (nm)	ITO _{simple} (pm/V)	ITO _{rigorous} (pm/V)	ZITO _{simple} (pm/V)	ZITO _{rigorous} (pm/V)	NW-ITO _{simple} (pm/V)	NW-ITO _{rigorous} (pm/V)
1315	33	32	31	34	35	30
1550	24	23	24	25	21	23

The commercial ITO demonstrated the largest deviation from the simple model at 1315 nm, which was accounted for in the rigorous model. The fit at 1550 nm was less than ideal, most likely from alignment issues during the measurement. Overall, modifying the ITO will not significantly improve the accuracy of the Teng-Man measurement at

45°. The poling efficiency was essentially unaffected by the different electrodes.

The resulting r_{33} values for the poled polymer films on each of the electrodes were within experimental error of each other. This experiment showed that although modifying processing steps and dopants can slightly improve the transparency of ITO, it is still absorbing in the NIR and the best solution to this problem would be to use the rigorous fit in future EO calculations. The simple model does not provide reasonable fit for the imaginary EO coefficient and the rigorous fit should be used to determine s_{33} . Even though the real EO coefficient did not change significantly, the rigorous model demonstrates a better fit with the experimental data, especially at 1550 nm. The difference between the simple and rigorous model is on the order of 10^{-4} for the higher angles of incidence, which is partially dependent on the absorption of the polymer. Section 5.5 will demonstrate that material absorption exerts a much more predominant effect on the deviation from the simple model.

5.5 Material Contribution

Studies in the early 1990s introduced the effects of material absorption on the EO measurement with limited resolution.[2, 7] The polymers of today differ considerably different from those tested in the past, and as the EO materials have shifted further to longer wavelengths and the chromophore loading has increased, the experimental error also has increased. In Figure 5.10 the measured values with the Teng-Man technique vary from 132 pm/V at position A to 420 pm/V at position B. The average value of 276 pm/V is reasonable, but this degree of error is not.

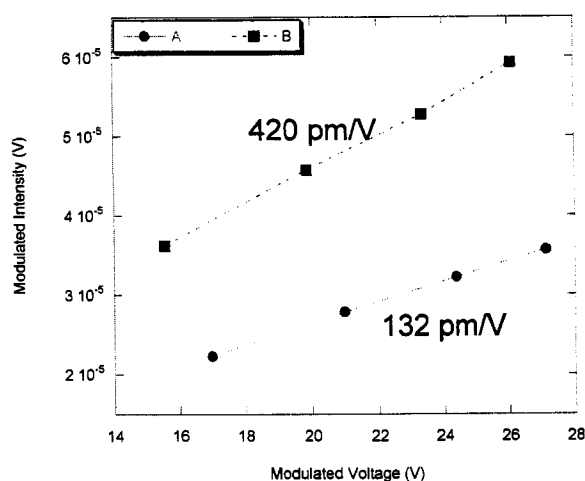


Figure 5.10. Modulated Intensity versus Modulated Voltage

In the following experiment we used the multi-angle method with a set of materials doped into amorphous polycarbonate (APC) between 25 and 30% by weight with varied absorption peaks (λ_{\max}). The experiment was designed to see the extent of deviation from the simple model and its relation to the material absorption. When fitted with the simple model [5], these results did not show a clear trend in the material's absorption and measurement error. To better understand these results, we used the rigorous model that included the effects of the ITO, gold and the EO polymer film. Figure 5.11 represents the absorption spectra for the materials measured in this study. Their chemical structures are shown in Figure 5.12.

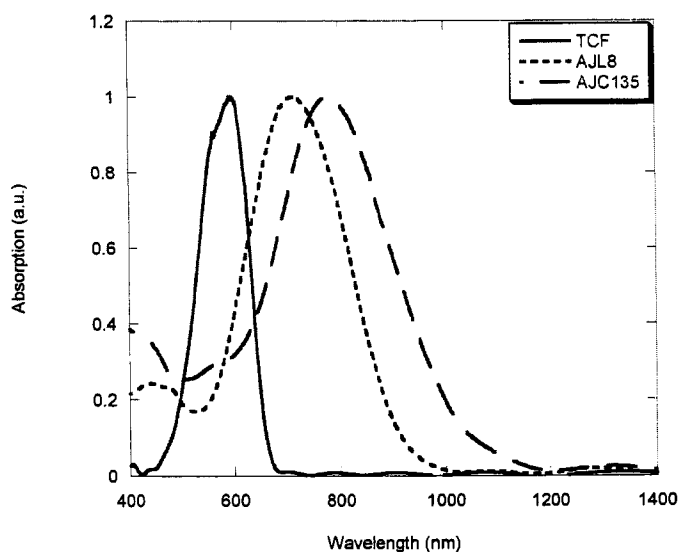


Figure 5.11. Absorption Spectra of the TCF, AJL8, and AJC135 Chromophores

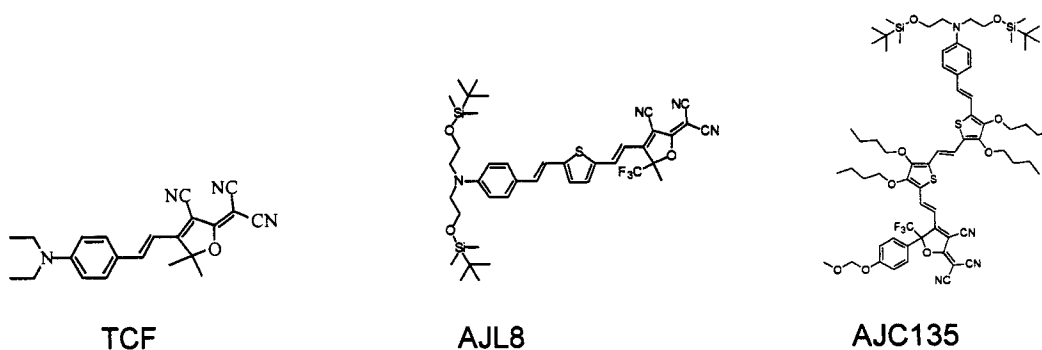


Figure 5.12. Chemical Structures of the TCF, AJL8, and AJC135 Chromophores

The absorption at the 1315 nm measurement wavelength increases as the absorption peak shifts from TCF's peak of 594 to AJC137's 800 nm peak. Figures 5.13 and 5.14 illustrate that the experimental data deviate further from the simple model as the absorption peak and chromophore content increase. Figure 5.13 shows the change in the separation from the simple and rigorous models for the TCF chromophore; again, the experimental and rigorous fit deviate from the simple at the higher angles.

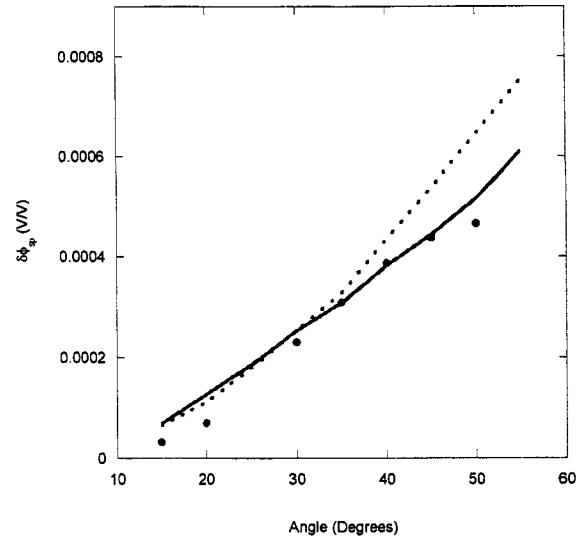


Figure 5.13. $\delta\phi_{sp}$ versus Measurement Angle 1315 nm

The trend of the experimental data and the rigorous model is similar to the previously discussed AJL8 samples; however, the scale of the deviation at the higher angles is on the order of 10^{-5} versus AJL8's 10^{-4} . This makes sense since TCF's absorption peak is considerably blue shifted from AJL8 and further limits the experimental error to only ITO absorption.

The change from AJL8 to AJC135 begins to show the real effects of the material absorption. Figure 5.14 illustrates $\delta\phi_{sp}$ versus measurement angle for AJC135 (a) and $\delta b/b$ versus measurement angle (b). The average EO coefficient for the simple model was 40 pm/V while the rigorous model fit had an average EO coefficient of 48 pm/V. Since the continuing focus of this research has been on increased EO coefficients, a 15% loss in value due to experimental error is not acceptable. Figure 5.14 (b) demonstrates that the key contribution to the reflectivity modulation of $\delta b/b$ is the rigorous correction term. The s_{33} value for this sample was fitted to be 10 pm/V and was very sensitive to the thickness of the polymer.

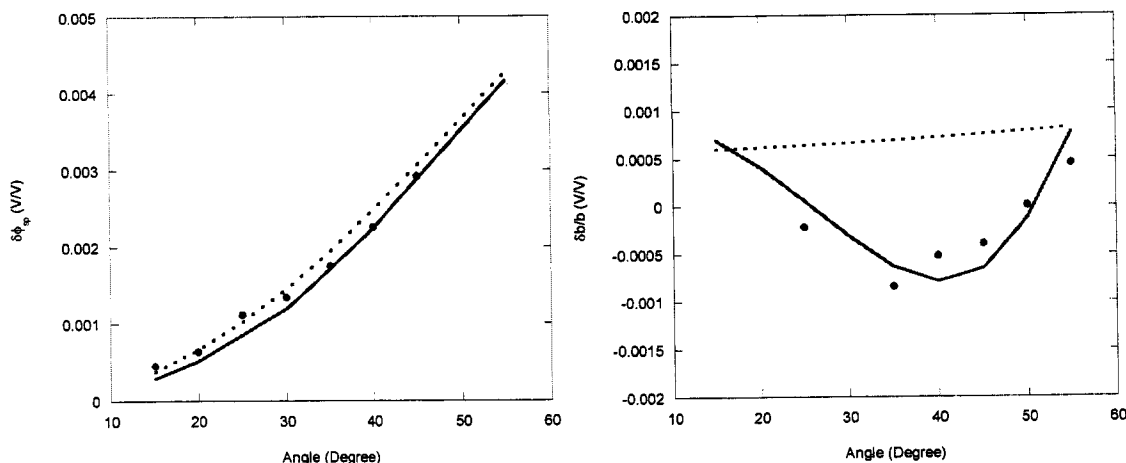


Figure 5.14. (a) $\delta\phi_{sp}$ versus Measurement Angle (b) $\delta b/b$ versus Measurement Angle at 1315 nm for the AJC135 Chromophore

As the material absorption further increases so does the separation from the simple and rigorous model. The Jen research group at the University of Washington developed the AJ302 organic glass, Figure 5.15. This material differs from the previously discussed materials because it has an unprecedented chromophore content of 100% by weight. This blended material contains a one-to-one ratio of the AJC146 chromophore and the AJC168 chromophore.

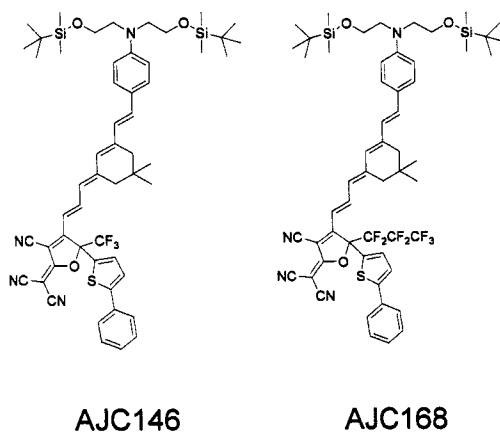


Figure 5.15. Chemical Structure of AJ302 Organic Glass

The large increase in chromophore content pushed the absorption peak to 804 nm and broadened the overall peak considerably. The effect of this change produced the type error in the Teng-Man results shown in Figure 5.10. Figure 5.16 demonstrates the expected large deviation from the simple model.

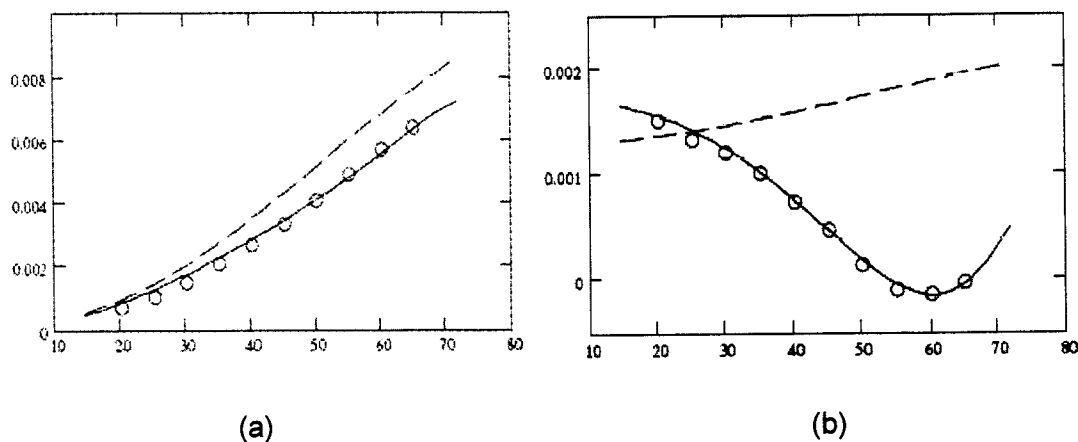


Figure 5.16. (a) $\delta\phi_{sp}$ versus Measurement Angle (b) $\delta b/b$ versus Measurement Angle at 1319 nm for the AJ302 Organic Glass [3]
Dashed line = simple model, solid line = rigorous model, and open circles = experimental results

The variation between the two models is on the order of 10^{-3} and unlike TCF and AJL8, the deviation is not limited to only the higher angles of incidence. This is not a surprising result because the chromophore content is significantly higher than in the previously discussed materials. As the EO coefficients increase, the discrepancy between the simple model and the experimental data also increases, resulting in significantly reduced EO coefficients (250 pm/V versus 290 pm/V). The s_{33} value was fitted to be 17 pm/V.[3]

Table 5.2 illustrates the change in the real EO coefficients and lists the absorption peak, chromophore content, and polymer film thickness.

Table 5.2. Material Properties of Multi-Angle Test Materials

Acceptor	Chromophore Content (wt%)	λ_{\max} (nm)	Polymer Thickness (μm)	r_{33} (simple) (pm/V) _{1315nm}	r_{33} (rigorous) (pm/V) _{1315nm}
TCF	25	594	1.73	10	12
AJL8	25	712	1.30	33	32
AJC135	30	778	1.45	40	48
AJ302	100	804	1.10	250	290

In general the rigorous fit showed an increase of approximately 15% in the real EO coefficient when material absorption is present. The imaginary EO coefficient was almost nonexistent in the AJL8 and TCF samples and very difficult to fit due to the noise in the experimental data. The combination of the multi-angle measurement and rigorous model should be used for the more absorptive materials to obtain an accurate real and imaginary EO coefficient.

5.6 Conclusions and Future Work

The effects of the ITO at 1315 nm are small and data measured for a non-absorptive material at a single angle is fairly accurate. The resulting r_{33} values for the poled polymer films on each of the different ITO electrodes were within experimental error of each other. The rigorous model demonstrated a better fit with the experimental data, especially at 1550 nm. This experiment showed that even though ITO's transparency can be slightly improved by modifying processing steps and its dopants, it is still absorbing in the NIR and the rigorous fit should be used in future EO calculations at 1550 nm. To get a better feel for the variations of commercial ITO at the longer wavelengths, a study should be done on several pieces of commercial ITO with the

multi-angle measurement in addition to the rigorous model. Ideally, the thickness and sheet resistance of that piece of ITO would be measured prior to the sample preparation. Overall, the rigorous fit showed an increase in the real EO coefficient when material absorption was present. The primary contribution to $\delta b/b$ came from the rigorous correction term and should always be calculated for absorptive materials. To improve the data fits of future measurements the interval between the angles of incidence should be reduced from 5° to 2° .

Even with the rigorous model the assumption of $r_{33} \approx 3r_{13}$ is still needed. Recent work by Nagtegaele and Zyss demonstrated the use of a Wollaston prism to separate the s and p waves to enable the calculation of r_{13} and r_{33} independently.[15] This experiment only requires a slight modification to the current experimental set-up and sample preparation. However Nagtegaele and associates' calculation was based on that for a Fabry-Perot cavity, which is not trivial.[15, 16] Working through the meticulous calculation would be worth the advantage of eliminating the need for the assumption that $r_{33} \approx 3r_{13}$ and would provide an opportunity to study the relationship between the material structure changes and the ratio between r_{33} and r_{13} .

5.7 Experimental

All solutions were filtered through the 0.2- μm PTFE filter prior to spin coating. The thin-film preparation for all materials included spin coating onto half-etched ITO substrates. Spin coating speeds typically ranged from 800–1200 rpm depending on the solid content and desired film thickness. On average the film thickness ranged from 1–2 micron and solid content varied from 8–15% by weight in cyclopentanone. The

samples were soft baked at 65°C for approximately 10 minutes and hard baked under vacuum for more than 12 hours after spin coating. All samples were baked under vacuum in a Napco 5851 oven. The guest-host APC samples were hard baked under vacuum at 85°C. All polymer film thickness measurements were made on a Daktek 3030 profilometer. Sputter coating for each sample was done with a Denton Desk II sputter coater for 2 minutes, resulting in an approximately 100 nm thick gold electrode. The UV/VIS spectrum was measured for all discussed materials by using a Perkin-Elmer Lambda 9 UV/VIS/NIR spectrophotometer. The poling conditions were carried out under a N₂ atmosphere and a fresh sample was used for each measurement. All poling was done with a Mettler FP800 oven, Stanford Research Systems, Inc. (SRS) high-voltage power supply PS 350, and a Keithley 617 programmable electrometer.

The simple reflection technique at the University of Washington was carried out using 630 nm, 830 nm, 1315 nm, and 1550 nm LaserMax diode lasers, a Tektronix TDS520D oscilloscope, Stanford Research Systems, Inc. (SRS) 560 low-noise pre-amplifier, a SRS DS345 synthesized function generator, a SRS SR850 DSP lockin amplifier, a SRS SR540 chopper controller, and a Trek 610C voltage amplifier. All multi-angle measurements were made at the Lumera Corporation in Bothell, WA. The index of the ITO was calculated based on the sheet resistance and film thickness.[17] The refractive index of the gold was obtained from Johnson et al.[18] All refractive index measurements were made with the Metricon 2010 prism coupler. The ITO thickness was determined by atomic force microscopy.

Notes to Chapter 5:

1. Teng, C.C. and H.T. Man, *Simple reflection technique for measuring the electrooptic coefficient of poled polymers*. Applied Physics Letters, 1990. **56**(18): p. 1734-1736.
2. Levy, Y., et al., *Reflection method for electro-optical coefficient determination in stratified thin film structures*. Molecular Crystal Liquid Crystal Science Technology - Section B: Nonlinear Optics, 1993. **4**: p. 1-19.
3. Park, D.H., et al., *Nonlinear ellipsometric analysis of poled organic glasses having very large electro-optic coefficients*. Proceeding SPIE, 2005. **5935**.
4. Chollet, P.A., et al., *Electro-optic coefficient determination in stratified organized molecular thin-films - application to poled polymers*. Thin Solid Films, 1994. **242**(1-2): p. 132-138.
5. Michelotti, F., et al., *On the measurement of the electro-optic properties of poled side-chain copolymer films with a modified Teng-Man technique*. Chemical Physics, 1999. **245**(1-3): p. 311-326.
6. Azzam, R.M.A. and N.M. Bashara, *Ellipsometry and Polarized Light*. 1977, New York: North-Holland Publishing Company.
7. Clays, K. and J.S. Schildkraut, *Dispersion of the complex electro-optic coefficient and electrochromic effects in poled polymer films*. Journal of the Optical Society of America B-Optical Physics, 1992. **9**(12): p. 2274-2282.
8. Schildkraut, J.S., *Determination of the electrooptic coefficient of a poled polymer film*. Applied Optics, 1990. **29**(19): p. 2839-2841.
9. Shuto, Y. and M. Amano, *Reflection measurement technique of electro-optic coefficients in lithium niobate crystals and poled polymer films*. Journal of Applied Physics, 1995. **77**(9): p. 4632-4638.
10. Kuzyk, M.G. and C.W. Dirk, *Characterization Techniques and Tabulations for Organic Nonlinear Optical Materials*. 1998, New York: Marcel Dekker, Inc.
11. Prasad, P. and D.J. Williams, *Introduction to Nonlinear Optical Effects in Molecules and Polymers*. 1991, Hoboken: Wiley-Interscience.
12. Michelotti, F., et al., *Measurement of the electro-optic properties of poled polymers at $\lambda=1.55 \mu m$ by means of sandwich structures with zinc oxide transparent electrode*. Applied Physics Letters, 2003. **83**(22): p. 4477-4479.
13. Ni, J., et al., *MOCVD-derived highly transparent, conductive zinc- and tin-doped indium oxide thin films: Precursor synthesis, metastable phase film growth and*

- characterization, and application as anodes in polymer light-emitting diodes.* Journal of the American Chemical Society, 2005. **127**(15): p. 5613-5624.
14. Filmetrics, *Taking the mystery out of thin-film measurement.* 2003.
 15. Nagtegale, P., E. Brasselet, and J. Zyss, *Anisotropy and dispersion of a Pockels tensor: a benchmark for electro-optic organic thin-film assessment.* Journal of the Optical Society of America B-Optical Physics, 2003. **20**(9): p. 1932-1936.
 16. Toussaere, E. and J. Zyss, *Ellipsometry and reflectance of inhomogeneous and anisotropic media: a new computationally efficient approach.* Thin Solid Films, 1993. **234**: p. 432-438.
 17. Edwards, P.P., et al., *Basic materials physics of transparent conducting oxides.* Dalton Transactions, 2004(19): p. 2995 - 3002.
 18. Johnson, P.B. and R.W. Christy, *Optical constants of the noble metals.* Physical Review B, 1972. **6**(12): p. 4370.

Bibliography

- Aillerie, M., N. Theofanous, and M.D. Fontana, *Measurement of the electro-optic coefficients: description and comparison of the experimental techniques*. Applied Physics B-Lasers and Optics, 2000. **70**(3): p. 317-334.
- Azzam, R.M.A. and N.M. Bashara, *Ellipsometry and Polarized Light*. 1977, New York: North-Holland Publishing Company.
- Bosshard, C.H., K. Sutter, Ph. Pretre, J. Hulliger, M. Florsheimer, P. Kaatz, and P. Gunter, *Organic Nonlinear Optical Materials*. 1995, New York: Taylor & Francis.
- Burland, D.M., R. Miller, and C. Walsh, *Second-order nonlinearity in poled-polymer systems*. Chemical Review, 1994. **94**: p. 31-75.
- Cai, Y.M. and A.K.Y. Jen, *Thermally stable poled polyquinoline thin film with very large electro-optic response*. Applied Physics Letters, 1995. **67**(3): p. 299-301.
- Chen, A.T., et al., *DC biased electro-optic polymer waveguide modulators with low half-wave voltage and high thermal stability*. Optical Engineering, 1999. **38**(12): p. 2000-2008.
- Chollet, P.A., et al., *Electro-optic coefficient determination in stratified organized molecular thin-films - application to poled polymers*. Thin Solid Films, 1994. **242**(1-2): p. 132-138.
- Clays, K. and J.S. Schildkraut, *Dispersion of the complex electro-optic coefficient and electrochromic effects in poled polymer films*. Journal of the Optical Society of America B-Optical Physics, 1992. **9**(12): p. 2274-2282.
- Dalton, L.R., *Rational design of organic electro-optic materials*. Journal of Physics: Condensed Matter, 2003. **15**: p. R897-R934.
- Dalton, L.R., *Nonlinear optical polymeric materials*. Advances in Polymer Science, 2002. **158**: p. 1-86.
- Dalton, L.R., et al., *From molecules to opto-chips: organic electro-optic materials*. Journal of Materials Chemistry, 1999. **9**: p. 1905-1920.
- Dalton, L.R., et al., *Synthesis and processing of improved organic second-order nonlinear optical materials for applications in photonics*. Chemistry of Materials, 1995. **7**: p. 1060-1081.
- Edwards, P.P., et al., *Basic materials physics of transparent conducting oxides*. Dalton Transactions, 2004(19): p. 2995 - 3002.
- Eldada, L., *Advances in telecom and datacom optical components*. Optical Engineering, 2001. **40**(7): p. 1165-1178.

- Filmetrics, *Taking the mystery out of thin-film measurement*. 2003.
- Grote, J.G., et al., *Effect of conductivity and dielectric constant on the modulation voltage for optoelectronic devices based on nonlinear optical polymers*. Optical Engineering, 2001. **40**(11): p. 2464-2473.
- Haller, M., et al., *A novel lattice-hardening process to achieve highly efficient and thermally stable nonlinear optical polymers*. Macromolecules, 2004. **37**(3): p. 688-690.
- Harper, A.W., et al., *Translating microscopic optical nonlinearity into macroscopic optical nonlinearity: the role of chromophore-chromophore electrostatic interactions*. Journal of the Optical Society of America B-Optical Physics, 1998. **15**(1): p. 329-337.
- Heavens, O.S. and R.W. Ditchburn, *Insight into Optics*. 1991, New York: Wiley and Sons.
- Hecht, J., *WDM Solutions*, 2001: p. 100-104.
- Jen, A.K.Y., et al., *Synthesis and characterization of highly efficient, chemically and thermally stable chromophores with chromone-containing electron acceptors for NLO applications*. Advanced Materials, 1999. **11**(6): p. 452.
- Johnson, P.B. and R.W. Christy, *Optical constants of the noble metals*. Physical Review B, 1972. **6**(12): p. 4370.
- Kajzar, F., K.-S. Lee, and A.K.-Y. Jen, *Polymeric materials and their orientation techniques for second-order nonlinear optics*. Advances in Polymer Science, 2003. **161**: p. 1-85.
- Kim, T.-D., et al., *Molecular engineering of highly efficient and thermally stable nonlinear optical polymers for electro-optics*. Polymeric Materials: Science and Engineering, 2004. **91**: p. 273.
- Kuzyk, M.G. and C.W. Dirk, *Characterization Techniques and Tabulations for Organic Nonlinear Optical Materials*. 1998, New York: Marcel Dekker, Inc.
- Kwart, H. and K. King, *The reverse Diels-Alder or retrodiene reaction*. Chemical Review, 1968. **68**(4): p. 415-447.
- Levy, Y., et al., *Reflection method for electro-optical coefficient determination in stratified thin film structures*. Molecular Crystal Liquid Crystal Science Technology - Section B: Nonlinear Optics, 1993. **4**: p. 1-19.
- Liu, S., et al., *Focused microwave-assisted synthesis of 2,5-dihydrofuran derivatives as electron acceptors for highly efficient nonlinear optical chromophores*. Advanced Materials, 2003. **15**(7-8): p. 603-607.

- Luo, J.D., et al., *Nanoscale architectural control and macromolecular engineering of nonlinear optical dendrimers and polymers for electro-optics*. Journal of Physical Chemistry B, 2004. **108**(25): p. 8523-8530.
- Luo, J.D., et al., *A side-chain dendronized nonlinear optical polyimide with large and thermally stable electrooptic activity*. Macromolecules, 2004. **37**(2): p. 248-250.
- Luo, J.D., et al., *Highly efficient and thermally stable electro-optic polymer from a smartly controlled crosslinking process*. Advanced Materials, 2003. **15**(19): p. 1635-+.
- Luo, J.D., et al., *Large electro-optic activity and low optical loss derived from a highly fluorinated dendritic nonlinear optical chromophore*. Chemical Communications, 2002(8): p. 888-889.
- Luo, J.D., et al., *Design, synthesis, and properties of highly efficient side-chain dendronized nonlinear optical polymers for electro-optics*. Advanced Materials, 2002. **14**(23): p. 1763-1768.
- Ma, H., et al., *Highly efficient and thermally stable electro-optical dendrimers for photonics*. Advanced Functional Materials, 2002. **12**(9): p. 565-574.
- Ma, H., A.K.-Y. Jen, and L. Dalton, *Polymer-based optical waveguide materials, processing, and devices*. Advanced Materials, 2002. **14**(19): p. 1339-1365.
- Marder, S.R., J.E. Sohn, and G.D. Stucky, *Materials for Nonlinear Optics: Chemical Perspectives*. ACS Symposium Series 455. 1991, Washington D.C.
- Michelotti, F., et al., *Measurement of the electro-optic properties of poled polymers at $\lambda = 1.55 \mu\text{m}$ by means of sandwich structures with zinc oxide transparent electrode*. Applied Physics Letters, 2003. **83**(22): p. 4477-4479.
- Michelotti, F., et al., *On the measurement of the electro-optic properties of poled side-chain copolymer films with a modified Teng-Man technique*. Chemical Physics, 1999. **245**(1-3): p. 311-326.
- Nagtegaale, P., E. Brasselet, and J. Zyss, *Anisotropy and dispersion of a Pockels tensor: a benchmark for electro-optic organic thin-film assessment*. Journal of the Optical Society of America B-Optical Physics, 2003. **20**(9): p. 1932-1936.
- Ni, J., et al., *MOCVD-derived highly transparent, conductive zinc- and tin-doped indium oxide thin films: Precursor synthesis, metastable phase film growth and characterization, and application as anodes in polymer light-emitting diodes*. Journal of the American Chemical Society, 2005. **127**(15): p. 5613-5624.
- Page, R.H., et al., *Electrochromic and optical wave-guide studies of corona-poled electrooptic polymer-films*. Journal of the Optical Society of America B-Optical Physics, 1990. **7**(7): p. 1239-1250.
- Park, D.H., et al., *Nonlinear ellipsometric analysis of poled organic glasses having very large electro-optic coefficients*. Proceeding SPIE, 2005. **5935**.

- Percec, V., et al., *Visualizable cylindrical macromolecules with controlled stiffness from backbones containing libraries of self-assembling dendritic side groups*. Journal of the American Chemical Society, 1998. **120**(34): p. 8619-8631.
- Pitois, C., A. Hult, and D. Wiesmann, *Absorption and scattering in low-loss polymer optical waveguides*. Journal of the Optical Society of America B-Optical Physics, 2001. **18**(7): p. 908-912.
- Prasad, P. and D.J. Williams, *Introduction to Nonlinear Optical Effects in Molecules and Polymers*. 1991, Hoboken: Wiley-Interscience.
- Robinson, B.H. and L.R. Dalton, *Monte Carlo statistical mechanical simulations of the competition of intermolecular electrostatic and poling-field interactions in defining macroscopic electro-optic activity for organic chromophore/polymer materials*. Journal of Physical Chemistry A, 2000. **104**(20): p. 4785-4795.
- Schildkraut, J.S., *Determination of the electrooptic coefficient of a poled polymer film*. Applied Optics, 1990. **29**(19): p. 2839-2841.
- Shi, Y.Q., et al., *Low (sub-1-volt) halfwave voltage polymeric electro-optic modulators achieved by controlling chromophore shape*. Science, 2000. **288**(5463): p. 119-122.
- Shuto, Y. and M. Amano, *Reflection measurement technique of electro-optic coefficients in lithium niobate crystals and poled polymer films*. Journal of Applied Physics, 1995. **77**(9): p. 4632-4638.
- Singer, K.D., M.G. Kuzyk, and J.E. Sohn, *2nd-Order nonlinear-optical processes in orientationally ordered materials - relationship between molecular and macroscopic properties*. Journal of the Optical Society of America B-Optical Physics, 1987. **4**(6): p. 968-976.
- Teng, C.C. and H.T. Man, *Simple reflection technique for measuring the electrooptic coefficient of poled polymers*. Applied Physics Letters, 1990. **56**(18): p. 1734-1736.
- Toussaere, E. and J. Zyss, *Ellipsometry and reflectance of inhomogeneous and anisotropic media: a new computationally efficient approach*. Thin Solid Films, 1993. **234**: p. 432-438.
- Unger, H.G., *Planar Optical Waveguides and Fibres*. 1977, Oxford: Clarendon Press.
- Wong, S., *Design, synthesis, and characterization of novel perfluorocyclobutyl (PFCB) aromatic ether polymers for optical waveguide applications*, in *Materials Science and Engineering*. 2003, University of Washington: Seattle.
- Zhang, C., et al., *Low V electrooptic modulators from CLD-1: chromophore design and synthesis, material processing, and characterization*. Chemistry of Materials, 2001. **13**(9): p. 3043-3050.

Zhang, C., et al., *Electric poling and relaxation of thermoset polyurethane second-order nonlinear optical materials: role of cross-linking and monomer rigidity*. *Macromolecules*, 2001. **34**(2): p. 235-243.

Zhou, M., *Low-loss polymeric materials for passive waveguide components in fiber optical telecommunication*. *Optical Engineering*, 2002. **41**(7): p. 1631-1643.

VITA

Marnie Ann Haller

Education

- Doctor of Philosophy, Materials Science and Engineering, University of Washington, 2005.
- Bachelor of Science, Ceramic Engineering, University of Washington, 2000.

Research Experience

- Characterization of highly efficient nonlinear optical polymers for waveguide applications. This research focuses on the development of molecular structure/property relationships based on the observed material behavior during the characterization process.
- Responsible for measuring electro-optic coefficients through simple reflection method based on the Pockels effect and designing and automating experiments through Labview.
- Work with various device teams to translate the small-scale characterization properties into devices.
- Lab skills include dielectric constant measurements, UV spectrometry, refractive index and loss measurements, spin coating, sputter coating, thin-film thickness measurements, glass transition measurements, poling materials, and photolithography.

Patents

- Highly efficient and thermally stable electro-optic polymers from reversible cross-linkable process, UW Tech-Transfer Number: 2636–3859

Work Experience

- Graduate Research Assistant, Department of Materials Science and Engineering, September 2000–September 2005.
- Teaching Assistant, Department of Materials Science and Engineering, September 2000–June 2001.
 - Fiber Composites Fall Quarter 2000
 - Kinetic Processes and Transformations Winter Quarter 2001
 - Mechanical Properties of Materials Lab Spring Quarter 2001
- Research Assistant, Battelle Pacific Northwest National Laboratories, June 2000–September 2000.
 - Researched the effects of radiation on the stability of spinel crystalline phases in waste glasses.
 - Researched the effects of heavy-ion beam damage on the optical properties of telluride glasses for photonics applications.

Publications

- Haller, M., J.D. Luo, H.X. Li, T.D. Kim, Y. Liao, B.H. Robinson, L.R. Dalton, and A.K.Y. Jen, *A novel lattice-hardening process to achieve highly efficient and thermally stable nonlinear optical polymers*. *Macromolecules*, 2004. **37**(3): p. 688–690.
- Kang, J.-W., T.-D. Kim, J. Luo, M. Haller, and A.K.-Y. Jen, *Very large electro-optic coefficients from in situ generated side-chain nonlinear optical polymers*. *Applied Physics Letters*, 2005. **87**(7): p. 1109.
- Liao, Y., B.E. Eichinger, K.A. Firestone, M. Haller, J.D. Luo, W. Kaminsky, J.B. Benedict, P.J. Reid, A.K.Y. Jen, L.R. Dalton, and B.H. Robinson, *Systematic study of the structure/property relationship of a series of ferrocenyl nonlinear optical chromophores*. *Journal of the American Chemical Society*, 2005. **127**(8): p. 2758–2766.
- Gray, T., R.M. Overney, M. Haller, J. Luo, and A.K.Y. Jen, *Low-temperature relaxations and effects on poling efficiencies of dendronized nonlinear optical side-chain polymers*. *Applied Physics Letters*, 2005. **86**(21).
- Sinyukov, A.M., M.R. Leahy, L.M. Hayden, M. Haller, L. Jingdong, A.K.Y. Jen, and L.R. Dalton, *Resonance-enhanced THz generation in electro-optic polymers near the absorption maximum*. *Applied Physics Letters*, 2004. **85**(24): p. 5827.
- Luo, J.D., M. Haller, H.X. Li, H.Z. Tang, A.K.Y. Jen, K. Jakka, C.H. Chou, and C.F. Shu, *A side-chain dendronized nonlinear optical polyimide with large and thermally stable electrooptic activity*. *Macromolecules*, 2004. **37**(2): p. 248–250.
- Luo, J.D., M. Haller, H. Ma, S. Liu, T.D. Kim, Y.Q. Tian, B.Q. Chen, S.H. Jang, L.R. Dalton, and A.K.Y. Jen, *Nanoscale architectural control and macromolecular engineering of nonlinear optical dendrimers and polymers for electro-optics*. *Journal of Physical Chemistry B*, 2004. **108**(25): p. 8523–8530.
- Kim, T.D., J.D. Luo, J.W. Kang, M. Haller, Y.Q. Tian, L. Dalton, B.Q. Chen, and A.K.Y. Jen, *Molecular engineering of highly efficient and thermally stable nonlinear optical polymers for electro-optics*. Abstracts of papers of the American Chemical Society, 2004. **228**: p. U438.
- Bhattacharjee, S., J.D. Luo, M. Haller, A.K.Y. Jen, and L.R. Dalton, *Reversible Diels-Alder type cross-linkable electro-optic polymers with pendant TCF-based chromophore*. Abstracts of papers of the American Chemical Society, 2004. **228**: p. U336.
- Liu, S., M.A. Haller, H. Ma, L.R. Dalton, S.H. Jang, and A.K.Y. Jen, *Focused microwave-assisted synthesis of 2,5-dihydrofuran derivatives as electron acceptors for highly efficient nonlinear optical chromophores*. *Advanced Materials*, 2003. **15**(7–8): p. 603–607.
- Luo, J.D., M. Haller, H.X. Li, T.D. Kim, and A.K.Y. Jen, *Highly efficient and thermally stable electro-optic polymer from a smartly controlled cross-linking process*. *Advanced Materials*, 2003. **15**(19): p. 1635–+.
- Jen, A.K.Y., H. Ma, J.D. Luo, S. Liu, M. Haller, S.H. Jang, L. Dalton, H. Zareie, B. Reed, and M. Sarikaya, *Nanoscale architectural control of organic functional materials for photonics and molecular electronics*. Abstracts of Papers of The American Chemical Society, 2003. **225**: p. U671.

- Luo, J.D., S. Liu, M. Haller, L. Liu, H. Ma, and A.K.Y. Jen, *Design, synthesis, and properties of highly efficient side-chain dendronized nonlinear optical polymers for electro-optics*. *Advanced Materials*, 2002. **14**(23): p. 1763–1768.
- Luo, J.D., H. Ma, M. Haller, A.K.Y. Jen, and R.R. Barto, *Large electro-optic activity and low optical loss derived from a highly fluorinated dendritic nonlinear optical chromophore*. *Chemical Communications*, 2002(8): p. 888–889.
- Ma, H., S. Liu, J.D. Luo, S. Suresh, L. Liu, S.H. Kang, M. Haller, T. Sassa, L.R. Dalton, and A.K.Y. Jen, *Highly efficient and thermally stable electro-optical dendrimers for photonics*. *Advanced Functional Materials*, 2002. **12**(9): p. 565–574.